Faculty of Metallurgy and Materials Engineering
VŠB-Technical University of Ostrava

DISSERTATION THESIS

Nano-particulate metal-based emissions from pyrometallurgy and road traffic

Mgr. Pavlína Peikertová

Chemical Metallurgy

Supervisor: doc. Mgr. Jana Kukutschová, Ph.D.

Ostrava, July 2014

Bibliographic identification

Author's name and surname: **Mgr. Pavlína Peikertová**

Name of dissertation thesis: **Nano-particulate metal-based emissions from pyrometallurgy and road traffic**

Name of dissertation thesis in Czech: **Emise nanometrických částic na bázi kovů z pyrometalurgie a dopravy**

Faculty: **Faculty of Metallurgy and Materials Engineering**

Study Programme: **Chemical Metallurgy**

Supervisor: **doc. Mgr. Jana Kukutschová, PhD.**

Year: **2014**

Keywords: pyrometallurgical sludges, friction composites for automotive brake linings, wear debris, Raman microspectroscopy

Keywords in Czech: pyrometalurgické kaly, frikční kompozity pro brzdové obložení osobních automobilů, otěrové částice, Ramanova mikrospektroskopie

Statement

I, Pavlína Peikertová declare that I have elaborated this work on my own. All literature and other sources from which I drew the preparation work I properly quoted in the list of references.

Ostrava, July 2014 Signature:

Acknowledgements

This research has been elaborated in the framework of the Nanotechnology – the basis for international cooperation project, reg. no. CZ.1.07/2.3.00/20.0074 supported by Operational Programme 'Education for competitiveness' funded by Structural Funds of the European Union and state budget of the Czech Republic.

Author would like to thank to doc. Mgr. Jana Kukutschová, PhD. for patient guiding of this work, for many good advices and versatile help. Author would like to thank to Mgr. Kateřina Mamulová Kutláková and Ing. Jana Zdrálková for XRPD analysis, to Marie Heliová, Mgr. Kateřina Dědková, and Klára Šafářová (Regional Centre of Advanced Technologies and Materials Faculty of Science Palacky University in Olomouc) for SEM analysis, and to doc. RNDr. Richard Dvorský for particle sizes measurements. Author would like also thank to Ing. Ivo Vávra, CSc. for the opportunity to measure samples on TEM device in Slovak Academy of Science in Bratislava. Significant thanks also go to all my colleagues for their support and advices. Also author would like to thank to Mgr. et Mgr. Marek Gajda for English corrections of the thesis.

Last but not least author wish to thank to Professor Peter Filip for the opportunity to stay and work in Center for Advanced Friction Study in Carbondale (Southern Illinois University, USA) and MUDr. Jana Tulinska PhD. for the opportunity to stay and work in Department of Immunology and Immunotoxicology (Slovak Medical University in Bratislava, Slovakia) thanks to support of the European Commission 7th FP for the Quality Nano project (FP7 INFRA-2010-1.1.31, Contract no: 214547-2).

Annotation

Anthropogenic activities, as pyrometallurgy and road traffic have plenty of benefits for the society; however they may also pose risks to the environment and human health as well. These risks are mainly connected to the production of wastes during these processes. With iron and steel production the generation and accumulation of fine-grained solid wastes are connected. These solid wastes are partially being recycled and partially they are landfilled. Potential risk of these wastes depends on amounts, chemistry and bioavailability of potentially hazardous metals present in wastes. These metals are persistent and may have significant negative impact on living organisms, so their long term presence in the environment may pose significant risks.

Non-combustion anthropogenic processes associated with road traffic, such as braking are also known to contribute to the environmental pollution. The friction contact between pad and disc during forced deceleration creates wear debris, which could be divided to the nonairborne and airborne fraction. The non-airborne fraction may settle on brake hardware, road surfaces, and in the vicinity of roads. These particles are considered to be large, but their surface may be "covered" with attached nano-sized particles, which can be potentially released to the environment.

Aim of the thesis was to evaluate the mobility of the nano-sized particles in the water environment and their morphology and chemistry characterization from five selected pyrometallurgical sludges (blast furnace sludge, blast furnace sludge treated in hydrocyclone overflow and underflow, tandem furnace sludge, and oxygen converter sludge), and nonairborne wear debris from two model brake pads (G6C and G6C/KATI), and two commercial brake pads (SMP1 and SMP2). Scanning electron microscopy, X-ray powder diffraction, FTIR spectroscopy, and Raman microspectroscopy were used for characterization of initial samples. According to European standard the suspensions were prepared from pyrometallurgical sludges. Also the sedimentation technique was used for suspension preparation of pyrometallurgical sludges and brake wear debris. Prepared suspensions were dried on a glass slide and characterized by scanning electron microscopy and Raman microspectroscopy. Transmission electron microscopy measurements were evaluated with liquid suspensions. These analytical techniques revealed presence of nano-sized metal based and some crystalline particles. Filtered aqueous leachate is inaccurately considered homogenous.

Keywords: pyrometallurgical sludges, friction composites for automotive brake linings, wear debris, Raman microspectroscopy

Annotation in Czech

Antropogenní činnosti, jako je pyrometalurgie a pozemní doprava jsou přínosem pro společnost, avšak přinášejí s sebou také jistá rizika pro životní prostředí a zdraví člověka. S těmito riziky je spojen například vznik odpadních produktů těchto procesů, které se uvolňují do životního prostředí. S výrobou železa a oceli je spojena produkce a akumulace jemnozrnných tuhých odpadů, které jsou částečně recyklovány a částečně skládkovány. Potenciální rizika těchto odpadů jsou závislá nejen na množství ale také na formě potenciálně rizikových kovů. Výskyt těchto kovů v životním prostředí představuje dlouhodobé riziko a může mít významný negativní vliv na živé organismy.

Nespalovací procesy, jako je brzdění automobilů, také hojně přispívají ke znečištění životního prostředí. Brzdný otěr vzniká při tření mezi komponenty brzdné soustavy a může být rozdělen na dvě frakce, a to „nonairborne“ a „airborne“. „Nonairborne“ frakce obecně může spadat na povrchy cest, nebo být zachycena na součástech automobilu. Tyto částice jsou považovány za „velké“, ale na jejich povrchu mohou být zachyceny nanometrické částice, které mohou být uvolňovány dále do prostředí.

Hlavním cílem této práce bylo určit mobilitu nanometrických částic ve vodném prostředí, jejich morfologii a složení v pěti vybraných pyrometalurgických kalech (kal z kyslíkového konvertoru, tandemové pece a vysoké pece, vysokopecní kal také po rozdružování na hydrocyklonu - výtok a přepad) a v brzdném otěru ze dvou modelových brzdových destiček (G6C a G6C/KATI) a dvou komerčních brzdových destiček (SMP1 a SMP2). Skenovací elektronová mikroskopie, rentgenová prášková difrakce, FTIR spektroskopie a Ramanova mikrospektroskopie byly použity pro charakterizaci všech původních vzorků. Podle evropské směrnice byly ze vzorků pyrometalurgických kalů připraveny vodné výluhy. Vodné suspenze byly také připraveny sedimentačním procesem pro oba typy vzorků. Připravené vodné suspenze byly nakápnuty na podložní sklíčko a nechány zaschnout pro analýzy skenovací elektronovou mikroskopií a Ramanovou mikrospektroskopií. Transmisní elektronová mikroskopie byla provedena přímo na připravených vodných suspenzích. Těmito technikami byly nalezeny nanometrické částice, některé i krystalického charakteru na bázi kovů. Připravené vodné suspenze podle normy jsou tudíž nesprávně považovány za homogenní výluh.

Keywords: pyrometalurgické kaly, frikční kompozity pro brzdové obložení osobních automobilů, otěrové částice, Ramanova mikrospektroskopie

Content

1. PREFACE

Anthropogenic activities, as pyrometallurgy and road traffic have plenty of benefits for the society; however they may also pose risks to the environment and human health. These risks are mainly associated with the production of wastes during these processes. In addition to the gaseous emissions, they generate enormous quantities of solid wastes, which are formed predominantly by fine-grained dust particles which may be released into the environment. In the case of the finest fraction it can be assumed, that these particles could enter the atmospheric environment. Air pollution is mostly connected to the activity of the heavy industry and road traffic. Especially the urban areas with industrial facilities rank among the most air polluted areas. It should be noted that this issue has already received considerable attention not only in scientific community, but also in public. Efforts are leading to the pollution reduction from both metallurgical and road traffic sources.

Iron and steel production go hand in hand with gaseous emissions and as well as production and accumulation of fine-grained solid wastes. Only in Moravian-Silesian Region (Czech Republic) thousands of tons of wastes are produced every year, partially they are being recycled and partially landfilled. Potential risk of these wastes depends on amounts, chemistry and bioavailability of the potentially hazardous metals, which may show toxic properties, such as cadmium, lead, zinc and others. These metals are persistent and may have significant negative impact on living organisms, thus their long term presence in the environment may pose significant risks.

Pollution generated by road traffic can be divided based on the sources by which pollutants are emitted to the combustion and non-combustion processes (friction processes), which contribute to the environmental pollution. Combustion processes has been more frequently studied, but nowadays attention is also paid to the friction processes associated with wear particles emissions (brake wear, tire wear, wear of automotive hardware (engine parts, etc.), road surfaces and traffic signs). Brake system is a very important part of each automobile safety operation. In general, automotive brake system consists of 3 main parts: rotating disc with caliper and a couple of brake pads. There are many types of formulations of brake pads, which contain different components and are manufactured in huge quantities. There is a tendency to control some potentially hazardous materials used for brake pads formulation (asbestos, copper etc.). Since the friction that occurs during braking is accompanied with high temperatures and pressures, and new compounds different from the

initial composition may be created. Therefore, the attention is drawn to the braking processes and its potential environmental impact.

Occurrence of high temperature is associated with both metallurgical and friction processes, which caused the creation of nano-sized metal-based particles subsequently released into the environment. These particles can be released directly to the air or could be attached on the surfaces of larger particles.

The thesis deals with selected pyrometallurgical sludges and nonairborne brake wear debris particles forcefully on creation of methodology of detection and characterization of micron and sub-micron particles in these particulate materials. This experimental design was applied on both groups of materials and the particles mobility in water media was investigated.

Aims of the work:

1) To design experimental methods for comprehensive characterization of fine-grained materials from two selected groups of anthropogenic sources, i.e. pyrometallurgy and road traffic non-combustion emissions, with a special focus on micron and submicron particles.
2) Application of the experimental design to the selected pyrometallurgical sludges (blast furnace sludge, tandem furnace sludge and oxygen converter sludge) and nonairborne wear particles generated during simulation of braking process of automobiles (commercial and model brake pads).
3) For the above mentioned materials to evaluate mobility of submicron particles in water environment and their morphology and perform chemistry characterization.

2. INTRODUCTION

2.1 PYROMETALURGY

No substance in the history has been as important as a metal. Iron, which is the most abundant in the Earth's surface, was processed for the first time about 2,000 BC, but about 1,500 BC the processing of iron was performed almost everywhere on a regular basis. By the 11th century BC it was discovered that properties of iron could be improved by adding carbon to it. If iron was reheated in a furnace with charcoal (containing carbon), some of the carbon was transferred to the iron. This new developed material was steel and replaced bronze weapons in the Middle East (birthplace of Iron Age) [1].

Historical developments in ferrous metallurgy can be found in a wide variety of past cultures and civilizations (Egypt, Greek, China, etc.) [2]. A lot of applications, practices, and devices associated or involved in metallurgy were established in ancient China. Georg Agricola "the Father of metallurgy", who published book titled De Re Metallica in a 16th century, describing the highly developed and complex processes of mining metal ores, metal extraction and metallurgy of the time [3]. In the past, the economic development of the state was assessed by the metallurgical progress.

Metallurgy, the technology of metals, is subdivided into ferrous metallurgy (black metallurgy) and non-ferrous metallurgy (colored metallurgy). Ferrous metallurgy involves processes and alloys based on iron. Non-ferrous metallurgy deals with other metals. The production of ferrous metals accounts for 95% of the entire world metal production [4].

2.1.1 Fine-grained Pyrometallurgical Wastes

Metallurgy (a field of heavy industry dealing with materials production based on metals, their mechanical, thermal and chemical treatment) has plenty of benefits for society. However, it is one of the biggest environment polluters and belongs to so called stationary sources. Pollutants could be released into the environment in solid, liquid or gaseous form. Nowadays, requirements for disposal and manipulation with this kind of solid metal-based wastes are a big issue. The scheme of iron and steel making processes is shown in the Figure 1.

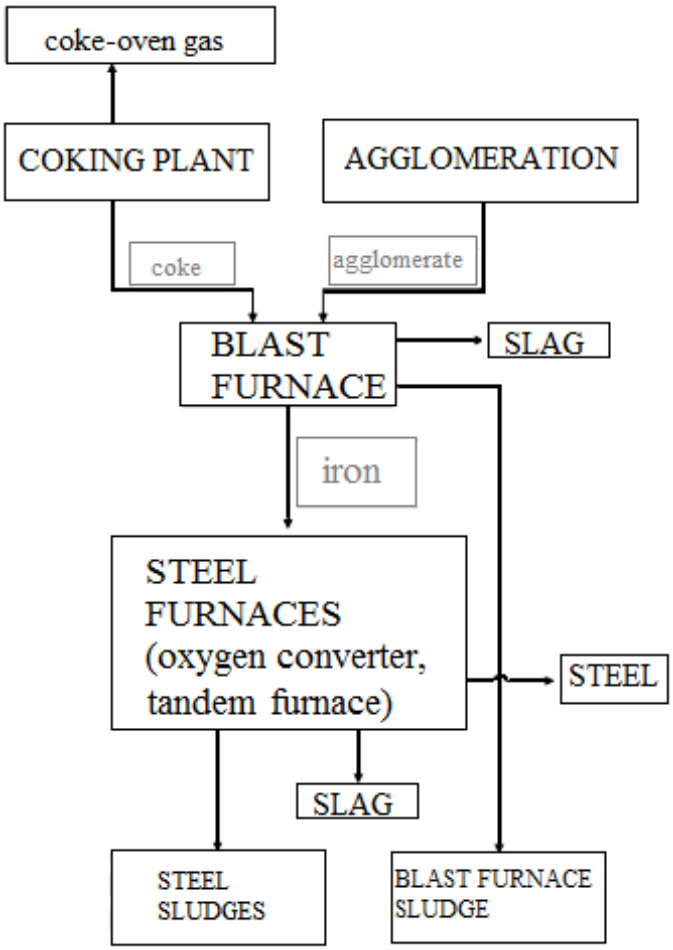

Figure 1: Iron and steel making process scheme modified from [5].

Metallurgical fine-grained solid wastes can be divided into two basic types according to their origin: blast furnace sludge and steel sludge. Other division could be made based on their potential risks. The Czech law on wastes ("Zákon o odpadech") No. 185/2001 Sb. [6] defined the term: "waste", as a movable object the holder discards, intends to discard or is required to discard. The same definition is given by European Union legislative (the Waste

Framework Directive) [7]. According to the Czech valid legislative wastes are cataloged in "Waste catalog" [8] to the 20 groups which could be divided by their chemical composition into the dangerous waste ("N"), other wastes ("O"), or wastes which are not mentioned in lists of "N" materials, but the category "N" was assigned to them after contamination ("O/N").

Even though 85% of pyrometallurgical wastes are included in the category "O" (others), slags from blast furnace and steel industry, scrap iron, and ash from coal and coke. 11% of metallurgical wastes (blast furnace and steel sludges) are assigned to the category marked "N" [6,8].

Only in Moravian-Silesian region of the Czech Republic thousands of tons of wastes are produced per year, partially they are recycled and partially if contain high amounts of zinc, lead and some others potentially hazardous metals they are landfilled [9]. For example, in 1998 about 105 kt of fine-grained wastes (agglomeration dusts, flue dust, and blast furnace sludge) and about 95 kt of fine-grained wastes from steelmaking plants (tandem furnace sludge, converter sludge etc.) were produced in North Moravian region of the Czech Republic. It could be concluded that fine-grained wastes represent 2% of the iron production and about 1.5% of the steel production in oxygen converters [10].

Metallurgical plants are currently making an effort to recycle all produced wastes, however only a part could be recycled, the rest is being landfilled. Previously, either terrain roughness or artificial wasteponds were used for wastes storage. According to Řepka et al. [11] about 854 kt of blast furnace sludge and 1183 kt of steel sludge is stored in Moravian region in wasteponds which were built of dams from slags and proof clays. Sludges can also be stored in caverns created from slag waste dump. In this way, 960 kt of blast furnace sludges contaminated by slags, and 400 kt of sludges from converters are stored. Converter sludges could be mined and used as an ingredient to the cement raw materials. Steel sludges could be deposited in a shoot up and mined space in a slag heap. Nowadays these sludges could be stored only in secure dumps with impermeable foils and monitoring [11,12]. Due to the high content and chemical form of potentially hazardous metals (e.g. zinc, lead and cadmium) in these sludges, the dumps represent a long-term risk of environment contamination, especially for surface and ground waters.

Metals contained in wastes have been for years disposed of in dumps and landfills. Le Guédard et al. [13] studied composition poplar leaves (*Populus nigra*) on a metal-contaminated landfill (Lyon, France), and on the uncontaminated roadside bordering this site. The impacts related to exposure to each of the following metals (Cr, Cu, Ni, Pb, Zn) were difficult to be evaluated, but according to the study [13] chromium in leaves plays a major

role in toxicity. The percentage of linoleic acid, which is mainly associated with thylakoid lipids, was significantly lower in tree species within the landfill than within the control area [13]. Guédard et al. [14] also exposed *Lactuca serriola* (prickly lettuce) *in situ* in the contaminated landfill to high levels of Cu, Cr, Ni, Pb and Zn, and the results showed that the lipid biomarker values were significantly lower in leaves of plants grown in the metallurgic landfills soil than in leaves of plants harvested on surrounding areas. The decrease in the lipid biomarker values *in situ* is positively solely correlated with Cr and Ni contents [14].

Two areas in Europe affected by presence of iron and steel factories have been extensively examined both for their metals content and speciation, and their pedological characteristics. One was localized in northeast France [15,16] and the other in southern Italy [17,18]. These soils were indeed characterized by a very high heavy metal contamination, but the evaluation of the potential mobility of pollutants gave contradictory results. The vertical metal transfer to the groundwater and to the above-ground vegetation is closely dependent on metal concentration and speciation, but also on soil characteristic and plant species [19,20].

It can be concluded that the metals which are present in the metallurgical wastes may pose risk to the environment, because the effect on the flora nearby the dumps and also the transfer to the soils and then to the water systems were proved. But the mechanism of the metals transfer and their chemistry is not yet entirely clear.

2.1.2 Recycling of Pyrometallurgical Wastes

The removal of metallurgical landfills is clearly unrealistic, due to the technical and financial considerations. One way to minimize the metal hazards in the environment is the recycling such a quantity of sludges as is possible, but this is connected to an increase in the cost of production [10]. However, raw materials used for the production of pig iron also contain non-ferrous metals, which are at minimal levels also present in final product (steel, steel blank), and it is suitable to remove these metals from production cycle as well. The removal of non-ferrous metals allows for the reuse of these materials in regular metallurgic processes (e.g. in blast furnace). Composition of fine-grained wastes varies and it is dependent on the method of collection, time of sampling (phase of a technologic cycle), type of raw materials used, and others [21].

For non-ferrous metals removal (mainly Cd, Zn) the process of evaporation of pollutants could be used at high temperature in the plasma heating oven, which leads to the thermal dissociation (high temperature reduction) of non-ferrous oxides. Plasma arc may reach high temperature, while above 4000°C substantially all oxides except CO, are thermodynamic unstable. During this process the metal-based compounds are decomposed and oxygen from oxides is bonded to the carbon. In order to maintain the metals in un-oxidized state, it is necessary to accelerate cooling to prevent reverse recombination of metal oxides [10].

Sintering plants have traditionally been used to recycle by-products in integrated steel plants. Recycled wastes may also have noticeable effects on sinter quality, sinter strength and productivity [22]. For example, the flue dust is generally recycled through sinter making. The Institute of Gas Technology, USA has developed a fluidized-bed process for recovering direct reduced iron from blast furnace flue dust. Up to 95% of the iron oxides contained in the waste stream could be reduced to the elemental iron. The yield of elemental iron depends upon the quantity of iron oxides present in the flue dust and generally ranges from 20 – 30% of the waste stream, but authors did not mentioned which iron oxides were mainly presented [23]. Another approach for processing fine-grained metal-based solid waste and for the decontamination of blast furnace sludge a hydrocyclone could be used (see Chapter 2.1.4).

2.1.3 Blast Furnace Sludge

Extractions of Fe from ores and its conversions into alloys are the most important metallurgical processes and take place in blast furnaces mainly [24]. There are several design variants of blast furnaces, but they always have a conical shaft, to which feed (ore, fuel, or fluxes) is continuously weighed. Following minerals contain suitable amount of iron and low content of undesirable components (Cu, Cd, Zn, Pb, and others) and therefore they can be used as a blast furnace feed: magnetite, hematite, limonite, siderite, chamosite or materials prepared therefrom. Some ores must be pretreated and they enter the blast furnace in the form of pellets or sinters. Coke is used as fuel and as a reducing agent as well [25].

In the iron-making process may be generate a hazardous metallurgical wastes as blast furnace sludge is. [26]. Undesirable metals (Cu, Cd, Zn, Pb, etc.) are introduced to the blast furnace with raw materials, partly from ores and mainly from scrap iron. Zinc, cadmium and lead have low melting points, and thus in the blast furnace they circulate in form of fumes and may leave the furnace with gaseous emissions or condense and subsequently attach to the surface of larger dust particles in the upper part of the blast furnace. Metals amount captured onto these particles is proportional to their surface, thus the biggest part is captured by the finest particles [27,28]. According to Vereš et al. [28] the concentration of Zn was observed to be highest on the finest dust particles. During the process between 8 and 12 kg of dust is produced per ton of pig iron.

Two products of blast furnace gas are named flue dust and sludge. Flue dust is a product of the rough cleaning in the anther, where almost 70% of dust particles can be captured. But author did not mentioned if the percentage is according to weight or volume. The flue dust may be further processed on the agglomeration and contains high amounts of carbon and low content of undesirable components based on Cd, Pb, Zn, etc. [9]. The dust is commonly being removed in the air pollution control system. Larger particles (> 50 μm) are removed from the flue gas in a dust bag and a cyclone. Since the content of zinc is generally low (<0.1 wt.% of zinc) it could be directly recovered in the blast furnace after sintering. Smaller particles (<50 μm) are washed out in a wet scrubber and generate sludge [24].

Blast furnace sludge is the second type of a blast furnace solid waste. Blast furnace sludge contains high amounts of hazardous components, and thus could be recycled by regular metallurgy processes only partially and the rest of it is settled in the wastepond until a suitable processing technique is available [9,29,30]. The Council Directive 96/61/EC [31] on integrated pollution prevention and control defined the term “best available techniques

(BAT)" as "the most effective and advanced stage in development of activities and their methods of operation which indicate the practical suitability of particular techniques for providing in principle the basis for emission limit values designed to prevent and, where that is not practicable, generally to reduce emissions and the impact on the environment as a whole." For example for blast furnaces, the techniques minimizing solid waste/by-products are considered as BAT. Description and list of others BAT techniques could be found in [32].

In Europe, about 5000 kt of blast furnace sludge is produced per year. Typically, blast furnace sludge (dry solid) contain 21 - 32 wt.% of iron, 15 – 35 wt.% of carbon, 1.0 - 3.2 wt.% of zinc, and 0.3 – 1.2 wt.% of lead [33,34] and PAHs which included the blast furnace sludge in the category "N". For example blast furnace sludge sample studied by Kursa et al. [10] contains the following amounts of metals: zinc 0.52 wt.%, lead 0.13 wt.%, iron 35.3 wt.%, and cadmium 0.015 wt.%.

A hydrocyclone (see Figure 2) could be used for separation and recycling part of the blast furnace sludge and thus to allow for separation of specific size fractions with specific chemical composition. A hydrocyclone is a device for classifying, separating or sorting particles in a liquid suspension based on the ratio of their centripetal force to fluid resistance. The feed is introduced under pressure through the tangential entry at a high speed. The motion of feed, mix of media and material particles form centrifugal force field [35].

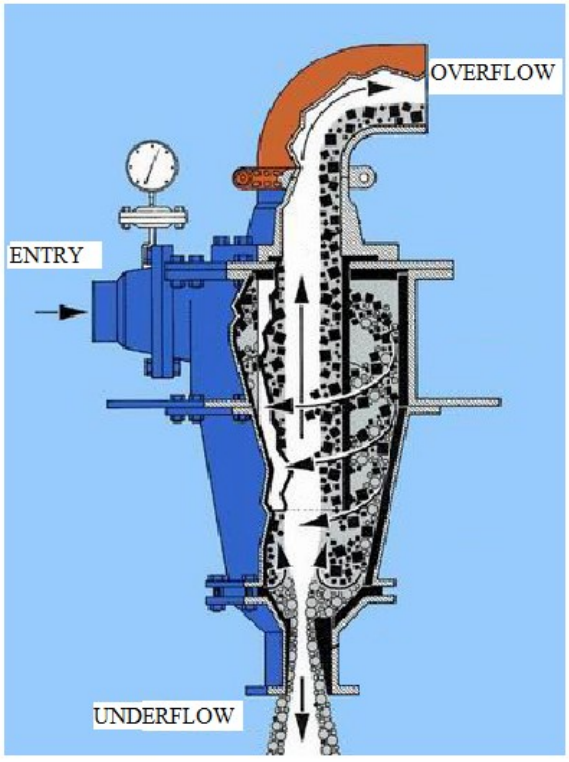

Figure 2: Hydrocyclone scheme [38].

Larger and heavier particles come to the hydrocyclone walls due to the centrifugal force and then go to the adjutage in the bottom part (underflow). Water that contains smaller and lighter particles flows to the upper part. The method uses the fact that, the amounts of metals are dependent on surface areas of dust particles. The finest particles have a large surface area and thus the highest amount of metals is captured on them. These particles with metals adsorbed are carried by stream and separated as fine fraction (overflow) [25,26,36,37].

In the work of Hlavatá [30] the separation in the hydrocyclone was studied and a large separation effect for both Zn (yield 80% in waste) and Pb (yield 70 % in waste) at low iron loss was observed. In the underflow fraction the metal content (undesirable metals as Zn, Pb, Cd, etc.) is very low, thus this material could be used as a secondary raw material. Materials with zinc content <1% could be processed into pellets and sintered in the agglomeration process [30]. This separation method may help to significantly reduce the amount of the landfilled materials and also to separate some hazardous components.

2.1.4 Steel Sludges

Steel is an alloy of iron, carbon and other metals (Mn, Si, S, etc.) that is widely used in construction and other applications because of its hardness and tensile strength. Manufacturing of steel is a refining process, which consists of reducing carbon and other elements content by the oxidation. The air, oxygen or iron oxides are used for the oxidation. Simultaneously chemical composition of steel and its structure are modified. Steel is mostly being manufactured in an oxygen converter, tandem furnace or an electric arc furnace. During the process fine grained sludges and dusts originate and may be potentially released into the environment [9].

According to its chemical composition steel could be divided into alloy and unalloyed steel. Unalloyed steel (carbon steel) is an iron alloy with carbon which usually contains accompanying elements (Mn, Si, P, S) without further additives, therefore the properties of the alloy is determined by carbon content only. Alloy steel contains other additives which improve its mechanical properties. The most common alloyants include Mn, Ni, Cr, Mo, V, Si, and B. The following elements are less common alloyants Al, Co, Cu, Ce, Nb, Ti, W, Sn, Zn, Pb, and Zr [25].

Tandem furnace sludge

Steelmaking in tandem furnaces is based on using enthalpy and reaction enthalpy of carbon dioxide to firstly preheat the solid and then the liquid feed. Iron refining with low phosphorus content is achieved by blowing oxygen onto the surface of the liquid metal. Tandem furnaces are two hearts furnaces, which use the heat of combustion products in one heart for heating the feed in the other heart [25]. The scheme of a tandem furnace is shown in Figure 3.

Generally, tandem furnace sludge contains about 60% of iron. Zinc and lead content depend on fabricated steel waste composition (0.8 – 13% zinc, 0.2 – 3% lead) [39]. Amounts and compositions are variable during the melting. The initial values of solid emissions are between 30 and 50 g/m^3, but at the end of the melting process the values are only between 5 and 10 g/m^3. Combustion products are subsequently cleaned in wet separators. Tandem furnace sludge could not be recycled due to high amounts of lead and zinc, but it is landfilled as a hazardous waste [9].

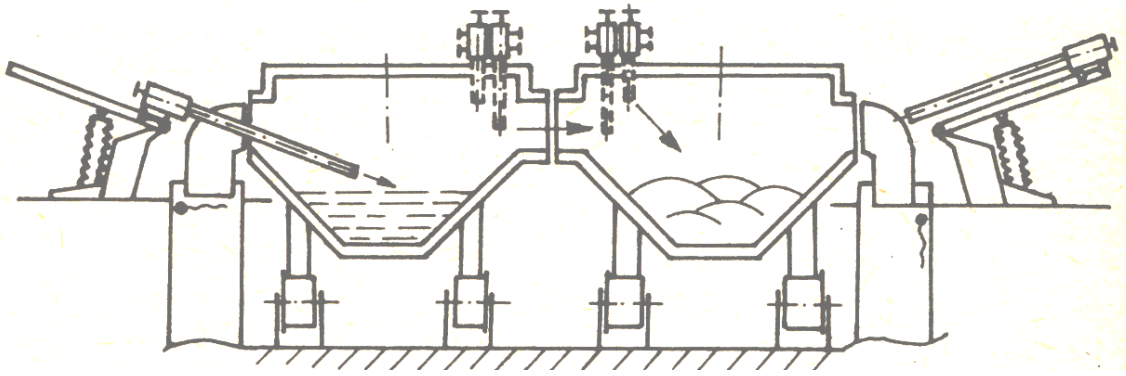

Figure 3: Scheme of tandem furnace [25].

Oxygen converter sludge

In the oxygen converter the bulk of the steel is produced. The essence of steel production in oxygen converters is injecting pure oxygen (min. 98.5 vol.%) into the molten pig iron, which may contain 0.1 – 0.2% of phosphorus). In the oxygen converter it is possible to produce iron with a greater range of chemical composition [25]. Oxygen converter sludge contains about 60 wt.% of total iron [40] and its production could be recycled in the agglomeration. Agglomerate is returned to the oxygen converter and the rest of the sludge is landfilled [9]. Two types of oxygen converter with sideway and upper blowing of oxygen are shown in Figure 4.

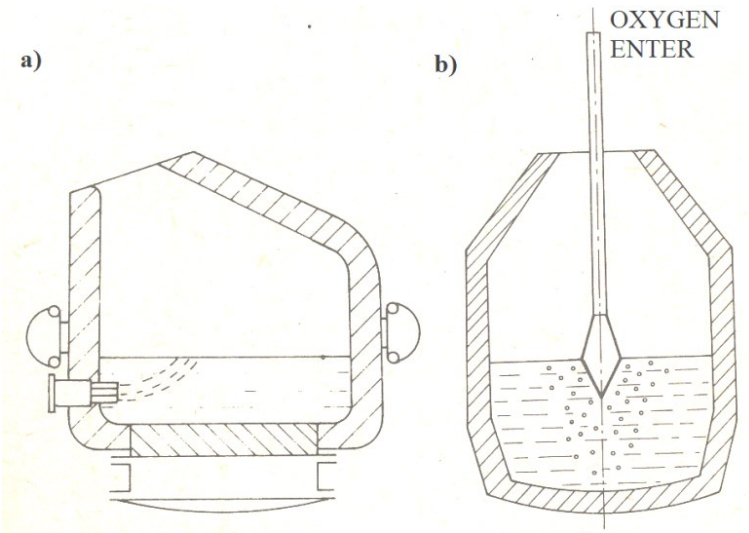

Figure 4: Scheme of oxygen converter with sideways blowing of oxygen (a) and with upper blowing of oxygen (b) [25].

Based on the previous information it is obvious that pyrometallurgy has a huge potential to significantly contribute to environmental pollution caused by gaseous and particulate emissions, including the nanoparticulates. Therefore, proper strategies are highly needed to precisely monitor and control these emissions to have a possibility to modify the capturing systems which are currently in use to be able to separate the nano-fractions as well and do not let them enter the atmospheric environment and thus contribute to the impairment of air quality in the vicinity of these stationary sources. And also to develop suitable techniques for recycling the largest amount of the generated wastes or storage technology and thus eliminated the transfer of potentially hazardous metals to the environment from landfills.

2.2 ROAD TRAFFIC

Road transport is a transport of passengers or goods on roads. The history of road transportation goes back far into the past where the first means of transport were horses, oxen or even humans carrying goods. Nowadays, a road network is spreading and according to European vehicle market statistics [41] in 2010, there were about 1 billion registered cars and trucks on the roads worldwide. However by 2030, it is expected that the number will reach about 1.7 billion, with the strongest growth taking place in Asia and the Middle East [41].

Road traffic represents a significant source of the environment pollution not just in the form of gaseous emissions from combustion of fuel, which was often a subject of various research studies. Nevertheless a big issue is also release of particulate emissions from non-combustion processes. Emissions from the combustion processes have been studied abundantly and the general public is also interested in this issue. In European Union the emission limits for light-duty vehicles is estimated by Euro V and Euro VI legislative. The exact definition of the Standards could be found in [42,43].

According to Kittelson [44] diesel exhaust particles consist mainly of highly agglomerated solid carbonaceous material and ash, volatile organic and sulfur compounds, and metals as well. Most of the particle number emitted by engines is in the nanoparticles range ($D < 50$ nm), while the most of the mass is in the accumulation mode ($50 \text{ nm} < D < 100$ nm). Kittelson [44] estimated that nanoparticles are typically hydrocarbons or sulfate and form by nucleation during dilution and cooling of the exhaust, while accumulation mode particles are mainly carbonaceous soot agglomerates directly from combustion. Emissions standards on diesel engines have led to dramatic reductions in particle mass emitted [44].

The United States Environmental Protection Agency (U.S. EPA) has created standards for fine particles in the atmosphere [45]. These standards would maintain allowed levels of 50 $\mu g/m^3$ annual average concentration of PM_{10} (particles smaller than 10 μm aerodynamic diameter) and add an annual average standard of 15 $\mu g/m^3$ of the fine particles (particles smaller than 2.5 μm aerodynamic diameter) [45]. However the finest particle fractions are not affected by gravitational forces and therefore their mass is not the best parameter how to express the quantity of the released particles, because the finest fraction presents the highest risk to the environment and health due to their capability of translocation through biomembranes.

Numerous studies (e.g. Dockery et al. [46] or Pope et al. [47]) have shown an association between adverse health effects and the concentration of the finest particles suspended in the atmosphere. Particles smaller than PM_{10} are labeled as thoracic fraction, because they can penetrate through the upper respiratory tract (head airways) and enter the thoracic airways (lower respiratory tract). Particles smaller than 4 μm are known as respirable fraction, which penetrate deep into the lungs, i.e. the alveoli [48].

On the other hand, emissions from non-combustion processes are still paid less attention to. These non-exhaust processes could be divided into the brake wear, tire wear, hardware wear, road surface wear, and traffic signs wear [49]. Due to the extensive experience and instrumentation capabilities of Nanotechnology Centre VŠB-TUO the part of this study is focused only on the automotive brake pads, their wear and characterization of metal-based emissions from this mobile source of pollution in comparison with pyrometallurgy.

2.2.1 Braking System

Braking systems are one of the most important parts of vehicles in terms of their safe operation. Braking system must provide service, emergency, parking, and retarder braking. Brakes could be divided based on friction parts of brakes into the two following types: drum and disc brakes [50].

In 20th century the drum brakes were widely used in automobiles. The advantage of the drum brake is the location of the whole device inside the brake drum, and thus it is protected against the adverse effects of impurities from the surroundings. Also the durability of the linings in this system is longer [51]. The most important parts of drum brakes are brake drum, brake shoes, spacer devices, return springs and the backing plate (see the scheme in Figure 5).

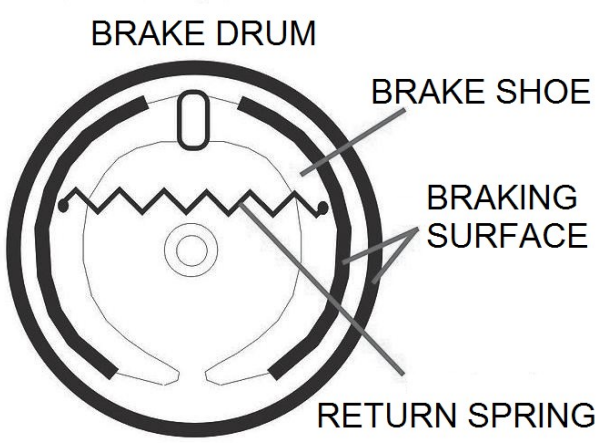

Figure 5: Scheme of drum brake [51].

However, the disc brakes (see the scheme in Figure 6) are more effective, and were combined with the drum brakes or nowadays they are more often used separately in passenger cars. Disc brakes are significantly lighter, more effective, and their cooling is easier and more effective, yet the wear rate is higher [51]. During braking, the friction surfaces of the brake pads are pressed against the surface of the rotating disc. The design of the disc brakes consists of a disc (grey cast iron or ceramic rotor), brake caliper, brake cylinder, and a couple of brake pads [51]. The automotive brake system works as follows: First of all the driver presses the brake pedal; the brake fluid from the cylinder creates hydraulic pressure and pushes the pistons in the caliper forward. Then the brake pad inside the caliper will get in contact with the disc producing friction forces, which convert kinetic energy of a vehicle mostly into heat generated by the friction between friction material and the disc [52].

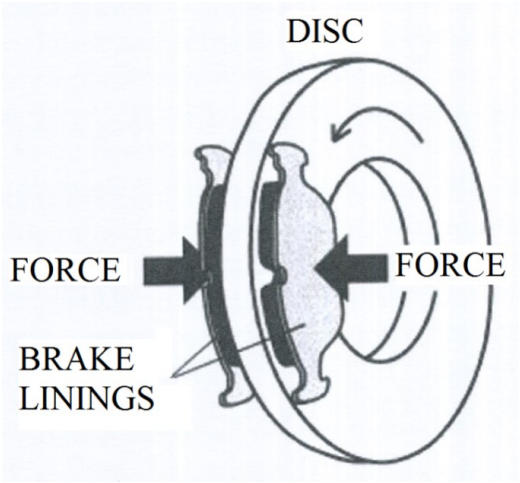

Figure 6: Scheme of a disc brake [51].

The science and engineering of interacting surfaces in relative motion is called Tribology and includes the study and application of the principles of friction, lubrication and wear. Tribology is a multidiscipline science field involving physical and chemical aspects of surface interaction, mechanics of this operation, technical and technological consequences of these processes [53]. The tribological processes between composite for brake linings and friction surface occur only in limited area, about 15 – 20% of the total area, so called contact plateaus [54].

Nowadays emphasis is also placed on the comfort properties of the brakes (reduction of noise, vibrations, and regulation of harshness) not only to the basic properties (friction performance, stability of friction coefficient with different temperatures, service life etc.) [51]. The design and development of friction materials is a very challenging discipline, because the influence of each component used is not easy to be predicted precisely due to very specific conditions which occur during braking (high temperatures and pressures). Disc brakes of passenger cars generally work with the pressures of about 1MPa and drum brakes with pressures about 0.2 MPa [51,55,56]. The temperature during friction processes could reach 700°C on the surface, but the maximum temperature of small asperities could exceed 1,000°C at short time intervals. Formed friction layer is depleted of organic matter, on the other hand is enriched with inorganic constituents (metal particles). Higher temperatures cause the oxidation of metals in the surface layer and thermal degradation of carbonaceous components [54,57-59].

Frictional contact between brake system components during a forced deceleration takes off very tiny amount of the brake material as wear debris according to Ostermeyer and

Müller [60] who presented a friction theory only in a very small area of brake system with one SiO_2 particle for simplicity (see Figure 7).

Figures 7 a-d show the growing of this particle. The contact between the metallic brake disc and the friction composite will unhinge wear particles out of the brake pad. A part of the wear is stuck on the brake disc outside the brake pad area. These particles will reach the contact zone with next revolution again. When the SiO_2 particle reaches surface, the wear flow will be disturbed (Figure 7b). The hard SiO_2 particle nearly show no wear, but due to the wear of the surrounding area the particle will be pressed more and more into the matrix during the braking process and the temperature grows. Figures 7 c-d show the creation of the thin SiO_2 layer resulting from a high temperature and pressure achieved. The destruction of the layer and its release into the environment due to mechanical and thermal loads are shown in Figures 7 e-f [60].

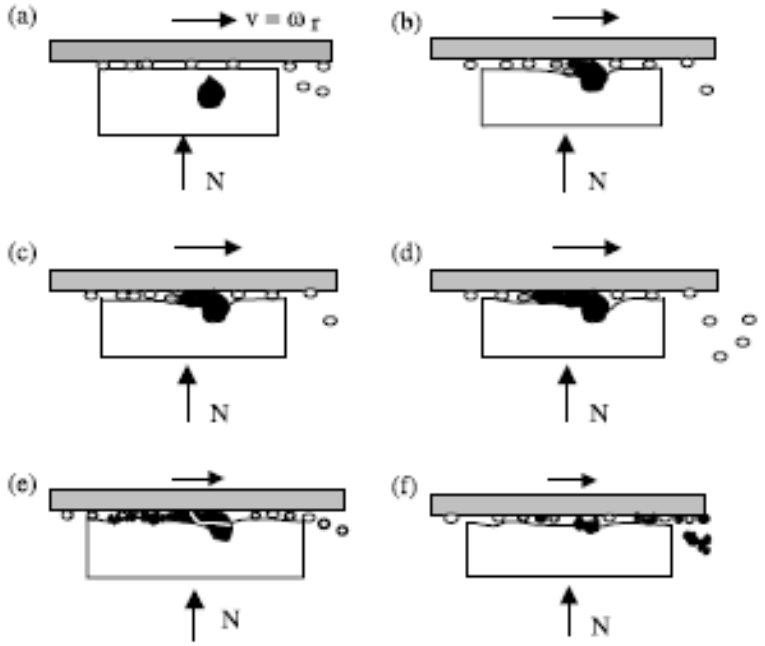

Figure 7: Demonstration of abrasive wear mechanism of SiO_2 particle (black), retrieved from [60].

2.2.2 Friction Composites for Automotive Brake Linings

Brakes belong to critical elements of traffic safety. Besides their construction, the formulation of friction composites is important parameter as well and plays a significant role in their proper function [51]. Automotive friction composites are multicomponent materials formulated of more than 10 components, whereas manufacturers could use up to 2,000 different components for the production of their mixtures. Each component has unique physical and chemical properties, therefore influences its specific function in a final brake pad. The information about formulation and amounts of each component are considered proprietary by manufacturers and is therefore rarely fully disclosed. However, it is known that in general regular automotive brake pads contain five basic types of components (see Table 1) [49].

Friction composites for automotive brake linings were mainly classified into three categories: semi-metallic, non-asbestos organic (NAO), and ceramic [61]. Semi-metallic friction materials usually contain large amount of metals/metal compounds which could reach up to 80 wt.%. The most abundant are steel, copper and brass chips, iron and copper powder, and other metal oxides and sulphides [62]. NAO friction materials include low-metallic (5 – 15 wt.% of metals) and non-metallic composites according to Sai Balaji and Kalaichelvan [61]. Recently, a kind of new ceramic friction materials consists of ceramic fibers and fillers [61].

Table 1: Types of compounds used in brake pad formulations [49].

Name	Properties	Compounds	Amounts
Fibers	Provide mechanical strength	various metals, carbon, glass, Kevlar fibre	6 – 35%
Abrasives	Increase friction, cleanliness between surfaces in contact	aluminium oxide, iron oxides, quartz, zircon	~ 10%
Lubricants	Stabilization of frictional properties in high temperatures	graphite, metal sulphides	5 – 29%
Fillers	Improve manufacturability	barite, calcite, mica	15 – 70%
Binders	Maintaining of structural integrity under mechanical and thermal stress	phenolic resin	20 – 40%

2.2.3 Brake Wear Debris

As mentioned above (see chapter 2.2.2), the frictional contact between brake system components during forced deceleration creates wear debris after each application of a brake. Due to this fact, wear of brakes is the important source of particulate matter emissions into the environment, especially in urban areas with heavy traffic.

The data obtained by Querol [63] from seven selected European regions showed that exhaust and non-exhaust sources contributed to the total traffic particulate matter (PM) emissions almost equally [63]. Exhaust and abrasions sources contribute to the PM emissions by 35-55 wt.% of PM_{10} and 40-60 wt.% of $PM_{2.5}$. Heavy industry in the studied areas contributes to the PM emissions only by 15-25 wt.% of PM_{10} and 20 wt.% of $PM_{2.5}$ [63]. Sanders et al. [64] revealed that approximately 50 wt.% of the wear debris became airborne within all the vehicles tested, which includes low-metallic, semi-metallic and NAO lining materials. Further, 35% of the brake pad mass loss was emitted as airborne particles; 86 wt.% of the airborne particles contribute to the PM_{10} while 63 wt.% to the $PM_{2.5}$. The average size of the emitted particles was estimated to be of 6 μm in diameter, with particle size maxima at 0.5 and 2 μm, tails extending to sizes < 10 μm [64]. The differences in size distribution between the different linings tested were observed to be small and not considered to be significant. Garg et al. estimated that the total brake wear for a small passenger car ranges from 3.2 – 8.8 mg/km based on the tested brake pad [65]. Thus, a relatively huge amounts of brake wear debris are generated and released to the environment, but no legislative exist to control these wear debris.

The emitted particles may be according to their size released as airborne or nonairborne fraction. The airborne fraction is released to the air due to their small size and therefore the minimum gravitational settling could be spread for long distances from a source and remain suspended in the air for long periods of time. The airborne fraction may contain nano-sized particles based on carbon, iron, copper and antimony, based on the brake formulation and also a driving style of each driver. The size of released nano-sized particles may be 20 nm in diameter and with concentrations as high as several millions of particles per cubic centimeter [66]. It is well known that nano-sized particles pose a potential risk to the environment and also to the human health, due to their small size they could penetrate through the cell membranes and may subsequently cause oxidative stress and inflammation which might finally cause mutations leading to a cancer [67-69].

The emitted nonairborne fraction may settle on road surfaces, vicinity of roads, and brake hardware. These particles are considered to be relatively large, but their surface may be "covered" with attached nano-sized particles, which can potentially be released [70]. Afterwards, they can enter the soil, ground waters, biogeochemical cycles, and enter the food chain subsequently. Nanosized particles could pose a higher risk than micro-sized particles, due to their larger surface area and a considerably higher reactivity with biomolecules [67].

As was mentioned above, there are many components used in brake pad formulations (see Chapter 2.2.3). Some of the raw materials which are still in use might be potentially hazardous and could cause various adverse effects, such as pulmonary toxicity and mutagenicity [71,72]. Toxicity and mutagenicity are mainly caused due to the metal based and organic compounds present in the brake pad formulation (e.g. copper and antimony components, phenolic resin).

Earlier asbestos was widely used in brake pad formulations, but it was found that all forms of asbestos are carcinogenic, thus phasing-out of asbestos lead to the development of safer/eco-friendlier alternatives of the brakes pads [64,65]. However, the selection of good and harmless raw material is not a sufficient solution, because the high temperatures and pressures could change the initial components and create hazardous compounds to be released.

For example, antimony pentoxide (Sb_2O_5) and Laves Sb_2Fe phase were formed from antimony trisluphide (Sb_2S_3) during a simulation of a braking process [73,74]. According to the International Agency for Research on Cancer (IARC), Sb_2S_3 is not classified as a carcinogen to humans, but the antimony oxides are classified as potentially carcinogenic. The toxicity of antimony compounds depends on their solubility and their valence, where $Sb^{(V)}$ is less toxic than $Sb^{(III)}$ [72].

Copper is one of the most common friction modifiers, and is used for its ability to mitigate/eliminate thermal fade of brakes pads as well as improve the thermal conductivity [75]. Copper has been used in brake pad materials for decades and its usage in automotive brake pads has increased by almost 40% in the past few years, which has had a negative impact on the environment [76]. Brake wear emissions with size $PM_{2.5-10}$ may be responsible for 50 – 75% of the total copper emissions to air in Western Europe [77]. Although the brake wear debris is released onto the road surfaces or into the air and it may end up in the water systems eventually. In addition copper can be toxic to the aquatic organisms, e.g. copper harms salmon's sense of smell, making them vulnerable to predators and unable to find their spawning streams [78]. It is an inherent property of copper that it is antimicrobial; it kills

microbes and wear of brakes containing copper and its compounds has to be paid attention to [79].

In March 2010, Washington State passed the SENATE BILL 6557 (Brake Friction Material-Restriction on Use). This document restricts the use and content of hazardous constituents and their compounds in the brake friction material. Therefore the content of antimony, copper, nickel, and zinc and their compounds in brake pads available in Washington State will be monitored. Furthermore, a restriction of less than 5 and 0.5 wt.% of copper amount in brake pads will be effective by January 1, 2021 and January 1, 2023, respectively [80]. Some other American Sates consider similar laws (state of California, New York) [81-83]. In view of the regulations, the developing of environmentally friendly (eco-friendly) brake pads is important. The elimination of copper and other potentially hazardous materials in brake pad formulation as well as the reduction of the hazardous wear is the goal.

3. MOTIVATION

Every year 45 kt of dusts and sludges from blast furnaces and agglomerations and 100 kt dusts and sludges from steel industry is produced in North Moravian region (Czech Republic), but only 70% and 60%, respectively is being further processed [84]. A relatively large portion cannot be reused and therefore it is landfilled. Three localities are found in the area of Ostrava city (Odval a.s. Vítkovice, Arcellor Mittal, and Třinecké železárny a.s.). According to Botula and Řepka [84] in the area of Třinecké železárny landfill oxygen converter sludges were reused in the manufactory of cements. Now about ¼ of the initial amounts of sludges remains in the area [84]. Other two localities were a subject to drilling research and this research has shown that the materials contain the highest amounts (60 - 90%) of the finest size fractions (<0.02 mm) of particles [84]. Another issue is represented by the mixtures of the sludges in the landfills, which are mutually contaminated and thus their further recycling is impossible.

However, an accurate risk assessment on contaminated landfills should consider the risk of metals transfer both to the groundwater and to the above ground vegetation [85]. This transfer will be closely dependent on the metal content, chemical speciation and particle size, but also on the soil characteristics and plants species [19,20]. The removal of metallurgical landfills is clearly unrealistic, due to technical and financial considerations. One way to minimize the metal hazards in the environment is recycling such a quantity of sludge as is possible, however, this is connected to an increase in the production costs [10]. The other way is to control and stabilize the existing landfills.

On the other hand, the brake wear is not stored anywhere and is being emitted by mobile sources. Wear debris is released into the air environment in the case of the airborne fraction or settled onto the road surfaces, brake hardware and vicinity of the roads in case of the nonairborne fraction. Some of the raw materials used might be potentially hazardous. However, there are newly formed particulates with different chemistry as compared to original bulk materials released during the friction processes accompanied with complex physico-chemical interactions on the surface [66].

Different approaches are adopted when addressing the impact of braking on the environment, but a complex study of these impacts is still missing. The amounts of the particulate emissions from non-exhaust process are significant, e.g. brake and tire wear correspond to 19% (5.8 kt per year) of the national total $PM_{2.5}$ in Finland [86]. The study of the brake wear impacts is also made more difficult due to the determination of the origin of

the released particles. According to some researchers, the antimony is the main element of wear of brake linings [87,88], but according others barium is the best tracer of particles released from brakes [89]. Although the information about brake wear tracers is not complex yet, the following possible tracers are used in studies: Cu/Sb ratio [87], Cu, Sb, and Mo correlation [90], and Ba [91]. Copper and antimony is now used less than barium in brake pad formulations, thus barium/barite is possibly the best brake wear tracer [92].

Some studies tried to determine the impact of the brake wear on the plants, because plants could be used as a good biomarker of automotive-pollution, e.g. Verma et al. found changes in foliar configuration of plants *Ficus religiosa L.* and *Thevetia nerifolia L.* [93]. Naszradi et al. [94] determined that content of zinc, lead and cadmium increases in meadow herbs with a closer distance from the motorway (*Arrhenatherum elatius L., Anthoxanthum odoratum L., Bromus erectus L., Bromus mollis L., Lolium perenne and Agropyron repens L.*). Some studies try to determine the impact on the aquatic animals, e.g. salmon. Sandhal et al. found that copper-containing stormwater has potential to cause chemosensory deprivation and increase predation mortality in exposed salmon [95].

Limited information is available about the impact on the health of humans. It is known that the exposure to fine PM air pollutants ($PM_{2.5}$) affects the heart rate variability parameters, and the levels of serum proteins associated with inflammation, homeostasis and thrombosis. Riediker et al. [96] studied nine healthy young non-smoking male troopers and found out that $PM_{2.5}$ originating from speed-changing traffic including engine and brake emissions modulates the autonomic control of the heart rhythm, increases the frequency of premature supraventricular beats and elicits proinflammatory and pro-thrombotic responses in healthy young men [96]. It cannot be concluded, that the issue results from the influence of brake wear solely, but from traffic emissions in general.

It is possible to capture the brake wear debris by laboratory simulations of various braking scenarios using the full-scale dynamometer test, which is strictly controlled and it is clear what particles are released from the braking process only. The dynamometer test is also good for studying the mechanical properties of brake pads. Thus in the beginning it is better to characterize the brake wear debris in the isolated lab conditions for a better understanding of its complex influence on the environment.

In both cases (pyrometallurgy and road traffic) it is important to have as much information about these materials as can be obtained, e.g. possibilities of particles mobility and its characterizations on which this study is focused.

4. EXPERIMENTAL

4.1 STUDIED SAMPLES

4.1.1 Pyrometallurgical Sludges

Five samples of blast furnace and steel fine-grained sludges were studied. All sludges were collected in Czech pyrometallurgical plants. The blast furnace sludge (BF) came from Arcelor Mittal Ostrava a.s. The BF sample was further treated in hydrocyclone at Institute of Environmental Engineering VŠB- Technical University of Ostrava and two fractions were obtained, the overflow (BFO) and underflow (BFU). Steel sludges were sampled from the oxygen converter (OC) of Vítkovice a.s. and from the tandem furnace (TF) of Arcelor Mittal Ostrava a.s.

4.1.2 Automotive Brake Pads

Two model brake pads and two commercial brake pads for mid-size passenger cars (Škoda Octavia I and Ford Crown Victoria) were selected for characterization. First model brake pad is named G6C, its formulation is shown in Table 2. The other model brake pad is the Cu-free eco-friendly brake pad. The copper was replaced by nanocomposite kaolinite/TiO_2 (KATI). Its formulation is the same as the formulation of G6C where the amount of copper was replaced by the same content of KATI. The brake pad is called G6C/KATI. For comparison, two types of commercial brake pads were selected (SMP1 and SMP2). SMP1 and SMP2 are commercial low-metallic brake linings, designed for mid-size passenger cars and approved for the European Union and U.S. markets. Since these are commercial samples, their exact composition is not known.

Model Brake Pad Preparation

Model brake pads were prepared during the internship in the Center for Advanced Friction Studies (CAFS), Southern Illinois University, Carbondale, USA. All components were weighted with a tolerance of ± 0.05 g. First, the heavier components (steel fibers, iron powder and copper) were mixed for 6 minutes with the lighter components (vermiculite and

twaron) for a better blending of all the components. Subsequently, the remaining components were added and mixed for another 6 minutes.

The mixture was placed to the compression mold (Figure 8a), which was pre-heated to 175°C and the walls were sprayed with Ease Release Spray (Mann Release Technology) for a better removal from the mold after the pressing.

Table 2: Formulations of model brake pad samples.

Constituent	**Weight [%]**	**Constituent**	**Weight [%]**
Steel Fiber	10	Twaron	2
Synthetic Graphite	5	Barite	9
Synthetic Graphitic Carbon	5	Aluminium Oxide	1
Coke	15	Magnesium Oxide	3
Iron Powder	3	Stibnite	3
Vermiculite	5	Tin	3
Zircon	2	Molybdenite	1
Nitrile Rubber	5	Phenolic Resin	24
Copper*	4	**KATI****	4

* Copper is only in formulation of G6C model brake pad
** KATI composite is only in formulation of G6C/KATI model brake pad

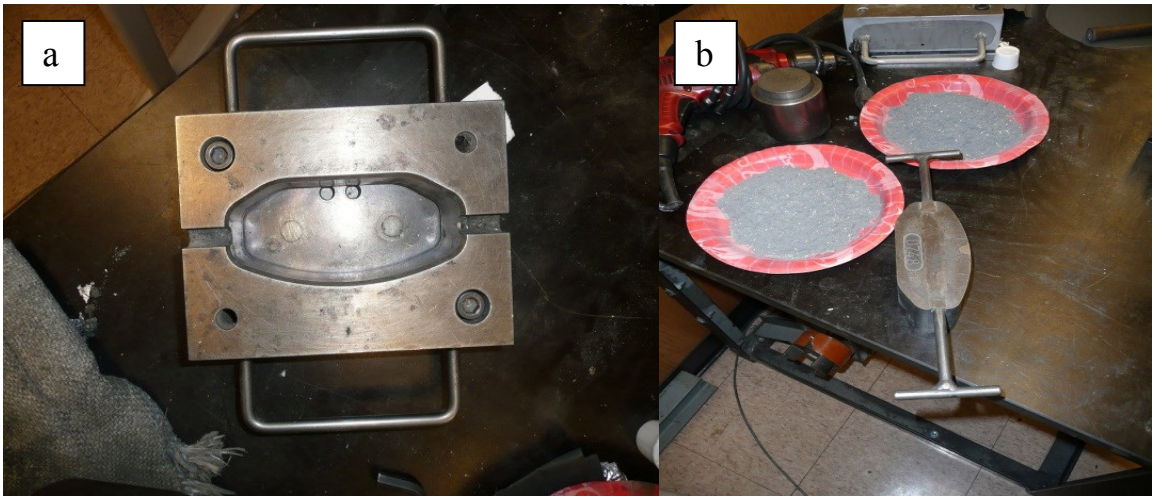

Figure 8: Empty compression mold (a), inside part of the compression mold and the composite mixtures (b).

The mixture and the required type of brake shoe were added to the compression mold. The brake shoe was painted with glue. The mold was inserted into the press for 20 minutes with a temperature of 175°C and 10,000 pounds. After pressing the friction composite was

removed and put to the kiln for 4 hours with a temperature of 180°C to stabilize the composite. The final brake pad (Figure 9) was cut off into a plane.

Figure 9: Prepared G6C brake pad.

The other model brake pad was prepared using the same procedure. This formulation could be considered as eco-friendlier. As mentioned above there is an effort to eliminate the use of copper in the brake pads formulations [75].

Nanosized TiO_2 is the most frequently studied photocatalyst which shows the most promising properties in anatase modification. Due to the fact that nanoparticles may pose risk to the environment, TiO_2 nanoparticles are anchored on the clay surfaces (e.g. vermiculite, bentonite, and kaolinite [97-101], which can prevent the nanoparticle from being released. The Nanotechnology Centre has extensive experience in the preparation and properties of the KATI composites. The KATI composite was tested in order to change the amount of copper in the brake pad formulation. The information about KATI photocatalytic properties and its preparation could be found in the paper published by Mamulová Kutláková et al. [97] and its antibacterial activity was evaluated by Dědková et al. [101]. Evaluation of the mechanical properties of the G6C/KATI brake pad is beyond the scope of this work.

Sampling of Brake Wear Debris

Brake wear debris was generated and obtained after a modified version of the AO4D brake dynamometer wear test procedure which simulates specific braking scenarios. The test consisted of instrument check, burnishing, effectiveness, fade, recovery, and two high-temperature wear tests. Similar wear test is used by manufacturers for brake pads characterization of friction linings of passenger cars. Brake dynamometer tests were performed using the Link Engineering Co. (USA) full-scale brake dynamometer model 2900

(CAFS, Southern Illinois University, Carbondale, USA) and M2800 (VŠB – Technical University of Ostrava) with an environmental chamber. Dynamometer M2800 can be seen in Figure 10.

Figure 10: Dynamometer Link M2800 (VŠB – Technical University of Ostrava) with detail of inside part.

The environmental chamber contains the entire front wheel with a disc and caliper (see the scheme in Figure 11), and it also contains a wind tunnel simulating a corresponding airflow. The chamber was cleaned before each test and the nonairborne wear debris was collected by sweeping the surfaces of a plastic bin placed at the bottom of the chamber. The controlled filtered air has a flow capacity of 25 l/min during the testing procedure. Applied braking simulation is a representation of sub-urban driving segments.

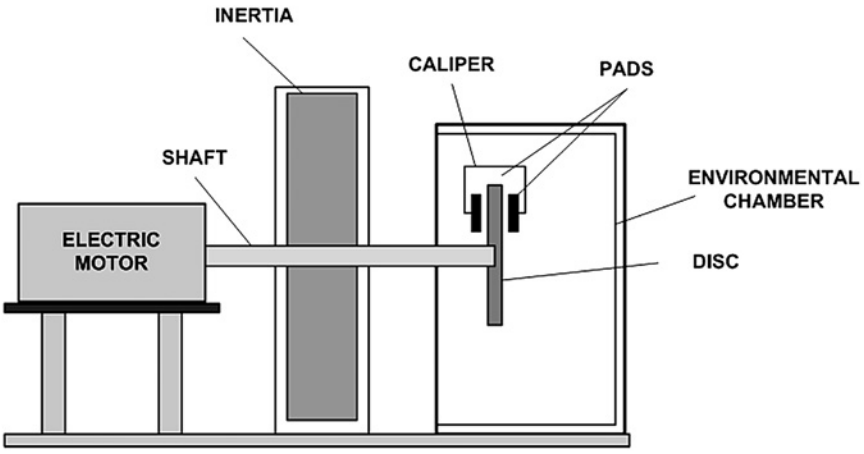

Figure 11: Scheme of the dynamometer with environmental [66].

4.2 SUSPENSION PREPARATION

In order to evaluate the release of nano-sized particles from pyrometallurgical sludges and brake wear debris into water, the suspensions were prepared. The amount of pyrometallurgical sludges available for these experiments was higher than the amount of wear debris generated and collected after dynamometer testing, thus suspensions could be prepared based on the European Standard as leachate only from studied sludges [102].

Leachates of pyrometallurgical sludges were prepared in liquid to solid ratio of 10:1 (i.e. 100 ml:10 g). All leachates were prepared with demineralized water in a bottle of inert material. Bottles with suspensions were shaken on a vertical shaker (Heidolph Reax 2, Vitrum) for 24 hours, and then the solid phase was separated through a nitrocellulose membrane filter (Pragopor, Pragochema s.r.o.) with an average pore size of 0.45 μm.

The second procedure carried out to obtain water suspensions was applied due to the small amount of the brake wear debris captured after a laboratory simulation of braking. The liquid to solid ratio was again 10:1 (i.e. 100 ml:10 g) for pyrometallurgical sludges and 100:1 for brake wear debris (i.e. 20 ml:0.2 g). Again the demineralized water and bottles of inert material were used. Suspensions were stirred for 5 minutes in an IKA® VORTEX Genius3 Mixer to assure better contact with water of the wear debris sample. The resulting mixture was further shaken for 30 minutes on a vertical shaker (Heidolph Reax 2, Vitrum) and subsequently subjected to sedimentation for 72 hours. The two phases were separated: the sediment at the bottom of the tube and the liquid phase followed. Only the liquid phase was removed for further analysis. The selected time of sedimentation allowed the submicron particles to settle [103,104] and for the larger particles to be separated. The collected liquid phase was further filtered using a 0.45 μm nitrocellulose membrane filter (Pragopor, Pragochema s.r.o.) for further analysis.

4.3 ANALYTICAL TECHNIQUES

Comprehensive characterization of the solid samples was performed by a combination of the selected analytical and microscopic techniques: infrared spectroscopy, Raman microspectroscopy, X-ray powder diffraction, scanning electron microscopy with energy dispersive X-ray detector, transmission electron microscopy and particle size analysis.

Infrared spectroscopy and Raman microspectroscopy has a tremendous potential to solve a wide variety of complex problems. Both techniques are completely complementary providing characteristic fundamental vibrations that are extensively used for the determination and identification of molecular structure [105]. The X-ray powder diffraction analysis was also used to evaluate phase analysis of initial samples. The scanning electron microscopy was used for morphology characterization and determination of the samples elemental composition and transmission electron microscopy for evaluation of the morphology and crystallinity of the finest particles present in the water suspensions prepared.

4.3.1Fourier Transform Infrared Spectroscopy (FTIR)

Mid-infrared spectra (4000 - 400 cm^{-1}) were measured by Nicolet 6700 FT-IR spectrometer (Thermo Nicolet, USA) using single reflection ATR technique with a diamond crystal. The Attenuated Total Reflectance (ATR) is a contact measurement technique that involves a crystal with a high refractive index and excellent IR transmitting properties. ATR is one of the most popular sampling techniques, because it is fast, non-destructive, requires no sample preparation and very small amount of a sample to be measured. The sampling depth of the ATR technique is approximately 2 – 15 μm (depends on a sample), is wavelength dependent, and increases with decreasing wavenumber [105].

Diamond crystal is commonly used, because it is very hard, with refractive index of 2.4. The operational wavenumber ranges for diamond are 4500 - 2500 and 1800 – 200 cm^{-1}, due to the limitation the measured spectra are shown without the range of 2500 – 1800 cm^{-1}. For further enhancements in throughput a turbo mode can be used, which is extra output for highly absorbing samples. Turbo mode is better to be used for samples, such as pyrometallurgical sludges and brake wear debris due to various components present in the samples. In Figure 10 you can see the difference between spectra measured with and without the turbo mode. Turbo mode also positively influences the noise to signal ratio.

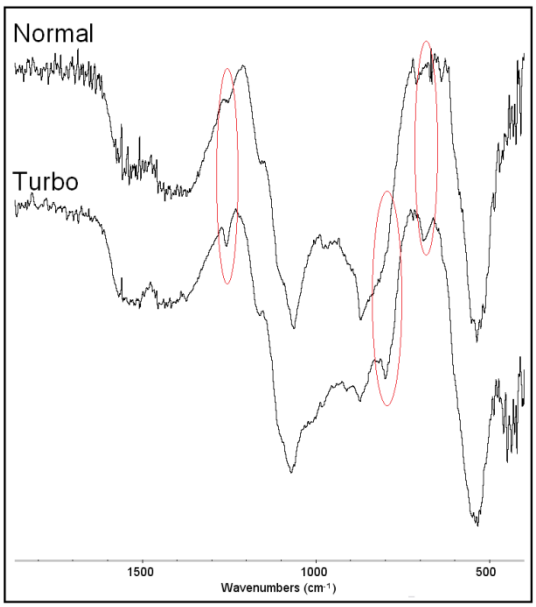

Figure 12: Comparison of FTIR spectra measured with the turbo mode (A) and without turbo mode (B). Red markings point to the newly appeared bands after measurements with turbo mode.

Infrared spectroscopy was used only for the characterization of the initial samples of pyrometallurgical sludges and collected wear debris. Since the water molecule has a very small moment of inertia on rotation, it creates very rich vibrational-rotational spectra in the vapor containing tens of thousands up to millions of absorption lines. The overlap of many of the absorption bands gives rise to very broad and intensive bands of water [106] which overlap bands of small amounts of components suspended in water. A sample dried on a glass slide could not be measured because of the thin layer of the sample and glass absorption in the mid-infrared region.

The measured spectra were modified by ATR and baseline corrections which are fully automated by OMNIC software.

4.3.2 Raman Microspectroscopy

As was mentioned above, the Raman spectroscopy is a complementary method for the sample characterization. In general, Raman spectroscopy is the best for the symmetric vibrations of non-polar groups, while IR spectroscopy is the best for the asymmetric vibrations of polar groups.

Initial samples and also dried water suspensions were measured by Smart Raman Microscopy System XploRA™ (HORIBA Jobin Yvon, France). Raman spectra were acquired with 532 nm (20 – 25 mW) excitation laser source, and 1200 gr./mm grating in the range 100

– 4000 cm^{-1}. The intensity of the laser beam was changed based on the sample signal. 0.1, 1, 10, 25, 50 or 100% of laser beam is possible to use for measurements. As the Raman system is coupled with a microscope, the powder samples were measured with a 50x objective and dried samples on the glass slides were measured with a 100x objective of the optical microscope Olympus BX41/51. Detection of Raman radiation is carried out by 1,024 pixel 1''CCD chip, which is high sensitive and air-cooled.

The advantage of Raman microspectroscopy is the possibility of measuring individual points, which is better for multicomponent samples. Raman spectroscopy also provides better information about the metal components than mid-infrared spectroscopy. However, Raman microspectroscopy is very time-consuming and fluorescence of the sample can overlay the Raman spectrum.

Initial powder samples need no further treatment prior to the Raman microanalysis. Although the arrangement of the device allows measurements of liquids, the point analysis in a specific selected particle is not possible due to the Brownian motion of particles. From this reason the suspension was dropped on a microscopic glass slide and dried in multilayers, which means that one drop was allowed to dry and then another drop was put at the same place. This procedure was applied ten times.

Measured spectra were corrected by baseline correction and in some cases by noise corrections which are fully automated by LABSPEC software.

4.3.3 X-Ray Powder Diffraction (XRPD)

Diffraction patterns of pyrometallurgical sludges were acquired under CuKα irradiation using the diffractometer Ultima IV (Rigaku). Measurements were carried out in the reflection mode with scintillation counter. The diffraction patterns of the collected brake wear debris were recorded under CoKα irradiation using the Bruker D8 Advance diffractometer (Bruker AXS) equipped with a fast position sensitive detector VÅNTEC 1. Measurements were carried out in the reflection mode, powder samples were pressed in a rotational holder. Phase composition was evaluated using database PDF-2 Release 2004 (International Centre for Diffraction Data).

The layer of the dried samples was too thin with small amount of particles to obtain relevant information from XRPD measurements that is why only the powder samples were characterized by XRPD.

4.3.4 Scanning Electron Microscopy (SEM)

SEM uses a focused beam of high-energy electrons to generate a variety of signal at the surface of solid specimens analyzed. The signals which derive from electron – sample interaction reveal information about the morphology (texture) of a sample. Interaction of an electron beam with a sample produces a variety of emissions, including X-Ray. An Energy Dispersive X-Ray detector (EDS) separates the X-Ray radiation of different elements. Therefore EDS could be used for the evaluation of the sample element composition [107].

Studied samples were analyzed using Hitachi SU6600 (operating at 0.5 - 30 kV), SEM Philips XL 30 (operating at 0.5 – 30 keV) and Quanta FEG 450(operating at 0.5 – 30 kV) all devices were equipped with EDS detectors. The suspensions were analyzed in a dried form on glass slides, prepared same as for the Raman measurements.

4.3.5 Transmission Electron Microscopy (TEM)

The transmission electron microscope operates on the same basic principles as the light microscope, but electrons are used instead of light. Electrons as a "light source" and their much lower wavelength make it possible to get resolution a thousand times better than with a light microscope [108].

TEM analyses were performed only for the prepared water suspensions. Analyses were performed using a JEOL 1200EX electron microscope at 120 kV. Suspensions were deposited onto a TEM grid with amorphous carbon film. Images are recorded on Electron Image film producing very high resolution negatives.

4.3.6 Particle size distribution

Particle size distributions of the initial pyrometallurgical sludges were evaluated on Fritsch particle sizer – Analysette 22 and particle size distributions of suspensions from pyrometallurgical sludges were obtained by Malvern Zetasizer Nano. Suspensions of brake wear debris were diluted much and a very small amount of particles in these suspensions was available, therefore information about particle size distribution of brake wear debris suspensions is missing.

5. RESULTS AND DISCUSSIONS

5.1 PYROMETALLURGICAL SLUDGES

5.1.1 Initial samples

Non-treated pyrometallurgical sludges contain variety of particles, sizes, morphology and chemistry. Chosen SEM images can be seen in Figure 13-17 to demonstrate these differences. Steel sludges OC and TF contain mostly spherical particles (Figure 13a and 14a). Spherical particles could be found also in the sample BFO (Figure 15a). However, all blast furnace sludges contain particles with various shapes, some with sharp edges (Figure 15-17a). EDS from surface areas are shown in Figure 13-17b. These particles shapes are typical for high-temperature process where the thermally unstable components start to evaporate and by a condensation process round shape particles with no sharp edges originated [109].

The elements detected by SEM-EDS in the initial sludges are shown in Table 3. Iron and zinc were found in all the samples. Iron was also found almost in all measured points in the samples. The presence of lead was confirmed in all samples except the sample TF. Cadmium was not found in any of the samples by SEM-EDS. This is probably caused by presence of very small amount of Cd, which is 0.16 wt.% for BFO sample and under 0.06 wt.% for other samples [27]. According to Kukutschová [27] amounts of Cd, Pb, and Zn were higher in steel sludges, but the hydrocyclone treatment led to a significant increase of these metals content in the BFO fraction. Also other metals as Co (BFO and BFU samples), Cr (BF and BFU samples), Ni (BFO sample), and Ti (BFU sample) were found by the EDS analysis. These metals may come from blast furnace feed or from recycled scrap iron used.

Table 3: Detected elements in the initial pyrometallurgical sludges by SEM-EDS.

	Al	C	Ca	Co	Cr	Fe	K	Mg	Mn	Na	Ni	Pb	S	Si	Ti	Zn
OC	-	x	x	-	-	x	-	x	x	x	-	x	x	x	-	x
TF	x	x	x	-	-	x	x	x	x	x	-	-	x	x	-	x
BF	x	x	x	-	x	x	x	x	x	x	-	x	x	x	-	x
BFO	x	x	x	x	-	x	x	x	x	x	x	x	x	x	-	x
BFU	x	x	x	x	x	x	-	x	-	x	-	x	x	x	x	x

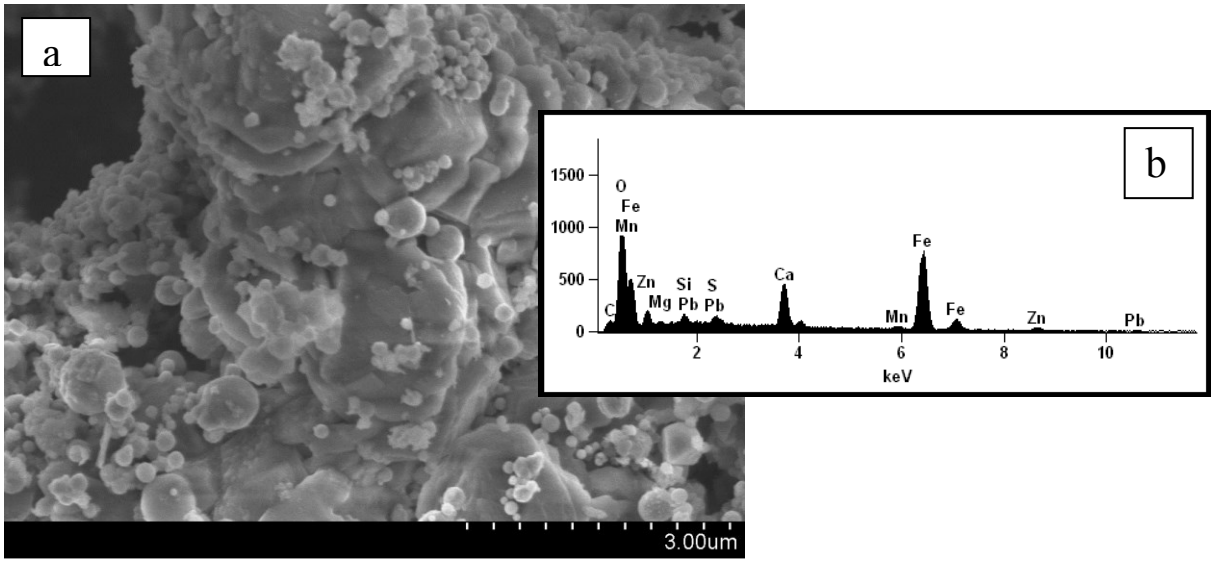

Figure 13: Chosen SEM image (a) with EDS pattern from surface area (b) of the OC sample.

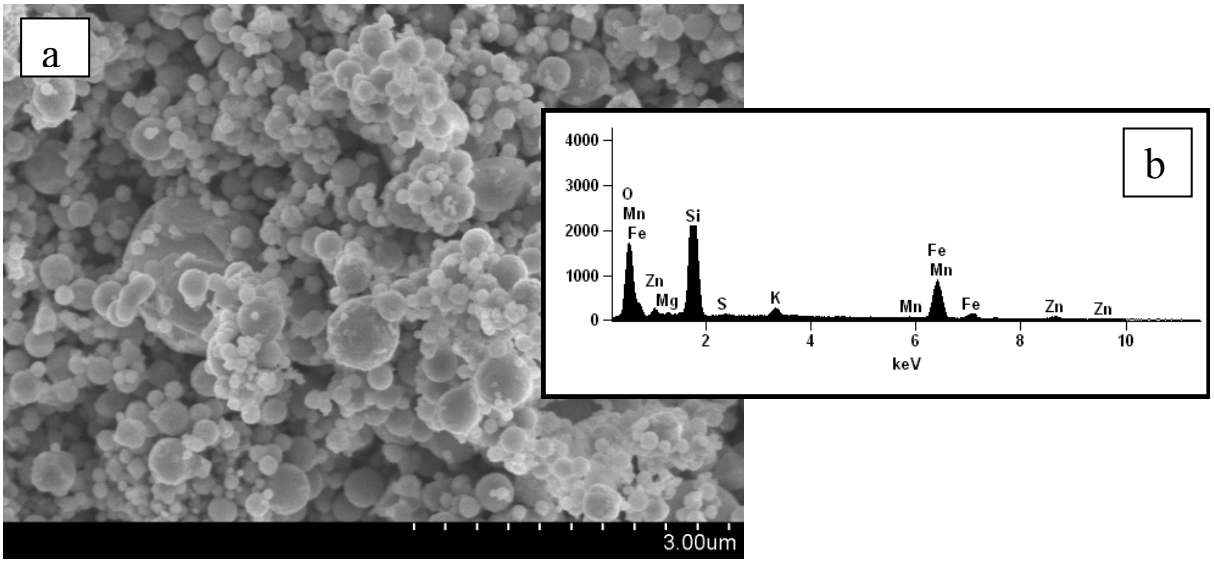

Figure 14: Chosen SEM image (a) with EDS pattern from surface area (b) of the TF sample.

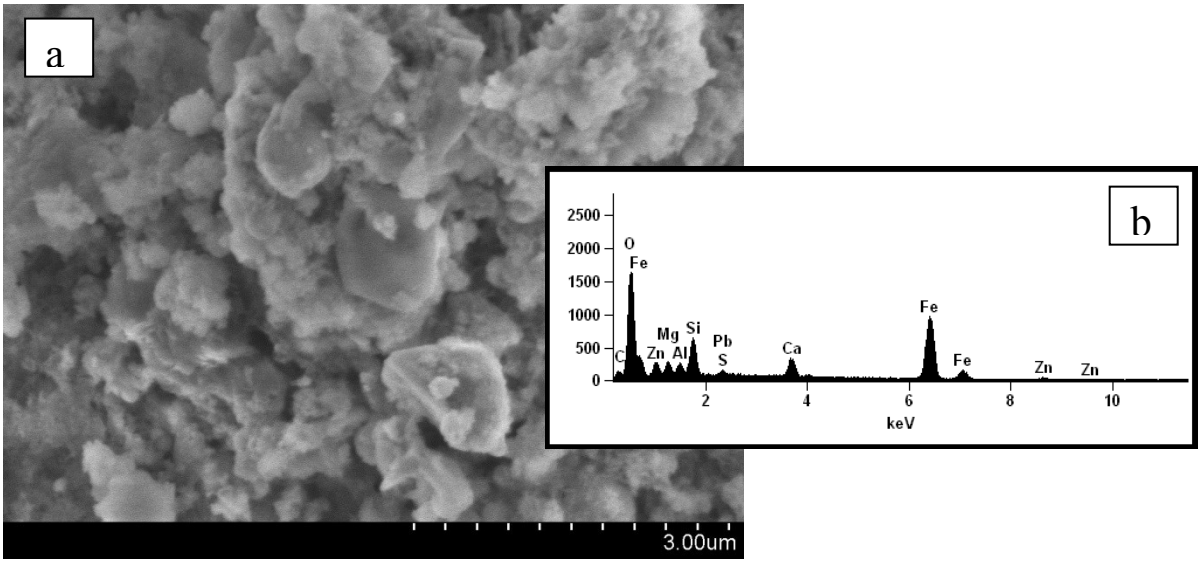

Figure 15: Chosen SEM image (a) with EDS pattern from surface area (b) of the BF sample.

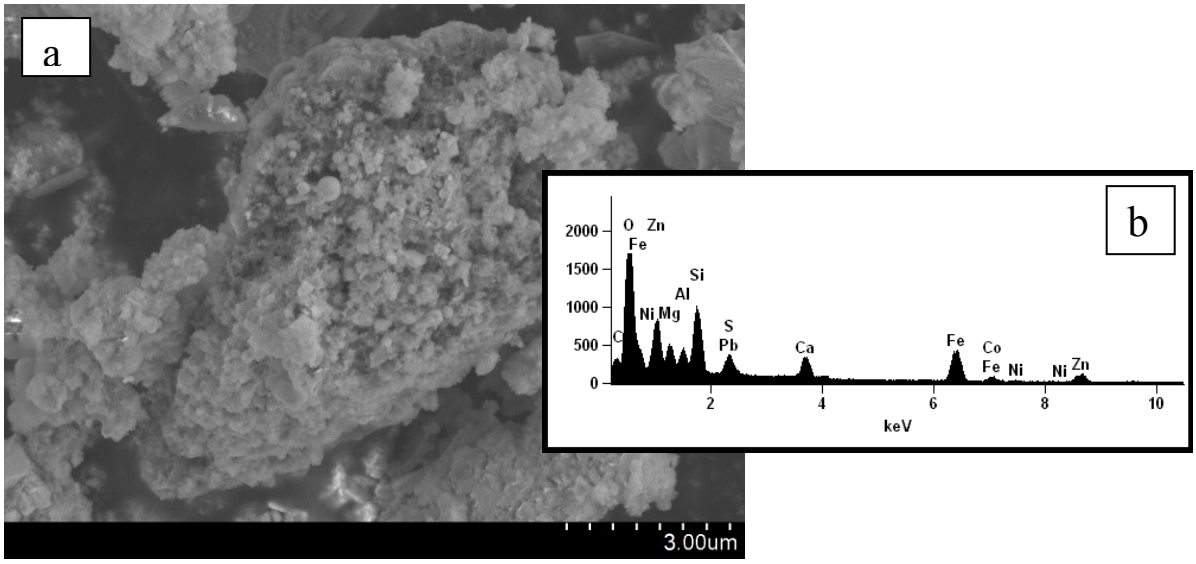

Figure 16: Chosen SEM image (a) with EDS pattern from surface area (b) of the BFO sample.

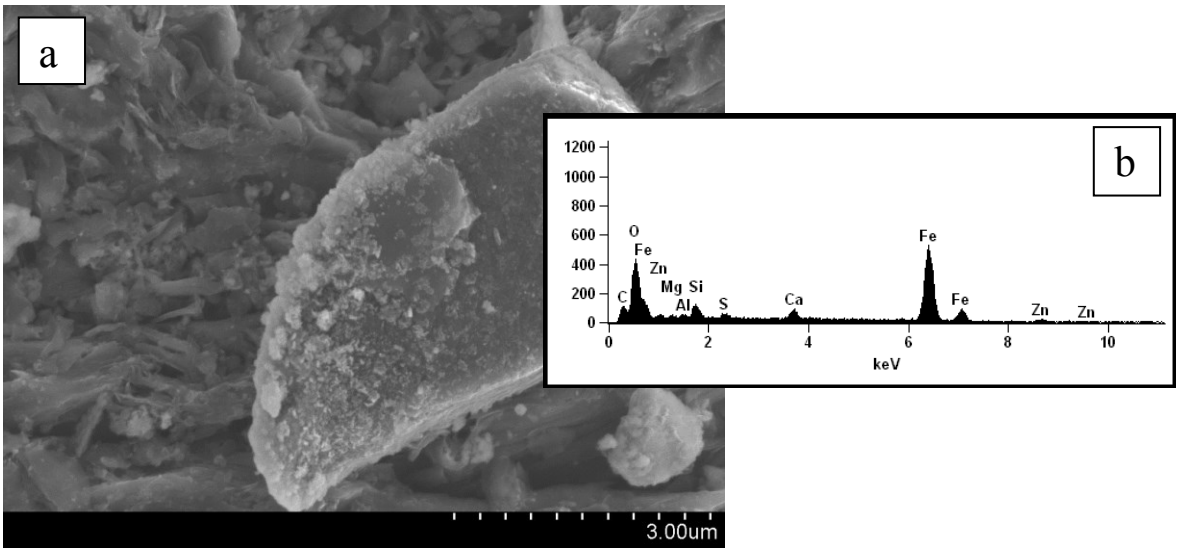

Figure 17: Chosen SEM image (a) with EDS pattern from surface area (b) of the BFU sample.

Information on exact quantities of elements from surface measured by EDS is not available, but elements content from measured points varies, for example in the sample TF was the measured range of iron content between 20 – 70 wt.%.

From SEM images it is evident that particles sizes are in wide ranges. These findings are in good accordance with granulometric measurements. Particle size analysis revealed that the steel sludges (TF and OC) are formed predominantly by fine particles with a diameter under 1.0 μm. Particle size distribution of the sample TF has bimodal character with the maxima at 1.0 μm and 15.0 μm. Particles in the sample are present in the size range 0.5 – 150.0 μm. The OC sludge is relatively different and it is formed by particles in the size range 0.7 – 450.0 μm and the particle size distribution has three maxima at 1.0, 25.0 and 250.0 μm. Sample BF

contains particles in the size range 0.8 – 400.0 µm, with only one maximum at 50 µm. Sample BFO is formed by particles in the size range 0.7 – 400.0 µm again with bimodal character with maxima at 1.0 and 15.0 µm, contrary to sample BFU contains larger particles in the size range 8.0 – 500 µm with only one maximum at 50µm. All obtained particle size distributions are shown in Appendix 1.

SEM-EDS determines only the elemental composition, thus the samples were further analyzed by spectroscopic techniques FTIR, XRPD and Raman microspectroscopy, which provide information about phase composition of a sample.

Achieved FTIR spectra are shown in Figures 18 and 19. FTIR analysis revealed the main functional groups in samples only. The spectrum of the OC sludge (Figure 18b) shows characteristic bands for carbonate groups (1793, 1409, 873 and 712 cm^{-1}), most probably for calcium carbonate [110]. Thus, very broad and intensive band with a maximum of about 3347 cm^{-1} corresponds to the O-H stretching vibration. Bending O-H vibration could be found at 1646 cm^{-1} as a weak broad band [111].

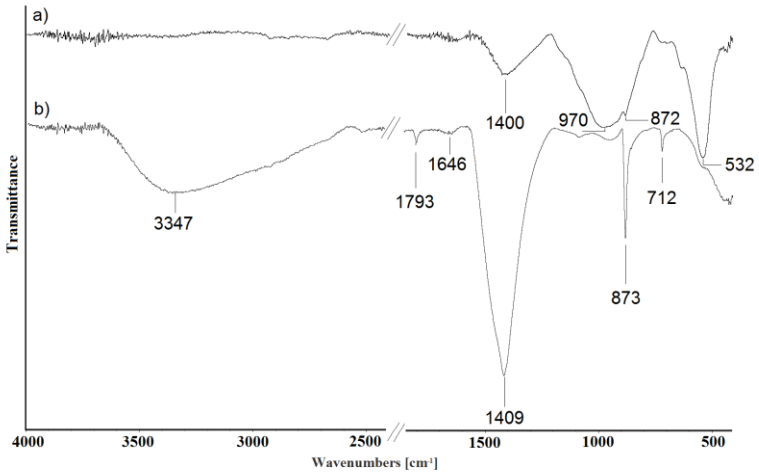

Figure 18: FTIR spectra of the steel sludges TF (a) and OC (b) with band numbers.

Other steel sludge (TF) (Figure18a) is significantly different. The broad band with the maximum of 1400 cm^{-1} could be assigned to the most intensive band of carbonates, which is in this case less intense and broad what could be caused by the amorphous character of this compound in the TF sludge. The little shoulder at 872 cm^{-1} could also be assigned to a vibration of C-O bonds in a carbonate in the OC sample this vibration was observed at 873 cm^{-1}. Broad band at 970 cm^{-1} could correspond to the stretching vibration of Si-O-Si bonds in $[SiO_4]^{4-}$ and the broad shape could be explained by its amorphous character. Very intensive band (532 cm^{-1}) corresponds to bending vibration of $[SiO_4]^{4-}$ [112]. Also it is evident that no O-H bonds are present in this sample, which corresponds to the missing broad and intensive

band about 3300 cm^{-1}. Therefore it can be stated that this sample contains no adsorbed or crystal water and also no structural hydroxyl groups.

The IR spectra of the BF and BFO samples (Figure 19 a-b) are very similar to each other. Both the spectra exhibit presence of O-H vibrations about 3350 and 1625 cm^{-1}. Very intensive band at 1004 cm^{-1} corresponds to the Si-O-Si vibrations. Only the spectrum of the BFO sample shows further a small band of Si-O at 1089 cm^{-1}, but other bands are the same for both spectra (BF and BFO) (Al,Fe)OH, (Al,Mg)OH, SiOAl, and SiOMg (874, 793, 539 and 433 cm^{-1}) [113]. All the spectra of blast furnace sludges contain band at 1420 cm^{-1}, which could be again assigned to the most intensive band of carbonate, in these cases again in amorphous form due to a broad shape of the band. Amorphous character is evident from all BFU spectra, where the broad band at 999 cm^{-1} could be classified as Si-O-Si vibration in silicates [113].

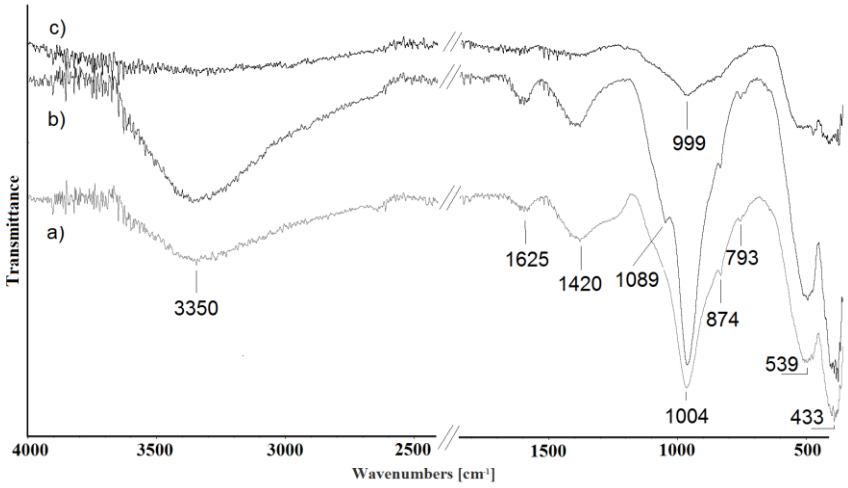

Figure 19: FTIR spectra of the blast furnace sludges BF (a), BFO (b), and BFU c) with band numbers.

The FTIR spectra of the OC, BF, and BFO samples show more crystalline character contrary to the spectra of the TF and BFU samples, which are mainly amorphous. All spectra except the spectrum of OC show presence of some silicate as the main component. The main component of the sample OC is carbonate according to the FTIR analysis. It has to be noted that due to a relatively low energy of the mid-IR light used for this analysis, no heavier elements can be detected in their bonds. Therefore, these data are not perfectly consistent with XRPD or Raman spectroscopy for instance. The Raman spectra detected in all sludges samples are shown in Figure 20. The advantage of the Raman microspectroscopy is the ability to perform the point phase analysis, which is useful for multicomponent and nonhomogeneous samples.

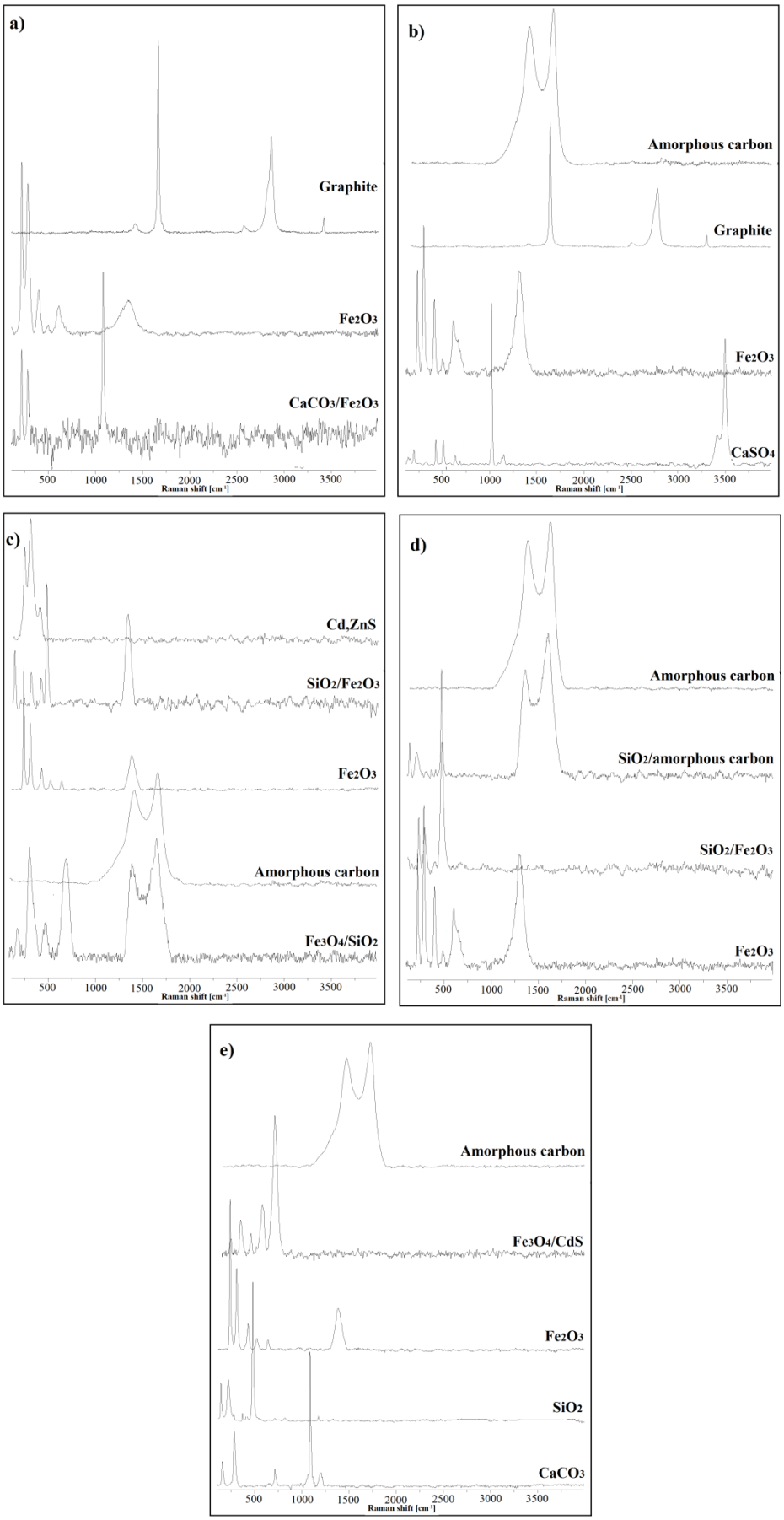

Figure 20: Raman spectra detected in the OC (a), TF (b), BF (c), BFO (d), and BFU (e) samples.

In the most measured points of the sample no spectra could be recorded. That could be caused by a fluorescence background of the sample and presence of the compounds which are Raman inactive. Except the OC sample, the amorphous carbon was found in all the remaining samples. Graphite, the other form of elemental carbon, was detected in both steel sludges (see Figure 20a and 20b) but was not detected in the blast furnace sludges. Iron oxides were detected in all the samples. Hematite (Fe_2O_3) was found in all samples and magnetite (Fe_3O_4) was found in the BF and BFU samples only. Magnetite was detected only together with other compounds, contrary to hematite which was detected solely (Figure 20a-e), but also in conjunction with SiO_2 (Figure 20c,d) and $CaCO_3$ (Figure 20a). SiO_2 was mostly present in the form of quartz, but in the BF sample also tridymite (high temperature polymorph of quartz) was found. The presence of cadmium compounds: (Cd,ZnS) and CdS in the BF and BFU samples was also observed.

XRPD also revealed graphite presence in the OC and TF samples and no presence in the BF, BFO, and BFU samples. Comparison of OC and TF diffraction patterns can be seen in Figure 21 and comparison of all blast furnace sludges is shown in Figure 22. All blast furnace sludges have relatively similar XRPD patterns, which differs only in intensities of diffractions. This is similar to the FTIR measurements because FTIR spectra of blast furnace sludges show also similarity to each other. Only quartz is missing in the BFO XRPD pattern. On the other hand XRPD analysis revealed more compound present in the samples than FTIR analysis.

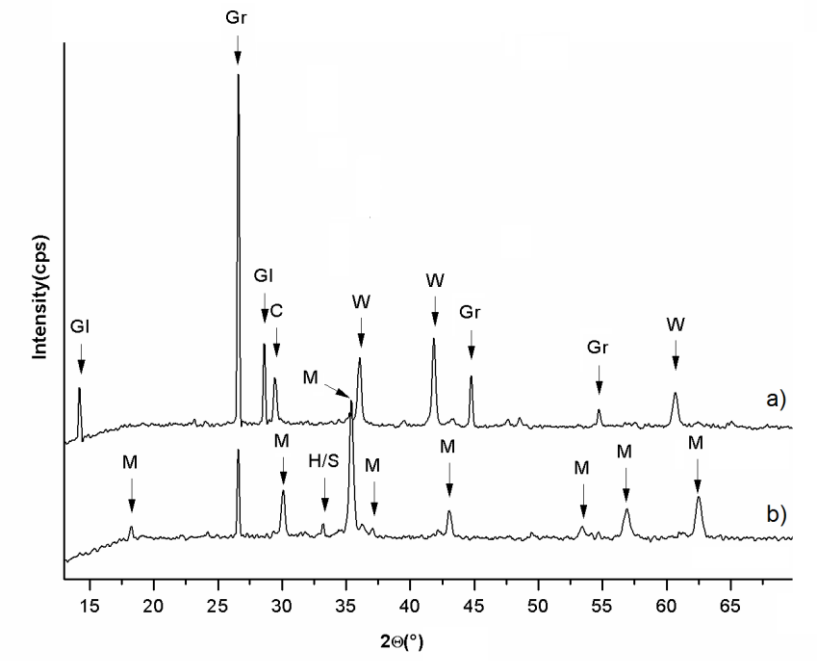

Figure 21: XRPD pattern of the OC (a) and TF (b) samples. The meaning of the symbols is as follows: C- calcite ($CaCO_3$), Gl – glauberite ($Na_2Ca(SO_4)_2$), Gr – graphite, H – hematite (Fe_2O_3), M – magnetite (Fe_3O_4), S- srebrodolskite ($Ca_2Fe_2O_5$), W – wüstite (FeO).

Although Raman microspectroscopy revealed quartz in the BFO sample, but only in conjunction with amorphous carbon or hematite, the quartz signal could have low intensity for the diffraction pattern and is probably below the detection limit of this method. XRPD patterns are in very good accordance with the Raman spectra, e.g. both methods determined calcite in the OC, BF, BFO, and BFU samples, but not in the TF sample. Also the iron oxides were determined in all samples analyzed.

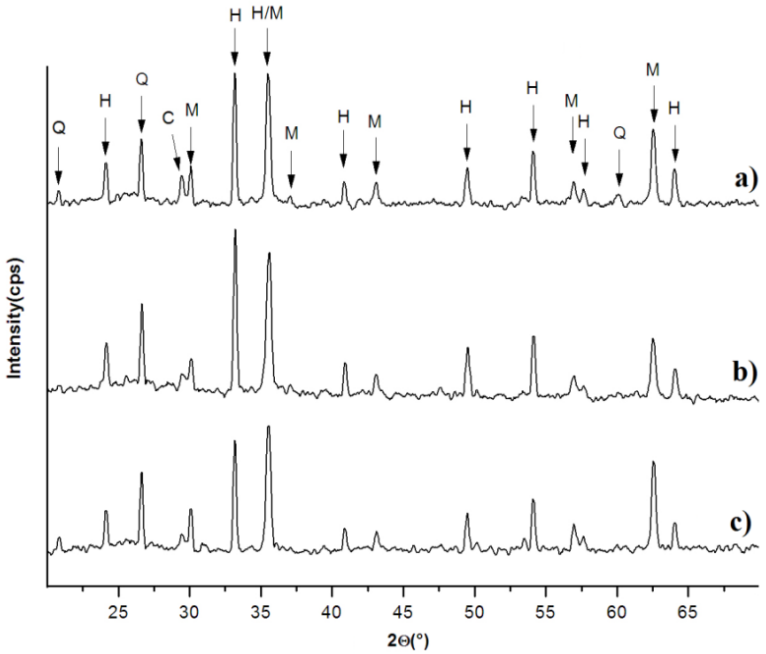

Figure 22: XRPD pattern of the BF (a), BFO (b), and BFU (c) samples. The meaning of the symbols is as follows: C – calcite ($CaCO_3$), H- hematite (Fe_2O_3), M – magnetite (Fe_3O_4), and Q – quartz (SiO_2).

5.1.2. Water Treated Pyrometallurgical Sludges – Prepared by Leaching

Water suspensions achieved after filtration according to the standard recommended procedure for preparation of a water leachate [102] contain very small particles. A bimodal character of the particle size distribution for all the suspensions was observed. Values are expressed as volume percentage and all obtained particle size distributions are shown in Appendix 1.

Suspension of the BFU sample contains the finest particles, 28.7% particles were in the size about 51 nm in diameter and 9.8% of particles were in size about 342 nm in diameter. The BFO sample contains particles with size 68 nm in diameter (36.7%) but the second maximum was higher about 615 nm (3.7%). The TF sample also contains particles with the size of 68 nm in diameter (40.7%) but its second maximum is lower at 342 nm contrary to BFO sample. This second maximum of the TF sample includes very small amount of particles, only 1.5%. The BF sample contains particles about 91 nm in diameter (26.6%) and 396 nm (5.2%). Contrary to the steel sludge, the OC includes larger particles; first maximum is 122 nm (28.6%) and the second is at 615 nm (2.8%).

Selected SEM images for all the measured samples of particles separated by filtration are shown in Figure 23 a-e. The elements detected by SEM-EDS are shown in Table 4. Following elements: Al, C, Ca, Cl, K, Mg, Na, O, S and Si are not shown in Table 4 because were detected in all samples and Table 4 would be less illustrative. Presence of the Al, Ca, K, Na, Mg and Si could be influenced by the glass slide, which was used for the analysis. However, all these elements were also found in the powder samples, thus cannot be accurately determined their origin. Another element detected in all samples was Fe. The cross in the SEM images (Figure 23 a-e) denotes the points where the iron was detected. For example in the BF sample of measured point which is shown in Figure 23c, the content of the iron was about 40 wt.%. However, in another measured point, there was only about 20 wt.% of iron detected, or none was found in other measured points. Iron was not found independently of others elements, thus its presence was always associated with some others phases.

Table 4: Detected elements by SEM-EDS in the water treated pyrometallurgical sludges prepared by leaching.

	As	Ba	Cr	Cu	F	Fe	Mn	N	P	Ti	Zn
OC	x	-	x	x	-	x	x	-	-	x	x
TF	-	x	-	-	x	x	-	-	x	-	-
BF	-	-	x	-	-	x	x	x	-	x	x
BFO	x	-	-	x	-	x	-	-	-	x	-
BFU	-	-	-	-	x	x	-	x	-	-	-

The SEM images of dried suspensions achieved after the standard leaching procedure show relatively large particles. It could be interpreted as the small metal based particles which were attached to the larger particles and formed agglomerates, probably with salts or silicates. Sulfur and silicon were detected in all samples by SEM-EDS. For example Figure 23c shows except metals (Fe, Cr, Zn) also Ca and S, which could be indicating the presence of $CaSO_4$. In the BFU sample less elements were detected, which is in accordance with the findings indicating that BFU contains the smallest amounts of the metals, which were separated by the hydrocyclone treatment [27].

Figure 23a (SEM image of dried suspension of the OC sample) shows a little "triangle-shaped particle" attached to a "fiber". In the "particle" C, O, Si, Cl, Ca, Mg, Fe, Mn, Cr, and Zn were determined. On the other hand, the "fiber" was formed by C, O, Si, Cl, Ca, Mg, K, and Na. Therefore the main composition is relatively similar, but the metals particles (Fe, Mn, and Cr) were attached only to the small "particle". Thus, the elements Fe, Mn, and Cr are present in the samples in minority and may tend to form aggregates. It could be caused by magnetic character of their compounds [113], which is discussed further.

Contrary to the SEM images, TEM images revealed the presence of ultrafine particles, which have a crystalline character. The TEM images are shown in Figure 24. The crystalline character of the finest particles is confirmed by the dark field TEM images, which is manifested by the presence of bright spots in the TEM images. The particles exhibit spherical character and create chains, which could be caused by their magnetic character. Thus, the presence of larger particles and aggregation of the particles could be explained by their magnetic character. Therefore iron could be present as magnetite or hematite, which are

ferrimagnetic and ferromagnetic, respectively. Also elemental iron shows magnetic character, but its presence is unlikely, since it is easily oxidizable.

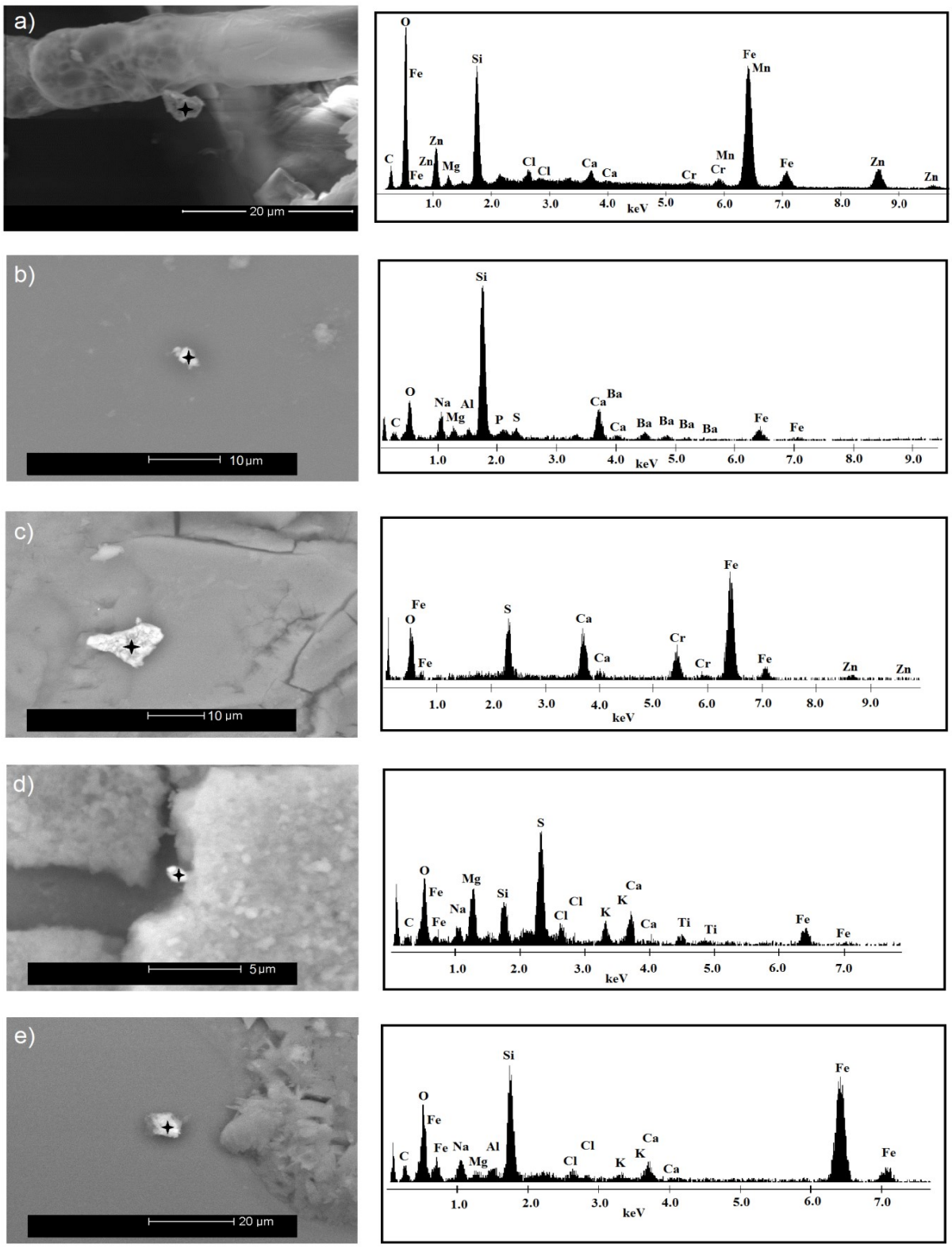

Figure 23: Selected SEM images of the OC (a), TF (b), BF (c), BFO (d), and BFU (e) samples prepared by leaching with corresponding EDS spectra. Crosses in the images show measured points.

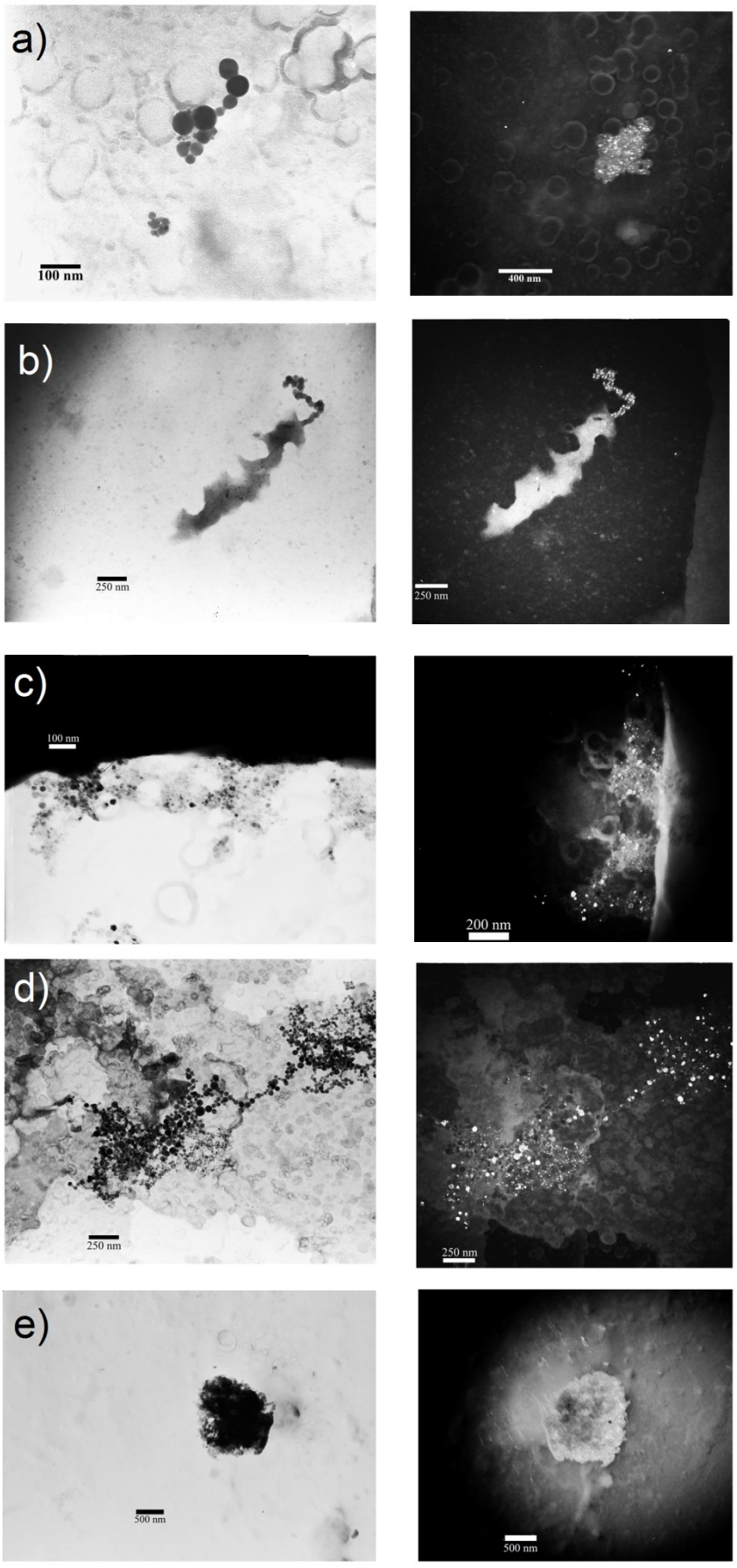

Figure 24: TEM images in bright (left side) and dark filed (right side) of the OC (a), TF (b), BF (c), BFO (d), and BFU (e) samples prepared by leaching.

In general, Raman microspectroscopy cannot detect single elements, but only bonding vibration. However, Raman measurements on the dried water suspensions prepared by leaching revealed no information about iron oxides presence in the samples. Only one detected iron compound was siderite ($FeCO_3$) in the OC, TF and BFU samples (Figure 25a). The lack of Raman response in relation to iron compounds in the samples could be caused by a small size of the particles present or because of their anchoring onto particles which are Raman inactive or have a big fluorescence background.

Another metal based component was found in the OC sample. It could be TiO_2 in the anatase form or γ-PbO (see Figure 25b). Since only one band is observed the interpretation is an issue, but according to the SEM-EDS analysis where the titanium was found in the OC sample without the presence of lead, thus anatase is more likely to be present. No more metal-based compounds were revealed by Raman microspectroscopy, but compounds based on silicates, sulfates, carbonates and amorphous carbon were also often found.

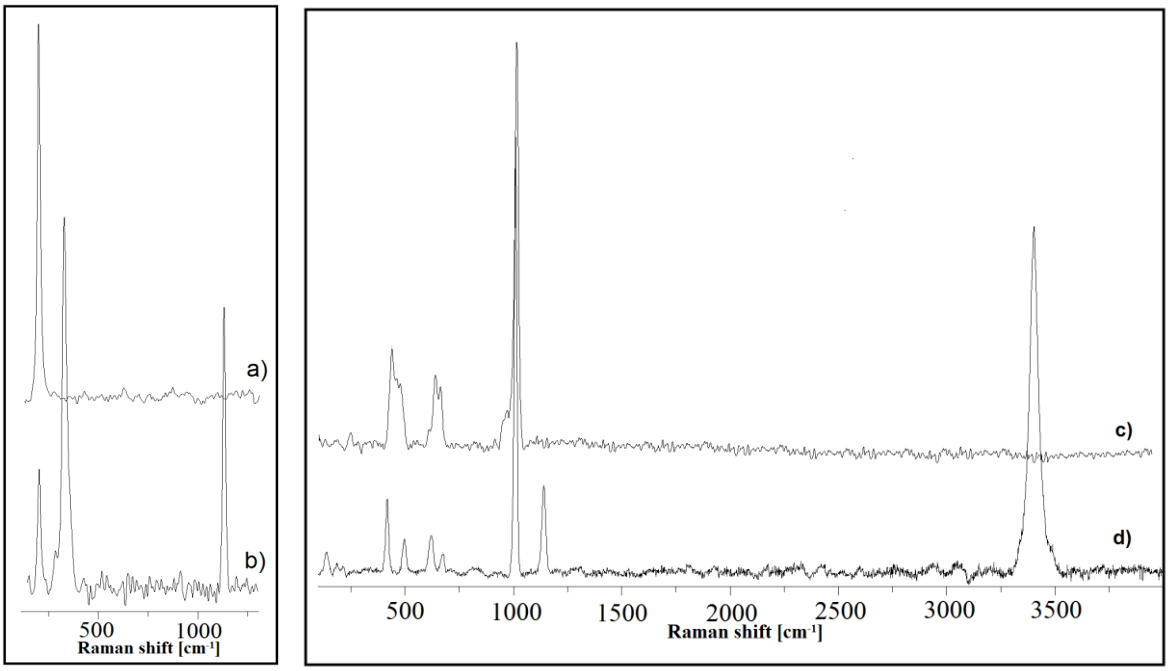

Figure 25: Raman spectra of measured metal compounds in suspension prepared by leaching – TiO_2 (a), $FeCO_3$ (b), $CaSO_4$ (c), and $CaSO_4.2H_2O$ (d) occurrence of these compounds in studied samples is described in text.

The interpretation of Raman spectra was very difficult, due to the following reasons: every measured spectrum has a large background (most likely due to fluorescence) and the most visible bands had low intensities. Only the spectra with relatively intensive bands were selected for interpretation. Nevertheless in some cases only type of compounds should be determined, such as sulfate, which was the most often detected compound in all the samples.

The presence of sulfates was confirmed by the presence of a very intensive band about 1010 cm^{-1}. But exactly determination was not possible, probably due to the presence of the sulfates mixtures. Therefore, $CaSO_4$ was undoubtedly determined. Calcium sulfate was revealed in two modifications: anhydrite ($CaSO_4$) (Figure 25c) and dihydrate ($CaSO_4.2H_2O$) (Figure 25d). The spectrum of dihydrate shows a relatively broad and intensive band at about 3400 cm^{-1}, which corresponds to the O-H vibration [114].

Although the carbon was found in all the samples by SEM-EDS, Raman microspectroscopy revealed the presence of amorphous carbon only in the samples BF and BFO, but in the remaining samples the $FeCO_3$ was found. All the obtained Raman spectra for each sample prepared by leaching can be found in Appendix 2.

5.1.3. Water Treated Pyrometallurgical Sludges – Prepared by Sedimentation

Suspensions prepared by sedimentation in water were also filtered prior to their TEM analysis, which prefers smaller particles for detection. Suspension prepared by sedimentation also contained very fine particles. Again for all the measured samples bimodal character was observed and values are expressed as volume percentage. All measured particle size distribution could be found in Appendix 1. In the OC, BF, and BFO samples, the same values for the first maximum as for the samples prepared as a leachate were obtained 122 (1.1%), 91 (17.5%), and 68 nm (25.3%), respectively. The following values were measured for the TF and BFU samples 79 (23.2%) and 91 nm (16.3%), respectively. The particle size distribution of the OC sample differs in the spectrum shape, where the first maximum contains fewer particles than the second maximum which contains 21.6% of particles with size of 825 nm in diameter. This size is much higher than pores in the membrane filter used. This is discussed in Chapter 5.1.4. Other determined second maxima are lower than the pore size of the used filter (0.45 μm): 295 (7.1%), 458 (6.7%), 220 (3.2%), and 458 (5.6%) for the TF, BF, BFO, and BFU samples, respectively.

The particles revealed by SEM analysis were similar (see Figure 26) to the particles which were present in the samples prepared by leaching. The larger size could be caused by adhering metal-based particles to the surface of some others particles/compounds, according to the EDS records probably to some sulfates or silicates. Table 5 shows selection of elements detected in studied samples. Ca, Mg, Na, O, Si were eliminated from Table 5, because they were found in all measured samples. Moreover, the presence of the Al, Ca, K, Na, Mg and Si could be affected by measurements on a glass slide, but not all of these elements were found in all samples.

Table 5: Detected elements by SEM-EDS in the water treated pyrometallurgical sludges prepared by sedimentation.

	Al	Ba	C	Cl	Fe	K	Mn	P	S	Sn	Zn
OC	x	-	-	-	x	-	x	-	-	-	-
TF	x	x	-	x	x	x	-	x	x	-	x
BF	-	x	x	x	x	x	-	-	x	-	-
BFO	-	x	-	x	x	x	-	x	x	x	x
BFU	-	x	-	x	x	x	-	-	x	-	-

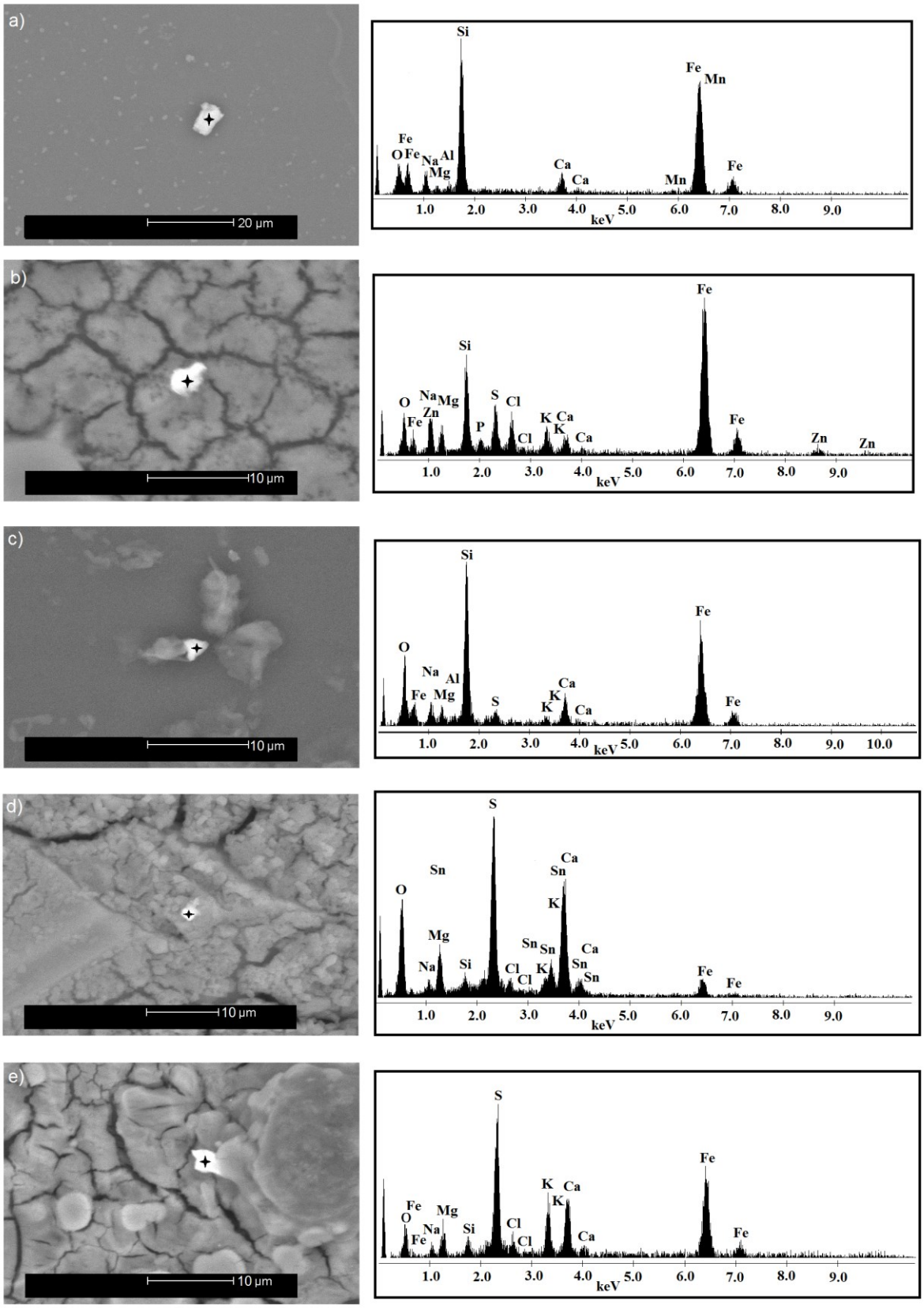

Figure 26: Selected SEM images of the OC (a), TF (b), BF (c), BFO (d), and BFU (e) samples prepared by sedimentation with corresponding EDS spectra. Crosses in the images show measured points.

Iron was again found in all measured samples and selected images (Figure 26 a-e) have depicted points (black cross) where the iron presence was confirmed. Contrary to the samples prepared by leaching the copper was not found, and neither was titanium, or chromium. However, tin was found in the BFO sample prepared by sedimentation, therefore no other technique revealed its presence in the sample.

The presence of barium was detected almost in all measured samples prepared by sedimentation, except the OC sample. In the points where the Ba was detected the presence of the sulfur was also recorded, which could point to the barite presence. Hazardous metals (Cd a Pb) in the pyrometallurgical samples were not determined by SEM-EDS in the samples prepared by sedimentation. The OC sample was the only one which contained Mn.

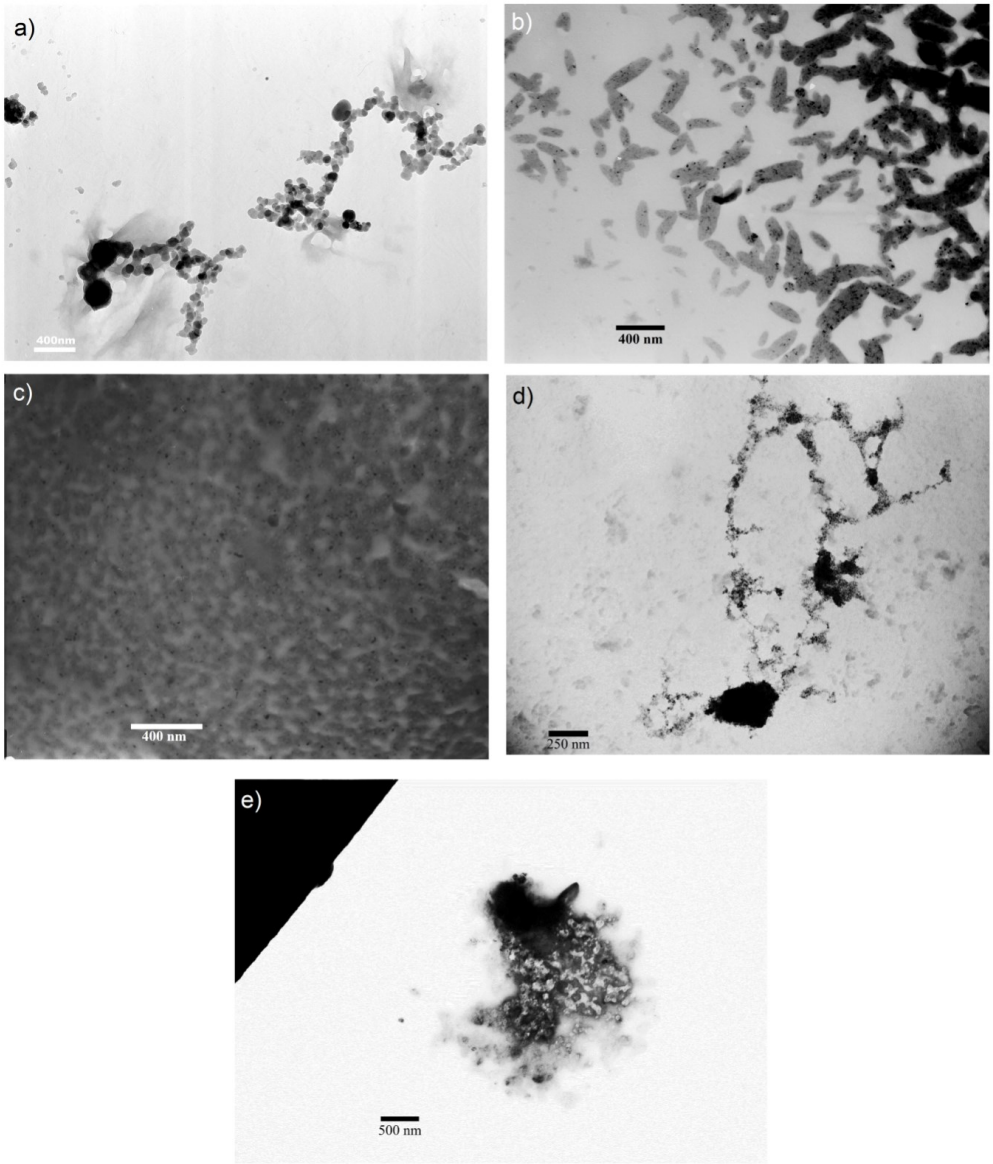

Figure 27: Selected TEM bright field images of the OC (a), TF (b), BF (c), BFO (d), and BFU (e) samples prepared by sedimentation.

The TEM analysis also revealed very fine particles which show a similarity to the particles determined in samples prepared by leaching, in Figure 27 is the similarity seen mainly for the OC, BFO, and BFU samples. Thus, the water treatment (leaching and sedimentation) did not generate different type of particles which was not expected. Figure 27 shows the selected images obtained from bright field TEM images. Dark field images were not measured for all studied samples, thus these images are not shown here. However, crystalline character of the present particles was revealed. For example, the bright field image of the TF sample (Figure 27b) shows larger particles covered with smaller darker particles, these particles in obtained dark field image are bright.

Raman measurements again provide no information about the presence of iron oxides in the samples prepared by the sedimentation. Thus, iron could be present as iron oxides but as very fine particles which are under detection limit of Raman microspectroscopy. Also iron oxides could be attached onto some other compounds which are not Raman active, thus the signal from iron oxides is hidden. Only one iron-based component was found, namely $FeCO_3$, but only in the BF sample. In the samples prepared by leaching $FeCO_3$ was found in the OC, TF, and BFU samples.

Contrary to the samples prepared by leaching, samples prepared by sedimentation contain more metal-based compounds which were detected by Raman microspectroscopy (ZnO, $BaSO_4$, and $PbSO_4$). In the TF sample the ZnO was found probably in conjunction with some carbonate or silicate according to the Raman spectral library. Considering the presence of zinc in the TF sample confirmed by SEM-EDS, without the presence of carbon, it could be probably a silicate in that measured point.

Carbon presence was revealed by SEM-EDS only in the BF sample, where Raman microspectroscopy determined the $FeCO_3$ (Figure 25b). No amorphous carbon was detected in the samples prepared by the sedimentation. Nonetheless, Raman microspectroscopy also revealed some organic compounds in the TF, BF, and BFU samples. It is not clear which organic compounds exactly are present, but the spectrum shows typical bands corresponding to C-H vibrations (2846 and 2879 cm^{-1}) [114]. Figure 28c shows the achieved spectrum. According to the spectral library the best match was with palmitic acid ($CaC_{32}H_{62}O_4$) or some polymer (e.g. polyvinyl acetate), however these particular compounds are probably not likely to be present within the pyrometallurgical processes. A better recognition was not possible, because the spectrum was relatively noisy with less intensive bands in lower wavenumbers. The membrane filter which was used for filtration was also measured by Raman microspectroscopy to reveal potential contamination from nitrocellulose, but the similarity

was not found. In studied pyrometallurgy sludges were determined several PAHs by gas chromatography [27], thus the organic compounds are present in the studied samples and could be transferred to the water suspensions.

The most abundant compounds in these samples were sulfates, in the case of the BFU sample $BaSO_4$ was found (Figure 28a). Another sulfate $PbSO_4$ (Figure 28b) was found in the BF and BFU samples, although no Pb was found by SEM-EDS. In Figure 28 it is clearly evident that the difference between $PbSO_4$ and $BaSO_4$ in their most intensive band is negligible. But the shift from 990 cm^{-1} ($BaSO_4$) to the lower wavenumbers 981cm^{-1} ($PbSO_4$) corresponds to the presence of heaviest element (Pb) in the compound or could be caused some changes in the structure of $BaSO_4$ which may be manifested by the shift of band.

A very good match was also recorded with $CaSO_4$, which was found as anhydrite ($CaSO_4$) (Figure 25c) and dihydrate ($CaSO_4.2H_2O$) (Figure 25d). In other cases of sulfate presence it is difficult to say with a certainty which sulfate was present in the samples. Probably the mixture of sulfates could also be present. Other measured spectra for all samples prepared by sedimentation are shown in Appendix 3.

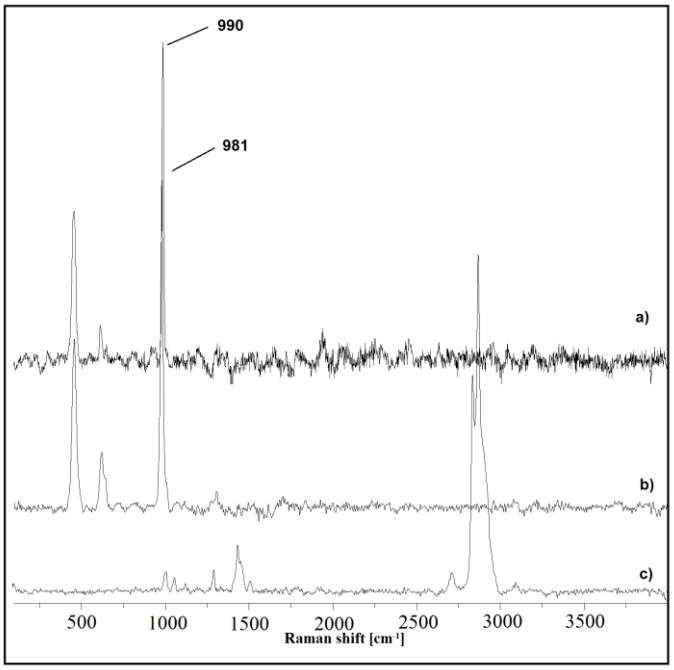

Figure 28: Raman spectra of $BaSO_4$ (a), $PbSO_4$ (b), and organic compound (c).

5.1.4 Comparison of Samples Prepared by leaching and Sedimentation

Particle size distributions for both types prepared samples show Table 6. Measurements of particle size distribution were complicated by very dilute suspensions and a lot of repetitions were applied to obtain relevant data. All measured particle size distributions measured for all samples are shown in Appendix 1.

A significant difference was observed in the OC sample. The OC sample contains the biggest particles and a different character of size distribution was obtained for sample prepared by sedimentation (second maximum contains more particles than first maximum). The initial OC sample shows a distribution with three maxima in the range 0.7 – 450 μm, but the samples prepared by leaching and sedimentation confirmed presence of much smaller particles which were probably attached to the surface of the larger particles in the initial sample and were released after water contact into the water environment. It is valid for all initial samples, which minimum particle size determined in the initial samples was higher than the detected size of the main particles in the suspensions. The detection of larger particles than the pore size of membrane filter used could be caused by the aggregating of the particles after filtration, irregular shapes of the particles, or an error in the measurements.

In general, samples prepared by sedimentation contain particles of similar sizes. Slightly larger particles in the samples prepared by sedimentation than in the samples prepared by leaching were observed in the TF and BFU samples for first distribution maxima.

Table 6: Particle size distributions: values of maxima and their percentage for both type samples preparation.

	OC		**TF**		**BF**		**BFO**		**BFU**	
	1st max **[vol.%]**	2nd max **[vol.%]**	1st max **[vol.%]**	2nd max **[vol.%]**	1st max **[vol.%]**	2nd max **[vol.%]**	1st max **[vol.%]**	2nd max **[vol.%]**	1st max **[vol.%]**	2nd max **[vol.%]**
Leach.*	122 **[28.6]**	615 **[2.8]**	68 **[40.7]**	342 **[1.5]**	91 **[26.6]**	396 **[5.2]**	68 **[36.7]**	615 **[3.7]**	51 **[28.7]**	342 **[9.8]**
Sed.*	122 **[1.1]**	825 **[21.6]**	79 **[23.2]**	295 **[7.1]**	91 **[17.5]**	458 **[6.7]**	68 **[25.3]**	220 **[3.2]**	91 **[16.3]**	458 **[5.6]**

*Leach. – samples prepared by leaching; Sed. – samples prepared by sedimentation

SEM images show relatively large particles with a similar character for both types of sample preparation. SEM-EDS revealed iron in all samples, but not alone, only with conjunction with other elements mainly sulfur or silicon. It could point to the attaching iron-based particles to the some sulfate or silicates. Presence of sulfate was confirmed also with Raman microspectroscopy. With no iron oxides, only $FeCO_3$ were determined by Raman

microspectroscopy; it could be caused by presence of iron oxides in very small sizes under detection limit of Raman spectroscopy or attached to particles which are not Raman active.

In the elements detected by SEM-EDS there are some differences. Some elements which were not found in initial powder samples were detected in the prepared suspension – As, Ba, Cu, F, N, and P (sample prepared by leaching) and Ba, Cl, P, and Sn (sample prepared by sedimentation). These elements should be present in the initial sludges in the minority, but was estimated in the prepared suspension. For example, barium was found in a form of $BaSO_4$ by Raman microspectroscopy, but only in one sample (BFU) prepared by sedimentation. Other sulfates were detected by Raman microspectroscopy ($PbSO_4$, $CaSO_4$, $Na_2Ca(SO_4)_2$) but in the most cases there was a problem to determine the exact measured sulfate. It could be caused by the mixture of components, so barite could be present in more samples. According to the spectral library the $PbSO_4$ was found in BF and BFU samples, but SEM-EDS detected no lead in all samples. Thus, this identification is not clear. In general, more metal-based compounds detected by Raman microspectroscopy were found in samples prepared by sedimentation.

TEM measurements revealed small particles with crystalline character in both prepared types of samples. Particle showed spherical shapes and created chains which could be marking of magnetic character. In some cases there was a problem with focusing the TEM microscope, which could probably be also caused by magnetic character of measured particles.

All analytical techniques used had some advantages and disadvantages and all in the complex shows character of particles released to the water. However the both type of suspension preparation not differ so much, thus the results from the samples prepared by leaching and sedimentation should be taken as complementary results. The mobility of the nano-sized crystalline particles was proved into water and filtered aqueous leachate is inaccurately considered homogeneous.

5.2 BRAKE WEAR DEBRIS

5.2.1. Nonairborne Brake Wear Debris

The nonairborne brake wear debris collected as settled fraction in the dynamometer chamber contains particles of various sizes, morphologies, and chemistry. The morphology of all collected brake wear debris samples is shown in Figure 29. Due to a mechanism of wear prevail specific morphologies are generated, i.e. mechanical (abrasive) wear produces irregular particles with sharp edges while oxidative wear generates round shape particles of the finest fraction. The brake wear particulate matter consists of larger isolated particles, but also smaller particles which tend to aggregate are attached on the surface of larger particles. A particle size analysis was not carried out for these samples. However it is known that particles of brake wear debris mostly range from millimeters to nanometers in size [66].

The elemental composition measured from the area of wear debris by SEM-EDS shows that the dominant element is iron in all measured samples. Brake wear debris is a multicomponent material as well as the initial friction composite. Thus some elements were not detected by SEM-EDS in measurements from surface, but only by point analysis. These elements are present in small amounts, or as small particles in brake wear debris. For example, in G6C brake pad formulation, presence of copper was not detected by SEM-EDS from the area measurements, but it was determined during the analysis of G6C brake wear debris. Copper was found in all brake wear debris samples except G6C/KATI sample, which is in accordance with brake pad formulation which was Cu-free (eco-friendly type of brake pad).

Table 7 shows elements detected by SEM-EDS in all measured samples. Although the formulation of the initial G6C and G6C/KATI samples is almost identical, differences were observed in the detected elements. G6C/KATI contained titanium in its formulation which was confirmed by SEM-EDS in brake wear debris. Nonetheless Al, Mg, Mo, and Sn were detected only in G6C sample but not in G6C/KATI which also contained these elements (Table 3). The difference in the detected elements was probably caused by non-homogeneous character of the samples or presence of these elements in small amounts in brake wear debris.

Table 7: Detected elements by SEM-EDS in all measured brake wear debris.

	Al	Ba	C	Ca	Cu	Fe	K	Mg	Mo	Na	O	S	Sb	Si	Sn	Ti	Zn
G6C	x	x	x	x	x	x	x	x	x	-	x	x	x	x	x	-	-
G6C/KATI	-	x	x	x	-	x	-	-	-	-	x	x	x	x	-	x	-
SMP1	x	x	x	x	x	x	-	x	-	x	x	x	-	x	-	x	-
SMP2	x	x	x	x	x	x	-	x	-	-	x	x	-	x	-	-	x

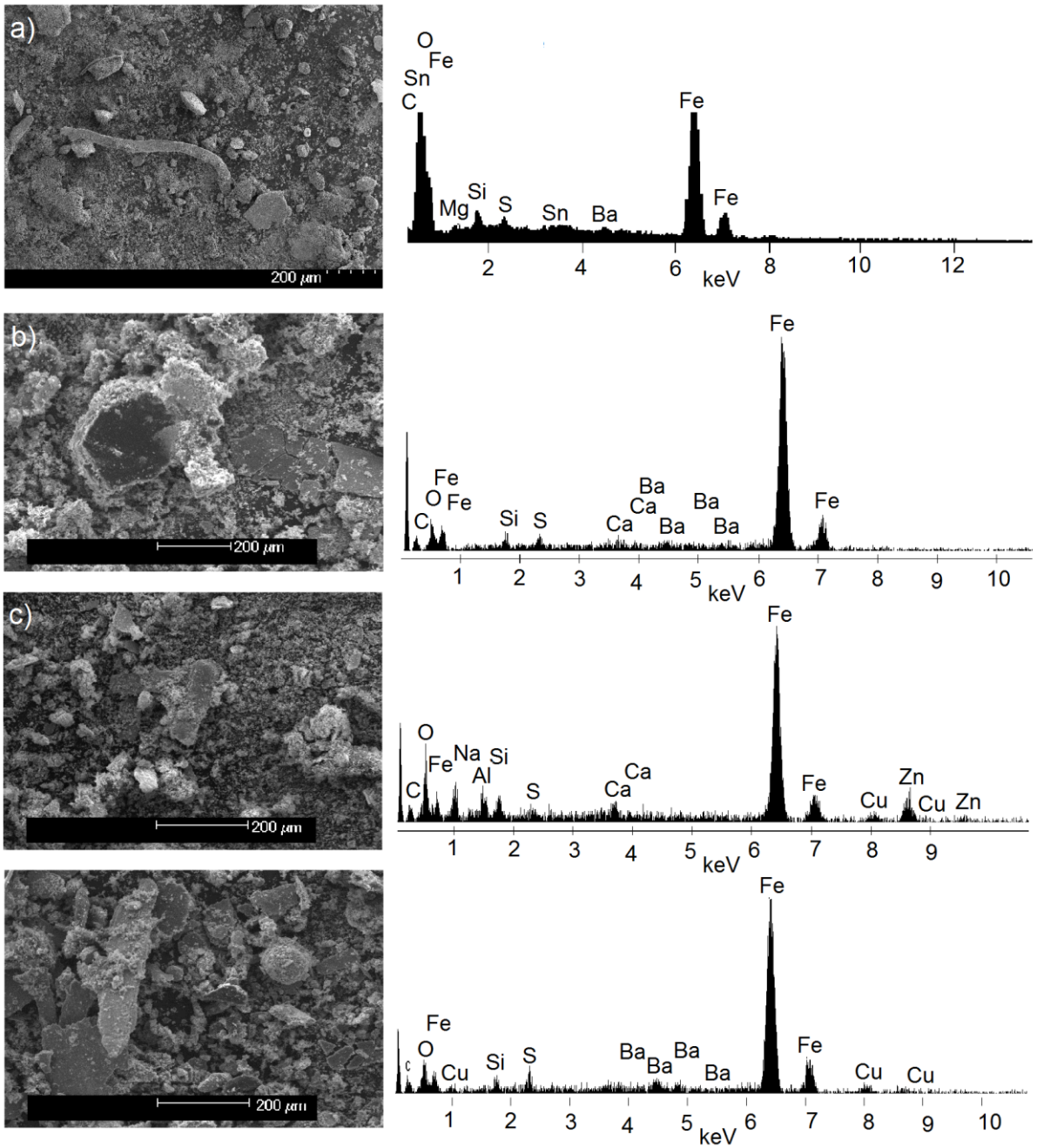

Figure 29: Selected SEM images with corresponding EDS patterns measured from surface area of the G6C (a), G6C/KATI (b), SMP1 (c), and SMP2 (d) wear debris samples.

No information is available about the formulation of commercial samples (SMP1 and SMP2) due to the secret know-how of each manufacturer, thus the detected elements could not be exactly correlated with the initial brake pad formulation. However, it is evident that wear debris of SMP2 sample as the only one contained zinc, thus zinc could be used in brake pad SMP2 formulation or it is an impurity of some material so not intentionally added. Brake wear debris of the SMP1 sample contained titanium as well as the sample G6C/KATI. Both commercial samples show a similarity with the model brake pad (G6C) in the elements detected. Ba, Al, Cu, Fe, Mg, S, and Si were detected in both commercial samples and in G6C. Therefore our model brake pad really correlates the real brake pads available in EU markets.

Figure 30 shows the FTIR spectra measured for all samples. The presence of organic compounds is confirmed by the bands at the wavenumbers about 2918 and 2846 cm^{-1}, which are corresponding to aliphatic hydrocarbons [114]. The C-H vibrations were confirmed in all samples, including sample G6C where these bands are less intensive. Their presence is caused by the remain amount of the phenolic resin, which is in initial formulation of the model brake pads (G6C and G6C/KATI) or by others organic compounds which are creating during friction process [115].

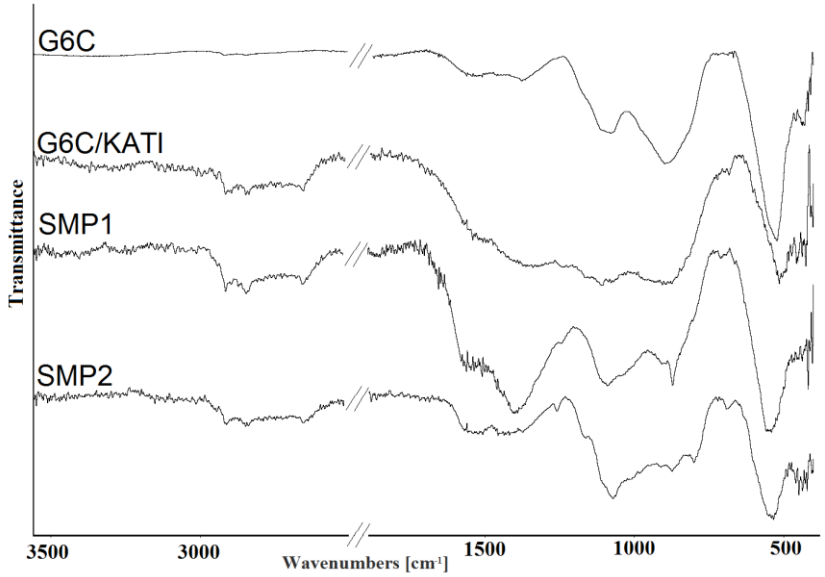

Figure 30: Measured FTIR spectra of all collected brake wear debris samples.

Due to the presence of many components in brake wear debris, amorphous components create the main character of the spectra and so the interpretation is very difficult. From Figure 30, it is clearly evident that the spectrum of G6C/KATI has only one very broad band, which was created by several bands overlapping of all presented components in the sample. Thus its interpretation is impossible. Problem with distinguish individual bands

related to each components is problem in all samples, due to bands overlapping and due to a relatively low energy of the mid-IR light used for analysis, thus no heavy elements can be detected in the samples.

Better results were obtained by XRPD measurements (see Figure 31). Iron was found in all brake wear debris in form of zerovalent iron and magnetite. Zerovalent iron is highly reactive and easily is oxidized to iron oxides, but Kukutschová et al. [116] showed that brake wear debris after dynamometer test contain nano-sized particles formed from Fe(0) core with iron oxide shell [116]. Hematite was found in all brake wear debris samples except the SMP2. Other iron oxide, FeO, was found in brake wear debris of G6C/KATI and SMP2, and nonstoichiometric iron oxide γ-$Fe_{21.34}O_{32}$ was determined in SMP1. These findings are in good correlation with SEM-EDS which determined iron as the most abundant element in the brake wear debris. From the comparison with the initial composite, it is evident that elemental iron was oxidized to iron oxides during friction processes. These iron compounds may come from oxidation of iron powder present in brake pads or from abrasion of cast iron discs. However, exact determination of the source of iron compounds is difficult. However, they contribute together to the pollution, thus its exact distinguish is not significant.

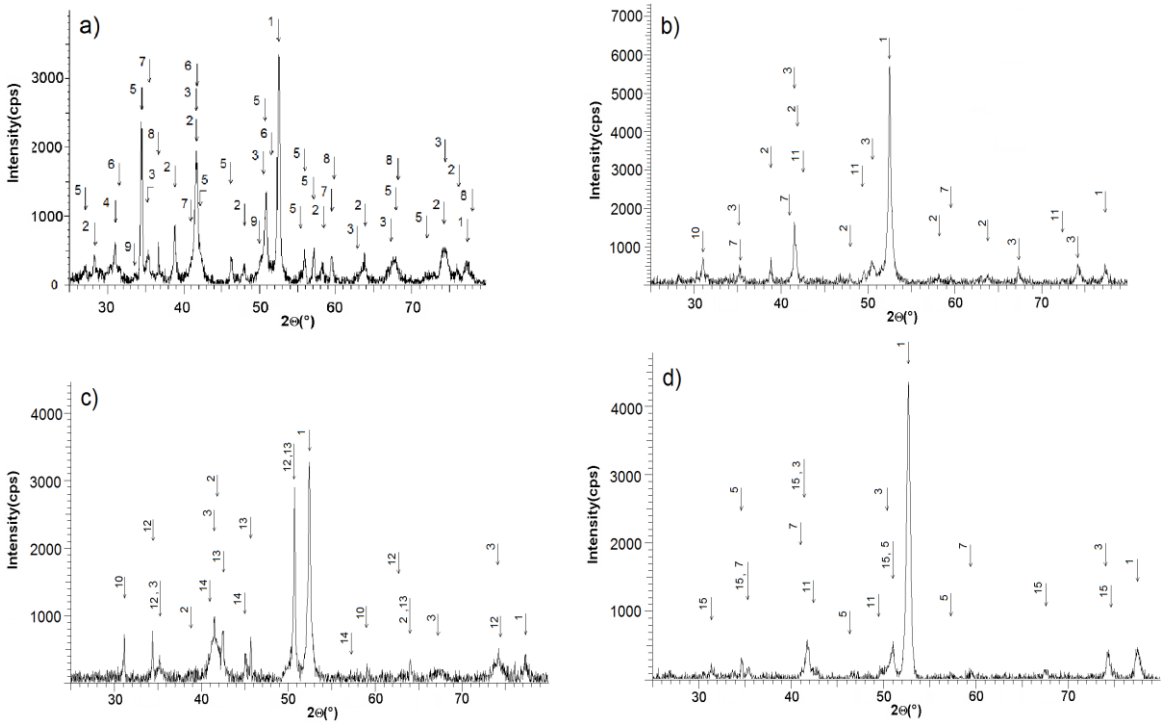

Figure 31: Measured XRPD patterns of G6C (a), G6C/KATI (b), SMP1 (c), and SMP2 (d). **1** - Fe, **2** – Fe_2O_3, **3** – Fe_3O_4, **4** – C (graphite), **5** – $(Mg_{0.064}Ca_{0.936})CO_3$, **6** – $ZrSiO_4$, **7** – Sb_2O_5, **8** - Sb_2Fe, **9** – $BaSO_4$, **10** – SiO_2, **11** – FeO, **12** – $BaZrO_3$, **13** – Zn, **14** – CuO, **15**– γ-$Fe_{21.34}O_{32}$.

Barium in form of barite was revealed only in sample G6C and in form of barium zirconium oxide in sample SMP1 by XRPD, but SEM-EDS determined barium presence in all samples. Barite is being used in brake pad formulations as filler. No information is available about the formulation of SMP2, but in formulation of G6C/KATI, barite was used (see Table 3). No determination of barite in sample G6C/KATI could be caused by its small amount which is under detection limit of XRPD method.

Two antimony oxides were found in samples G6C (Sb_2O_5 and Sb_2Fe), G6C/KATI (Sb_2O_5), and SMP2 (Sb_2O_5) by XRPD analysis. SEM-EDS revealed the antimony only in wear debris of the model brake pads (G6C and G6C/KATI). According to the model brake pad formulation (G6C), stibnite (Sb_2S_3) was used for brake pads as a solid lubricant. Obviously, antimony pentoxide (Sb_2O_5) and a Laves Sb_2Fe phase were formed from Sb_2S_3. Matějka and Jang et al. [73,74] showed the possible oxidation of Sb_2S_3 on the friction surface of semi-metallic friction composites containing steel fibers and concluded that the low content of iron in low metallic friction composites formulations leads to the formation of antimony oxides.

Silicon was revealed in the form of quartz (G6C/KATI and SMP1) and in form of $ZrSiO_4$ (G6C), but it was present in the model brake pads also as vermiculite and in G6C/KATI as kaolinite, which were not revealed by XRPD. The presence of copper was confirmed by XRPD only in the SMP1 sample in the form of CuO. Thus it can be concluded that for this kind of samples XRPD provides more information about phase composition than FTIR analysis.

All measured Raman spectra are shown in Appendix 4. Table 8 shows all determined components. Brake wear debris is multicomponent heterogeneous material and several components were found alone or with other in one measured point. Also a mixture of various components was found. Thus the interpretation of the mixtures was in some cases difficult. Also brake wear debris contained some components which have high fluorescence background or have no Raman spectrum that is why the achieved spectra are very noisy in some cases. Again only spectra with relatively intensive bands according to noise were selected for interpretation.

The example of the detected graphite, amorphous carbon, and their mixtures is shown in Figure 32. Raman spectrum of graphite (Figure 32c) shows two most intense bands, one at 1585 cm^{-1} labeled as a graphitic band (G band) and another at 2717 cm^{-1} (historically designated as the G' band) which is the most significant band that always appears in graphitic samples [117, 118]. This band is also called as the 2D band. Its presence in a spectrum of

Table 8: Detected compounds in brake wear debris samples by Raman microspectroscopy.

	G6C	G6C/KATI	SMP1	SMP2
amorphous carbon	x	x	x	x
graphite	x	x	x	x
Fe_2O_3	x	x	x	x
Fe_3O_4	x	x	x	x
$CaCO_3$	x	-	x	x
$CaSO_4$	-	x	x	-
MoS_2	x	x	-	-
$BaSO_4$	x	-	-	-
SiO_2	-	-	x	x
labradorite	-	-	x	-
Sb_2S_3	-	-	-	x

graphite is caused by the second-order zone boundary phonons, originating from a two-phonon double resonance process related to the band structure of the graphene layers [119]. The G band corresponds to the in-plane vibration of aromatic carbons in the graphitic structure. The band at 1350 cm^{-1} is labeled as the disorder band (D band). The D band is present in the spectrum due to the presence of heteroatoms or defects within the structure. The G band is characteristic for monocrystalline graphite [120]. Several bands are visible in the second order region and correspond to the overtones and combination scattering [121,122].

In Figure 32a broad character of the bands is assigned to amorphous phase [123,124]. The amorphous character is also clearly evident in Figure 32b, which shows mixture of two carbonaceous phases. The broad shapes indicate the amorphous character, but the presence of G' band in the spectrum confirms the graphitic structure. The mixture may be caused by a thin amorphous film, which covered the brake wear debris particles [66]. These two types of carbonaceous particles may be of different origin. While amorphous carbon is likely to be produced by oxidative wear, condensation, and subsequent deposition from related volatiles, the presence of graphitic particles in the deposited debris the most probably results from abrasive wear [66].

The presence of iron in all measured brake wear debris was confirmed by Raman microspectroscopy. Iron oxides (Fe_2O_3 and Fe_3O_4) were found in all samples (see Figure 33). Presence of zerovalent iron could not be determined by Raman microspectroscopy. Magnetite

is a poor Raman scatterer [125], therefore only one band at 670 cm^{-1} was observed, also the spectrum is very noisy. On the other hand, the spectrum of hematite was less noisy and contained very intensive bands. Very broad and intensive band at 1320 cm^{-1} is an overtone associated with a Raman-forbidden longitudial-optical phonon near 660 cm^{-1}. The two-magnon scattering is shown as a weak and broad band at 1525 cm^{-1} and it has magnetic origin [126,127].

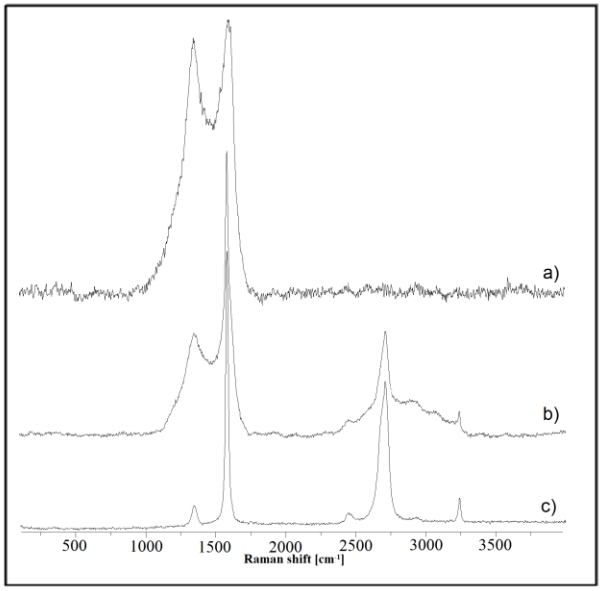

Figure 32: Measured Raman spectra of amorphous carbon (a), mixture of amorphous carbon and graphite (b), and graphite (c).

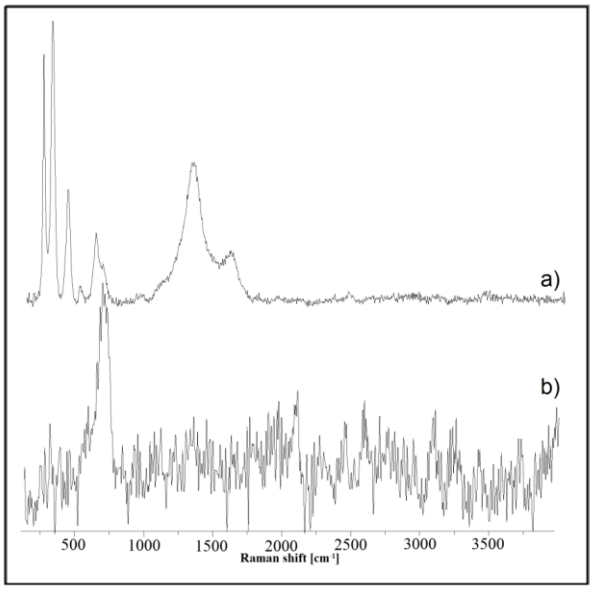

Figure 33: Measured Raman spectra of hematite (a) and magnetite (b).

Raman measurements were in very good accordance with the XRPD data, which reveals the $BaSO_4$ only in the G6C sample, although the Ba was found in all samples by SEM-EDS. But in the G6C/KATI sample also $CaSO_4$ was found, which has a similar spectrum to $BaSO_4$, thus the barite presence could be hidden in the mixture of sulfates.

5.2.2. Water Treated Nonairborne Brake Wear Debris – Sedimentation

Typical SEM images of the prepared water suspensions by sedimentation are shown in Figure 34 and Table 9 summarizes the measured elements. SEM images show relatively large particles again. The small particles which passed through the filter with 0.45 μm pore size might subsequently form larger aggregates.

In the case of the sample SMP2 the two elements found in dried water suspension were not detected in the initial brake wear debris (Bi and Se). It could be probably caused by small size of their particles and small amounts in brake wear debris and their weak attachment to larger particles which water contact allows their release into the water.

Iron was detected only in the sample G6C/KATI by SEM-EDS. The sample with the smallest number of detected elements was the SMP1 sample. Titanium was revealed by SEM-EDS in G6C/KATI and SMP1, this finding is in accordance with SEM-EDS of brake wear debris of these samples, where titanium was found. Au and Pd in SEM-EDS of sample SMP1 (Figure 34c) is present due to sputtering for better sample conductivity needed for SEM analysis. Barium, which was found in all initial brake wear debris, was not found in the SMP1 sample. Elements as Cu, Mo, Sb, Sn, and Zn were not determined by SEM-EDS in the dried suspensions. It could be caused by larger particles, which did not penetrate through the filter, or very small particles that were not found. The presence of the Al, Ca, K, Na, Mg and Si could be affected by measurements on a glass slide, but not all of these elements were found by SEM-EDS analysis in water treated brake wear debris.

Table 9: Detected elements by SEM-EDS in all measured suspensions of brake wear debris prepared by sedimentation.

	Al	Ba	Bi	C	Ca	Cl	Fe	K	Mg	Na	O	S	Se	Si	Ti	Zr
G6C	x	x	-	x	x	-	-	x	x	x	x	x	-	x	-	-
G6C/KATI	x	x	-	x	x	x	x	x	x	x	x	x	-	x	x	-
SMP1	-	-	-	-	x	-	-	x	-	x	x	-	-	x	x	x
SMP2	-	x	x	x	x	x	-	x	-	x	x	x	x	x	-	-

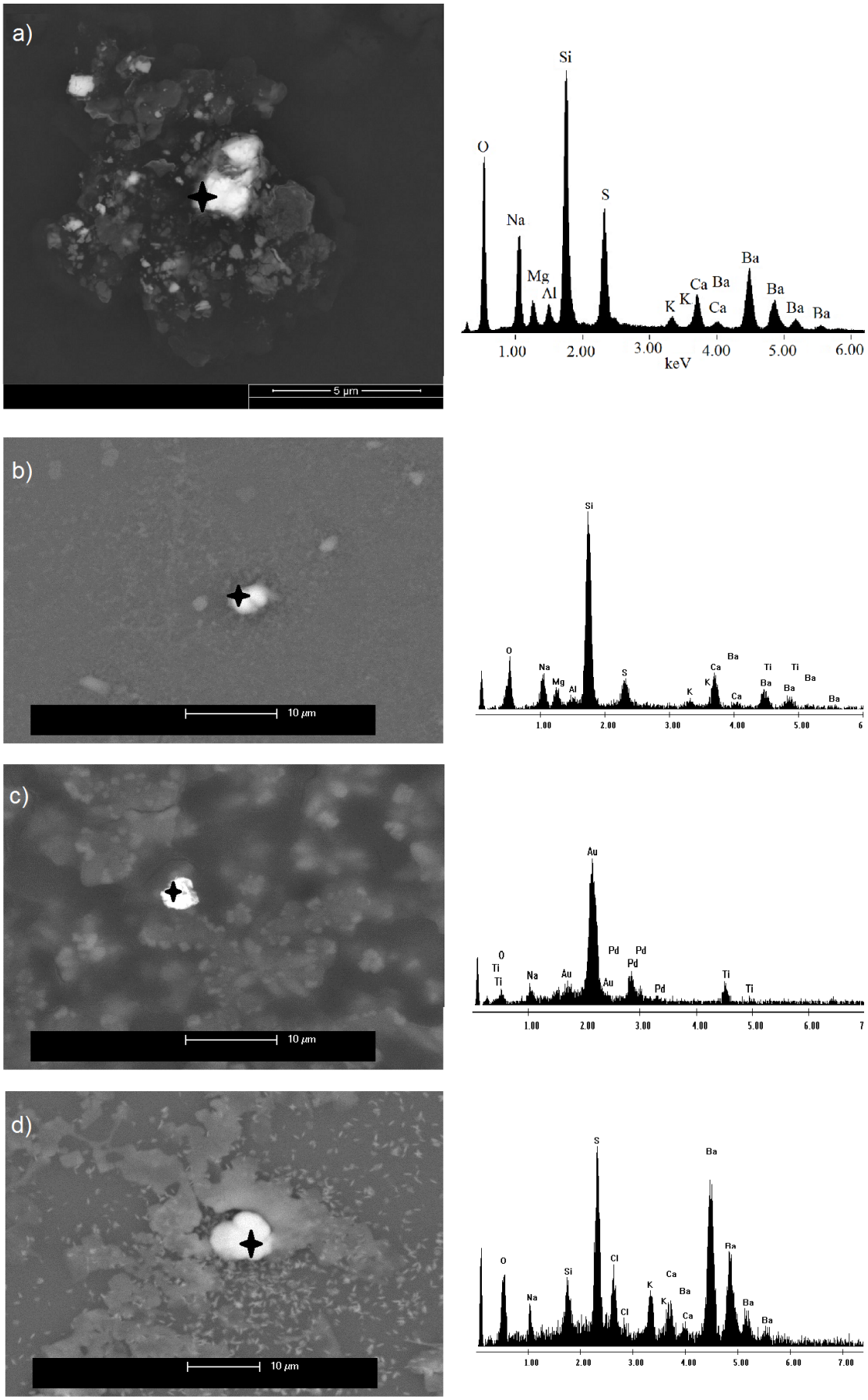

Figure 34: SEM images of detected particles in dried suspensions of brake wear debris with corresponding EDS patterns of G6C (a), G6C/KATI (b), SMP1(c), and SMP2 (d).

TEM images of samples G6C and SMP1 are shown in Figure 35, but the images of the samples G6C/KATI and SMP2 are missing because of the limited availability of TEM technique in Slovak Academy of Science, Bratislava. From TEM images (Figure 35a-b) presence of a large aggregate with smaller crystalline particles is clearly evident for the G6C sample. The smaller particles have a size of clearly below 100 nm. Contrary to the TEM images (Figure 35c-d) of SMP1 shows small spherical particles in chains. The similarity of pyrometallurgical sludges with TEM images was observed. And from the dark field image it is evident that small crystalline particles are attached to the surface of larger particles.

Particle size distributions were not evaluated for these water-treated brake wear debris samples, because the suspensions were diluted too much and no relevant data were obtained. However, the presence of nano-sized particles in the samples was revealed by TEM analysis for the G6C and SMP1 samples. It is therefore probable that the other two suspensions of G6C/KATI and SMP2 could contain some crystalline metal-based particles based on a Raman and SEM findings.

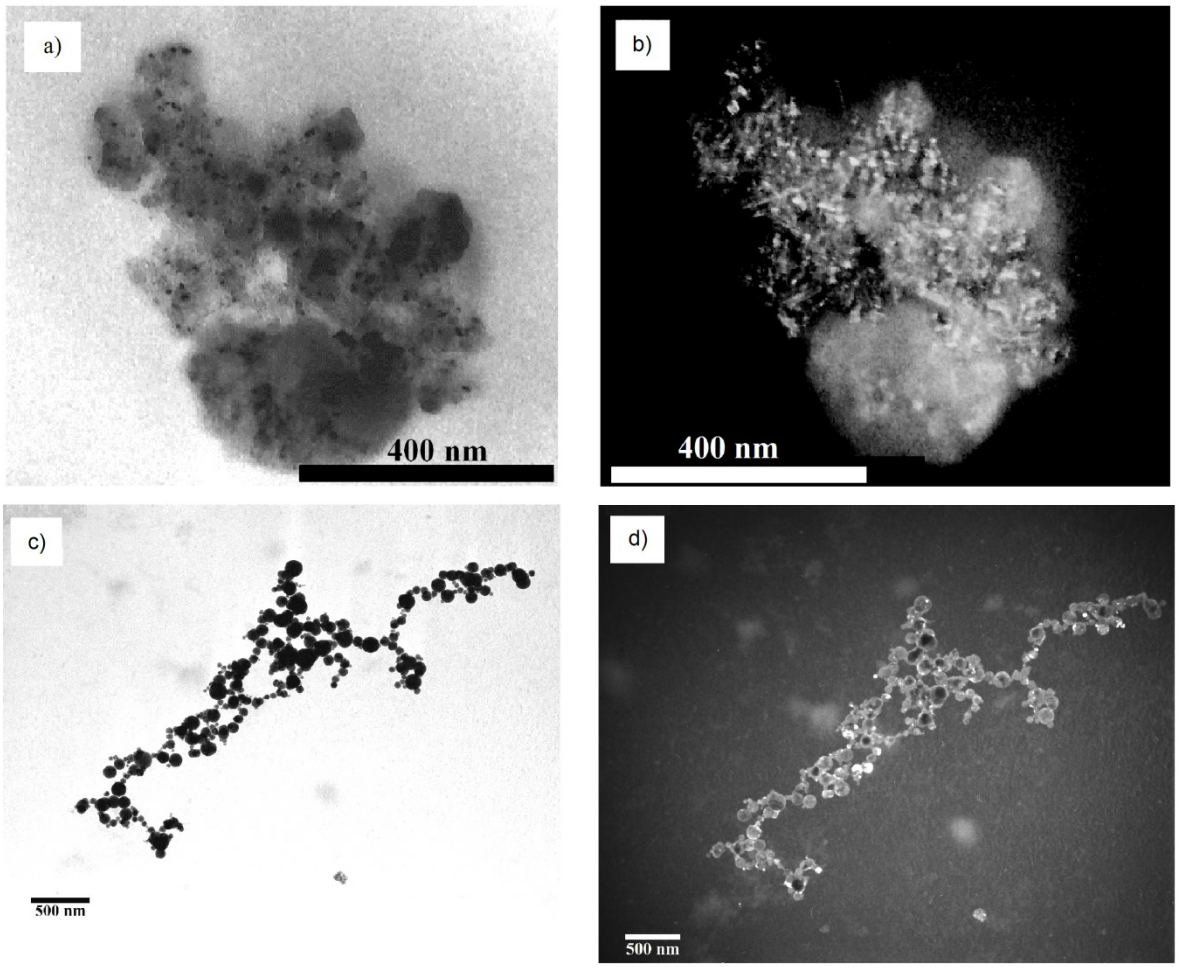

Figure 35: Bright field TEM images of G6C (a) and SMP1 (c), with corresponding dark field TEM images of G6C (b) and SMP1 (d).

Raman microspectroscopy revealed the presence of several compounds summarized in Table 10. All the measured spectra are shown in Appendix 5. Raman microspectroscopic measurements are in good accordance with the SEM-EDS results. For example, in all samples, calcium was detected and also Raman microspectroscopy revealed the presence of $CaCO_3$ in all the samples. Iron was found only in G6C/KATI by SEM-EDS and also Raman microspectroscopy revealed iron in form of $FeCO_3$ in this sample. Again no information about iron oxides was estimated by Raman microspectroscopy. According to TEM images, which show chains of small particles under the 100 nm, probably iron oxides are present as very small particles under detection of the Raman microspectroscopy.

Titanium was present in form of anatase and again the accordance between SEM-EDS and Raman microspectroscopy was obtained. Also presence of zirconium was confirmed in SMP1 in form of zircon, and also barium in form of barite was detected in same samples as by SEM-EDS (G6C, G6C/KATI and SMP2). Presence of barium in SMP1 was not proved by any technique in water treated suspension, it could be caused by barium presence in ionic form, which have no Raman spectrum or as very small particles, which are under the detection limit of Raman microspectroscopy.

Table 10: Detected compounds in all samples by Raman microspectroscopy.

sample	compounds
G6C	$BaSO_4$, $CaCO_3$
G6C/KATI	$BaSO_4$, $CaCO_3$, $FeCO_3$, TiO_2, $Na,Ca(SO_4)_2$, sulfates
SMP1	$CaCO_3$, TiO_2, $ZrSiO_4$, mixture of sulfates, graphite, amorphous carbon
SMP2	$BaSO_4$, $CaCO_3$, $CaC_2O_4.2H_2O$, $Na,Ca(SO_4)_2$, polyamide, sulfates

Previous studies [64-66,135] have proven that road traffic; especially wear of brakes can be a significant source of nano-sized particles suspended in the air; however none of the studies have addressed/demonstrated the release of nanoparticles into the water system so far. Based on the data obtained in this study, it is evident that some nano-sized particles are not tightly attached to the surface of larger wear particles and may be mobilized after a contact with water and enter biogeochemical cycles in the environment. Hence, the nonairborne brake wear debris may also contribute to water and soil pollution by nanosized particles. Raman findings were in good accordance with SEM-EDS, but its advantage is the determination of the chemistry of released particles.

5.3 POTENTIAL ENVIRONMENTAL IMPACT

Simulation of mobilization of the finest particles into the water environment by filtering demonstrated that nano-sized particles were suspended in water for both types of the studied samples (pyrometallurgical sludges and brake wear debris). It was estimated that shaking for 24 hours and as well as for a much shorter time allows for the mobilization of nano-sized particles. According to the valid Czech legislation [129,130], the definition and evaluation of waste is based on leachability tests and determination of selected pollutants in the dry state [102]. This procedure does not enable obtaining sufficient information leading to the assessment of potential toxicity and mobility of individual pollutants.

According to Kukutschová's study [27] leachates prepared from pyrometallurgical sludges (BF, TF, and OC) were estimated to have the leachability class IIb. And the aquatic toxicity was estimated by 3 bioassays. Two standard tests were performed in accordance with the valid legislation – immobilization test (*Daphnia magna*) [131], inhibition of growth (*Scenedesmus subspicatus*) [132]. Moreover one test was carried out in accordance with EN ISO (*Vibro fisheri*) [133]. The results did not prove the aquatic toxicity of the studied samples (BF, TF, and OC) and this finding underestimates the real toxic potential of these materials due to the fact that all the sludges came into contact with water previously while the capturing of particles in wet scrubbers.

Mutagenicity was evaluated in vitro for all sludge samples by SOS chromotest by Kukutschová [27] as well. In the test without metabolic activation none of the measured samples showed mutagenic activity. However, when the metabolic activity was used (i.e biotransformation was simulated), the mutagenic activity was observed. Higher SOS inducing potency (SOSIP) showed the sample OC (~0.02 SOSIP), under 0.01 SOSIP were values for the TF and BF sample. After the treatment on hydrocyclone, blast furnace samples show higher values SOSIP for the BFO sample and lower for the BFU sample than value for the BF was estimated. This corresponds to the findings that less metal-based particles were found in dried water suspensions of BFU. Thus, the sludges were found to be potentially hazardous.

It is known that the exposure to fine particulate air pollutants affects human cardiovascular systems, e.g. levels of serum proteins associated with inflammation, homeostastis and thrombosis [96]. Perrenoud et al. estimated that airborne brake wear debris may have cardiovascular effects [134]. Peikertová et al. [135,136] also found changes in the immune response of human blood cells exposed to the airborne brake wear debris. The

phagocytic activity of monocytes was decreased when exposed to the two highest concentrations of particles (15 and 75 μg/cm^2). The decrease in proliferative activity of T-lymphocytes stimulated with PHA mitogen seems to be dose dependent [135,136].

However, only little information is known about the potential impact of airborne brake wear debris and even less is known about the nonairborne fraction of brake wear debris, which is considered large and makes them non inhalable. However, this thesis concluded that contact with water could easily release nano-sized particles, which represent higher potential risks, due to their increased surface area and a considerably higher reactivity with biomolecules [137]. The potency of wear particles for interacting with DNA after metabolic activation, which indicates the presence of indirect mutagens, was obtained by Kukutschová et al. [71]. Moreover it was revealed that wear debris was toxic (killing bacteria cells) after metabolic activation [71].

Inhibition of growth of green algae (*Desmodesmus subspicatus* and *Raphidocelis subcapitata*) was evaluated by Kučová [138] on the nonairborne brake wear debris of sample G6C. However, the value of the IC_{50} i.e. the required parameter of toxicity was not determined because a small amount of sample, thus test were not performed by leaching of the sample but using water suspensions. Heterogeneity of the samples caused the main issue during the tests and more attention should be paid to the homogenization of the sample [138].

Although at the first sight the pyrometallurgical sludges and brake wear debris may appear to be different materials, in this work it was proved that both easily released the nano-sized particles after a contact with water. The composition of the detected compounds show similarity in particles shape and chemistry, e.g. Ba was revealed in water treated sludges samples (TF, BF, BFO, and BFU) as well as in brake wear debris (G6C, G6C/KATI, and SMP2). The presence of barite was confirmed by Raman microspectroscopy.

According to the study by Querol et al. [89] barium is the best tracer of particles released from brakes. Barite is assumed as extremely insoluble and therefore poses no risk [139, 140]. Nevertheless, barite may undergo anaerobic sulfate reduction in soil environment caused by specific bacteria. *Desulfovibrio desulfuricans* are commonly found in aquatic environments as well as in water-logged soils. The reduction, leads to a higher Ba(II) ions mobility due to consumption of the sulfate anions for respiration in the bacterial cells [140, 141]. These microorganisms reduce sulfate to sulfide (see Figure 36) [142,143], which increases barium solubility [144]. Contrary to the inert barite Ba(II) ions are way less inert in terms of interactions with living systems. Free Ba(II) is generally toxic to bacteria, fungi,

mosses, and algae which may have adverse effects on soil fertility. Barium is also known as muscle poison to mammals [145].

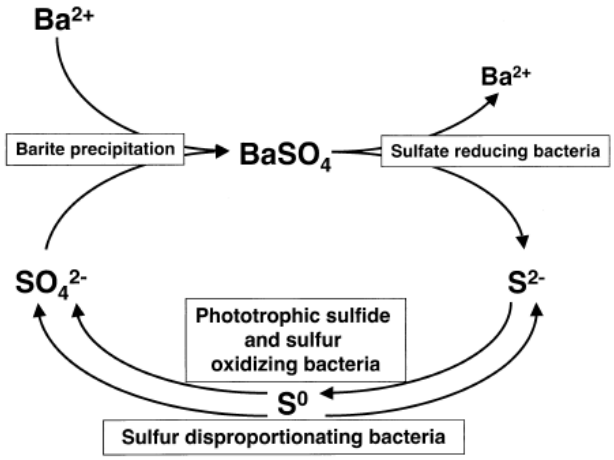

Figure 36: Bacterially mediated sulfur cycling reactions modulate the solubility of barite. Soluble barium can be released from barite by sulfate reducing bacteria and then reprecipitated as barite by bacterial processes that generate sulfate [146].

Iron was found in dried suspension of both type studied samples (sludge and wear), but its form was not revealed, either because very small size that is bellow the Raman detection limit, ionic form or due to the element form, which is Raman inactive, which is unlikely. The Fe(II) may participate in the Fenton reaction (see Figure 37), where the Fe(II) is oxidized by hydrogen peroxide to Fe(III), forming a hydroxyl radical and hydroxide ion in the process. Fe(III) is then reduced back to Fe(II) by another molecule of hydrogen peroxide, forming a superoxide radical and a proton. The free radicals generated by this process then engage in secondary reactions. For example pulmonary toxicity of inhaled dust particles is partially formed by hydroxyl radical caused by the presence of the iron ions onto the surfaces of the dust particles [147]. The presence of metals and reactive oxygen species (ROS) in cells may cause oxidative stress, which leads to biomolecules damage [148].

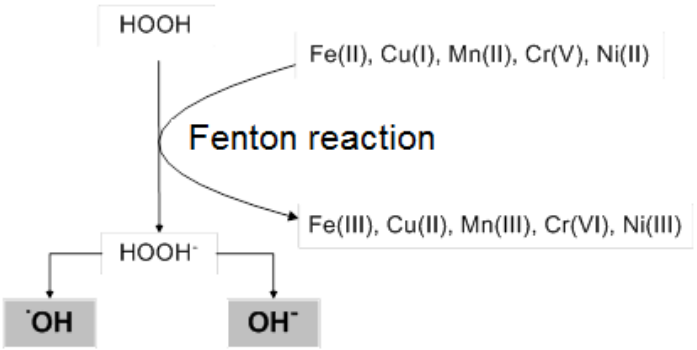

Figure 37: Scheme of Fenton reaction modified from [147].

Also antimony pentoxide (Sb_2O_5) and Laves Sb_2Fe phase were formed from antimony trisluphide (Sb_2S_3) during the braking [73,74]. According to the International Agency for Research on Cancer (IARC), Sb_2S_3 is not classified as a carcinogen to humans, but the antimony oxides are classified as potential carcinogenic. The toxicity of antimony compounds depends on their solubility and their valence, where $Sb^{(V)}$ is less toxic than $Sb^{(III)}$ [72].

Our previous studies also evaluated presence of metal-based particles in samples of some human tissues (tonsilar with tonsilitis, tonsilar squamous cell carcinoma, brain tissue – glioblastoma, etc.) and body fluids (amniotic fluids). In the study by Bielnikova et al. and Zelenik et al., the particles sizes were within the range of 500 nm to 25 μm. Metals, such as (Fe, Cu, Zn, Sn, Ba, Sb, and Ti) were found in these samples of human tissues and body fluids, and could be related to the combustion of fossil fuels or by friction processes during braking of automobiles [149,150]. The study by Peikertová determined the presence of Cu, Fe (see Figure 38), and Zn in amniotic fluids [151]. Thus it could be concluded that the nano-sized metal based particles which were not found in the samples of human tissues or body fluids naturally, but it is difficult to determine the exact source of these particles.

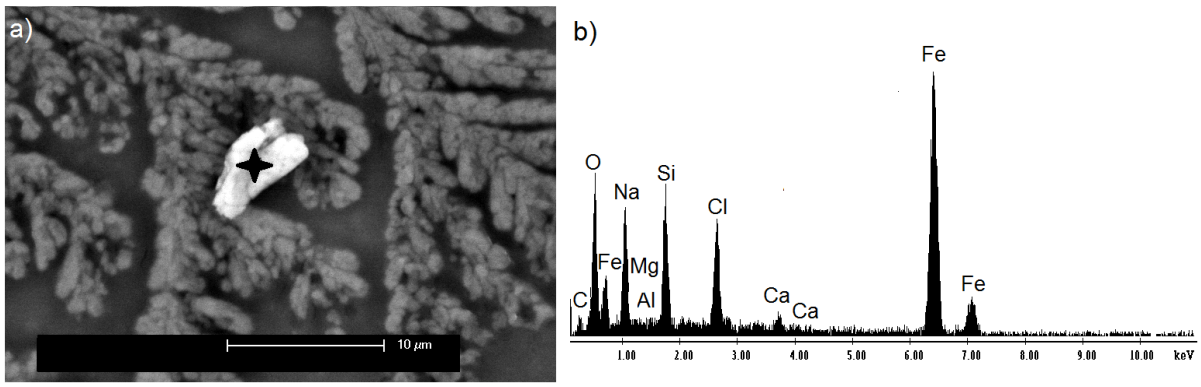

Figure 38: SEM image of particle detected in amniotic fluid (A) with EDS pattern of point analysis (B) [151].

Therefore it is very complicated to determine the environmental impact of brake wear debris *in situ*, because, as was confirmed, the origin of the detected particles in soil, water, plants and animal samples is difficult to distinguish. Moreover, there little information is available about the phase composition of metal-based compounds in human tissues and body fluids samples. Only the element compositions are evaluated in majority.

Same types of particles with similar chemistry were determined in both type of studied samples (pyrometallurgical sludges and brake wear debris). Thus the research should be targeted to characterization and evaluation of the potential impact of brake wear debris

collected after full-scale dynamometer test for better understanding of their complex impact in the environment.

Although the similarity of the detected elements and compounds was observed the potential hazard of the pyrometallurgical sludges is known and the sludges are disposed of with appropriate precautions (controlled waste dumps). However, the brake wear debris has not such a treatment, because they settle in the road surfaces and vicinity of the roads (nonairborne fraction) or are directly released into the air (airborne fraction). Both released fractions contain nano-sized metal-based particles, which afterwards may enter the soils, water systems, biogeochemical cycles and also food chain. Therefore this field requires further attention focused on the determination of brake wear impact to the environment and developing new eco-friendly materials which will not contain or create hazardous components thus pose no risks to the environment. In case of pyrometallurgy sludges further attention should be focused on recycling of the generated wastes or safe disposal/storage.

6. CONCLUSIONS

In the presented thesis the mobility in water, morphology and chemistry of the nano-sized particles released from selected pyrometallurgical sludges and brake wear debris were experimentally evaluated. Five selected pyrometallurgical sludges (blast furnace, blast furnace overflow, blast furnace underflow, tandem furnace, and oxygen converter sludges), wear debris from two model automotive brake pads (G6C and G6C/KATI), and wear debris from two commercial automotive brake pads (SMP1 and SMP2) were water treated and characterized by a combination of analytical techniques (SEM-EDS, XRPD, FTIR and Raman microspectroscopy). Suspensions of pyrometallurgical sludges were prepared by leaching and sedimentation in liquid to solid ratio 10:1 according to the European Standard. Due to a small amount of brake wear debris only sedimentation was used for suspensions preparation in liquid to solid ratio 100:1.

Various analytical techniques applied demonstrated various capacities in the particle detection. However a very good accordance of the results was observed and in complexity provides very good information about the released particles. All the initial samples were characterized by the FTIR spectroscopy, Raman microspectroscopy, XRPD, and SEM-EDS. Iron was the most abundant element in the samples of pyrometallurgical sludges as well as brake wear debris, and it was mainly present in the form of iron oxides (Fe_2O_3 and Fe_3O_4) or Fe(0) in case of brake wear debris which could have a core shell structure, because zerovalent iron is highly reactive. XRPD and Raman microspectroscopy were more beneficial than FTIR spectroscopy in the determination of the phase composition of these samples. FTIR spectroscopy reveal the presence of only the main functional groups in the case of pyrometallurgical sludges, but in case of brake wear debris it was less effective probably due to high amounts of amorphous components.

This thesis as one of the few used Raman microspectroscopy for phase determination of the pyrometallurgical sludges and brake wear debris. Raman spectroscopy with microscope combination is a very suitable technique for phase determination of multicomponent samples, because the point analysis, which enables to obtain a spectrum from a single point. Thus it is an advantage in case of nonhomogeneous samples. But fluorescence caused problems in the measurements.

Simulation of mobilization of the finest particles in water environments by filtering demonstrated that nano-sized particles were suspended in water after filtration and shaking for 24 hours and as well as for a much shorter time allows the mobilization of nano-sized particles. Presence of various metal based particles in water suspensions point to the

heterogeneous character of the suspension, thus filtered aqueous leachate is inaccurately considered homogeneous.

The combination of analytical techniques (Raman microspectroscopy, SEM-EDS, and TEM) revealed the presence of several metal-based and crystalline compounds in water suspensions. Particle size distributions were evaluated only for the suspensions of pyrometallurgical sludges, because the suspensions of brake wear debris were much diluted, which corresponds to the fact that brake wear debris suspension were prepared in liquid to solid ratio 100:1, while the pyrometallurgical sludges were prepared in ratio 10:1.

Although the pyrometallurgical sludges and brake wear debris may appear to be different materials at the first sight, similar compounds and elements were found in both samples types (e.g. $BaSO_4$, $FeCO_3$, TiO_2, $Na_2Ca(SO_4)_2$), also the iron was most abundant element detected by SEM-EDS in initial samples. Pyrometallurgical sludges rank among the category "N" (dangerous waste) and are stored in the special monitoring places. On the other hand, brake wear debris is uncontrollably released to the environment in two fractions (airborne and nonairborne). Both the fractions may contain nano-sized particles, and the mobility of nano-sized particles in water environment from nonairborne wear debris was proved. Brake wear is ubiquitous due to increasing road traffic and their potential environmental risk is still not clear. For example barium, which is assigned as brake wear tracer, was found in suspension of G6C, G6C/KATI, and SMP1, but as well as in the following samples (TF, BF, BFO, and BFU). Raman microspectroscopy reveals barite presence and undergoes anaerobic sulfate reduction in soil environment caused by specific bacteria, which could lead to higher Ba(II) ions mobility, which is generally toxic to bacteria, fungi, mosses, and algae which may have adverse effects on soil fertility and barium is also known as muscle poison to mammals.

The thesis provides new insights into the mobility of nano-sized particles present in pyrometallurgical sludges and nonairborne brake wear debris. Moreover, it was demonstrated that, the Raman microspectroscopy is a very suitable technique for detection of phase composition of multicomponent samples and particles in dried suspensions. From the obtained results it could be seen that both type materials could easily release nano-sized metal-based particles into the water and more attention should be focused on the determination of brake wear impact to the environment and developing new eco-friendly materials which will not contain or create hazardous components and in case of pyrometallurgy sludges further attention should be focused on recycling of the generated wastes or their safe disposal/storage.

6.1 CONCLUSIONS IN CZECH

V předkládané práci byla hodnocena morfologie, chemické složení a mobilita ve vodném prostředí nanometrických částic uvolňovaných z vybraných pyrometalurgických odpadů a brzdného otěru. Pět vybraných pyrometalurgických kalů (vysokopecní kal, vysokopecní kal přepad z hydrocyklonu, vysokopecní kal výtok z hydrocyklonu, kal z tandemové pece a kal z kyslíkového konvertoru), brzdový otěr ze dvou modelových brzdových destiček (G6C a G6C/KATI) a brzdný otěr ze dvou komerčních brzdových destiček (SMP1 a SMP2) byly charakterizovány stejnými analytickými technikami (SEM-EDS, XRPD, FTIR a Ramanovou mikrospektroskopií). Z těchto vzorků byly připraveny vodné suspenze a to formou výluhu v případě pyrometalurgických kalů a sedimentací u obou typů vzorků. Vodné výluhy u pyrometalurgických vzorků byly připraveny v poměru kapalné a pevné fáze 10:1, stejně tak suspenze připravené sedimentací. Vzhledem k velmi malému množství brzdného otěru byly suspenze připraveny v poměru kapalné a pevné fáze 100:1.

Rozdílné analytické techniky prokázaly různou účinnost při detekci uvolněných nanometrických částic, přesto byla ve výsledcích dosažená velmi dobrá shoda. Všechny původní vzorky byly charakterizovány FTIR, Ramanovou mikrospektroskopií, XRPD a SEM-EDS. Nejčastějším nalezeným prvkem ve vzorcích pyrometalurgických kalů, stejně jako ve vzorcích brzdného otěru, bylo železo a to ve formě Fe(0) v případě brzdného otěru a i ve formě jeho železných oxidů (Fe_2O_3 a Fe_3O_4) u obou typů vzorků. XRPD a Ramanova spektroskopie se projevily jako mnohem užitečnější techniky při určování složení daných vzorků, než FTIR spektroskopie. FTIR spektroskopie odhalila pouze hlavní složky studovaných vzorků pyrometalurgických kalů, ale v případě vzorků brzdného otěru byla ještě méně efektivní, pravděpodobně protože vzorky obsahují větší podíl amorfních složek.

Tato práce se jako jedna z mála zaměřuje na charakterizaci pyrometalurgických kalů a brzdného otěru pomocí Ramanovy mikrospektroskopie. Ramanova spektroskopie v kombinaci s mikroskopem je velmi užitečná technika pro fázové určení nehomogenních vzorků, jelikož bodová analýza umožňuje sejmout spektrum z jednoho konkrétního bodu. Ale při těchto měřeních, ale fluorescence vzorků tvoří velký problém.

Simulace mobilizace nanometrických částic do vodného prostředí po filtraci ukázala, že nanometrické částice jsou suspendovány do vodného prostředí i po filtraci a třepání i po podstatně méně než 24 hodin umožňuje mobilizaci nanometrických částic. Detekovaná přítomnost částic na bázi kovů ve vodné suspenzi ukazuje na heterogenní charakter vodné suspenze a tedy vodný výluh je nesprávně považován za homogenní.

Suspenze byly opět charakterizovány různými analytickými technikami (Ramanova mikrospektroskopie, SEM-EDS a TEM) a odhalily přítomnost kovových a krystalických složek. Distribuce velikosti částic byla stanovena jen u suspenzí připravených z pyrometalurgických kalů. Suspenze připravené z brzdného otěru byly příliš zředěné a nepodařilo se obdržet relevantní data. Toto odpovídá tomu, že suspenze z brzdného otěru byly připravovány v poměru 100:1, kdežto suspenze z pyrometalurgických kalů byly připraveny v poměru 10:1.

Ačkoliv se na první pohled může zdát, že pyrometalurgické kaly a brzdný otěr jsou dva úplně rozdílné materiály, přesto byly v obou typech vzorků nalezeny stejné sloučeniny a prvky (např. $BaSO_4$, $FeCO_3$, TiO_2, mix síranů a další). Pyrometalurgické kaly jsou řazeny do kategorie N (nebezpečný odpad) a jsou skladovány na speciálních místech a monitorovány. Naproti tomu brzdný otěr je nekontrolovatelně uvolňován do prostředí a to ve dvou frakcích („airborne“ a „nonairborne“). Obě frakce obsahují nanometrické částice a mobilita nanometrických částic z frakce „nonairborne“ byla v této práci prokázána. Díky rozšiřující se dopravě je brzdný otěr téměř všudypřítomný a jeho potenciální dopady na životní prostředí nejsou zatím zcela známy. Například barium, které je považováno za indikátor brzdného otěru, bylo nalezeno ve formě barytu Ramanovou mikrospektroskopií jak v otěru z modelových brzdových destiček (G6C a G6C/KATI), tak v komerčních vzorcích (SMP1). V půdě může být tak při anaerobické redukcí síranu přeměněno na barnaté ionty specifickými bakteriemi. Barnaté ionty jsou obecně toxické pro bakterie, plísně, mechy, řasy ale také jsou známy jako svalový jed pro savce.

Předkládaná práce přináší nový pohled na mobilitu nanometrických částic přítomných ve vzorcích pyrometalurgický kalů a „nonairborne“ brzdného otěru. Ukazuje, že Ramanova mikrospektroskopie prokazuje velmi dobrou účinnost při detekci složek multikomponentních vzorků a stejně jako při detekci částic uvolněných do vodného prostředí. Z dosažených výsledků vyplývá, že oba dva typy studovaných materiálů mohou jednoduše po kontaktu s vodou uvolňovat do okolí nanometrické částice na bázi kovů a další pozornost by měla být věnována v případě brzdného otěru vývoji nových materiálů, které nebudou obsahovat nebo uvolňovat do prostředí nebezpečné složky. V případě pyrometalurgických kalů by se pozornost měla dále věnovat recyklaci nebezpečných odpadů a případně jejich bezpečnému skladování, nebo likvidaci.

7. LIST OF REFERENCES

[1] History of Metallurgy. *History Worlds*. [online]. [cit. 20014-06-20]. Available from *http://www.historyworld.net/wrldhis/PlainTextHistories.asp?ParagraphID=ahh*.

[2] Tylecote R. F. *A History of Metallurgy*. London: Institute of materials, 1992. ISBN 0-901462-88-8.

[3] von Zittel K.A. *History of Geology and Palaeontology*. London: W.Scott, 1901.

[4] *The Great Soviet Encyclopedia*. 1979.

[5] Almaula S. Polycyclic Aromatic Hydro Carbons from Steelmaking. *Environmental Forensics* 6 (2005) 143-150.

[6] 185/2001 Sb. *Zákon o odpadech a o změně některých dalších zákonů*, 2001.

[7] Directive 2008/98/EC on Waste. *Waste Framework Directive*, 2008.

[8] 381/2001 Sb. *Vyhláška MŽP, kterou se stanoví Katalog odpadů, Seznam nebezpečných odpadů a seznamy odpadů a států pro účely vývozu, dovozu a trnazitu odpadů a postup při udělování souhlasu k vývozu, dovozu a tranzitu odpadů* (*Katalog odpadů*), 2001.

[9] Kret J. *Recyklace odpadů hutnictví železa*. Ostrava: VŠB – Technická univerzita Ostrava, 2003. ISBN 80-248-0511-1.

[10] Kursa M., Kárník T., Krištofová D., Leško J., Kret J., Botula J. Possibilities of Non-Ferrous Metals Removing from Fine-grain Metallurgical Wastes, In: *Conference Proceedings METAL 2000*. ISBN 80-85988-48-8.

[11] Řepka V., Botula J., Samková R. Odpady z výroby železa a oceli a jejich recyklace. *Acta Metallurgica Slovaca* 12 (2006) 334-337.

[12] Řepka V., Botula J., Kret J., Kursa M., Leško J., Vidlář J. Recyklace hutnických odpadů ze starých zátěží. *Final report of project GAČR 106/01/0122,* Ostrava: VŠB- Technická univerzita Ostrava, 2003.

[13] Le Guédard M., Faure O., Bessoule J.-J. Early Changes in the Fatty Acid Composition of Photosynthetic Membrane Lipids from *Populus nigra* Grown on a Metallurgical Landfill. *Chemosphere* 88 (2012) 693-698.

[14] Le Guédard M., Faure O., Bessoule J.-J. Soundness of *in situ* Lipid Biomarker Analysis: Early Effect of Heavy Metals on Leaf Fatty Acid Composition of *Lactuca serriola*. *Environmental and Experimental Botany* 76 (2012) 54-59.

[15] Venditti D., Durécu S., Berthelin J. A Multidisciplinary Approach to Assess History, Environmental Risks and Remediation Feasibility of Soils Contaminated by Metallurgical Activities. Part A: Chemical and Physical Properties of Metals and Leaching Ability. *Archives of Environmental Contamination and Toxicology* 38 (2000) 411-420.

[16] Venditti D., Berthelin J., Durécu S. A Multidisciplinary Approach to Assess History, Environmental Risks and Remediation Feasibility of Soils Contaminated by Metallurgical Activities. Part B: Direct Metal Speciation in the Solid Phase. A*rchives of Environmental Contamination and Toxicology* 38 (2000) 421-427.

[17] Buondonno C., Ermice A., Buondonno A., Murolo M., Pugliano M.L. Human-influenced Soils from an Iron and Steel Works in Naples, Italy. *Soil Science Society American Journal* 62 (1998) 694-700.

[18] Adamo P., Arienzo M., Bianco M.R., Terrible F., Violante P. Heavy Metal Contamination of the Soil Used for Stocking Raw Materials in the Former ILVA Iron Steel Industrial Plant of Bagnoli (southern Italy). *The Science of the Total Environment* 295 (2002) 17-34.

[19] Welch R.M. Micronutrient Nutrition of Plants. *Critical Reviews in Plants Science* 14 (1995) 49-82.

[20] Ernst W.H.O. Bioavailability of Heavy Metals and Decontamination of Soils by Plants. *Applied Geochemistry* 11 (1996) 163-167.

[21] Kursa M., Kursová M., Řepka V. Charakteristika jemnozrnných hutních odpadů z hlediska jejich vlivu na životní prostředí a využití jako suroviny na výrobu kovů. In: *Conference Proceedings METAL 2002.* ISBN 80-85988-76-3.

[22] Fleischanderl A., Pesl J., Gebert W., Heckmann H. Converting Wastes into Profit: Recycling of Steel Mill Wastes Through BOF/BF, RMF and COREEX-technology. In: *Learn Strategies for Coping with Steel Mill Wastes and Profiting from By-products*, 1999.

[23] Rehmat A., Mesinger M.C. Recovery of Direct Reduced Iron From Blast Furnace Dust. In: *Second international symposium on extraction and processing for the treatment and minimization of wastes*, 1996.

[24] van Herck P., Vandeasteele C., Swennen R., Mortier R. Zinc and Lead Removal from Blast Furnace Sludge with a Hydrometallurgical Process. *Environmental Science and Technology* 34 (2000) 3802-3808.

[25] Brož L. *Hutnictví železa*. Praha: SNTL, 1988.

[26] Mansfeldt T., Dohrmann R. Chemical and Mineralogical Characterization of Blast-furnace Sludge from Abandoned Landfill. *Environmental Science and Technology* 38 (2004) 5977-5984.

[27] Kukutschová J. *Hodnocení toxicity a mutagenity jemnozrnných metalurgických odpadů*. Ostrava, 2007. Dissertation thesis (PhD.). VŠB- Technická univerzita Ostrava. Fakulta metalurgie a materiálového inženýrství.

[28] Vereš J., Jakabský Š., Šepelák V. Chemical, Physical, Morphological and Structural Characterization of Blast Furnace Sludge. *Diffusion Fundamentals* 12 (2010) 88-91.

[29] Diner V., Kuraš M., Slivka V. *Odpadové hospodářství I.: praktická příručka*, Ostrava: VŠB – Technická univerzita Ostrava, 2006. ISBN 80-284-1245-2.

[30] Hlavatá M. *Odpadové hospodářství.* Ostrava: VŠB – Technická univerzita Ostrava, 2004. ISBN 80-248-0737-8.

[31] Council Directive 96/61/EC. *Integrated Pollution Prevention and Control (IPPC)*, 1996.

[32] Best Available Techniques Reference Document on the Production of Iron and Steel. *Registro Estatal de Emisiones y Fuentes Contaminantes.* [online] 2001 [cit. 2014-06-20]. Available from: http://www.prtr-es.es/data/images/siderurgia-c8226acf25c30184.pdf

[33] Das B., Prakash S., Reddy P.S.R., Misra V.N. An Overview of Utilization of Slag and Sludge from Steel Industries. *Resources, Conservation and Recycling* 50 (2007) 40-57.

[34] Dvořák P., Jandová J. Recycling of Blast Furnace and Basic Oxygen Furnace Dust. *Waste Forum* 6 (2002) 22-24.

[35] Hydrocyclones. *The Institute of Mining & Metallurgy Equipment, Changsha Research Institute of Mining & Metallurgy*. [online]. 2009 [cit. 2014-06-20]. Available from: *http://en.chinakyzb.com/news/en/kyzbProductsEn/2012/1025/1210251010407ADC604KE8G9DBE1713.html.*

[36] Kursa M. Komplexní výzkum jemnozrnných hutních odpadů. *Final report of project PZ – 01/30/98*. Ostrava: VŠB-TU Ostrava, 1998.

[37] Kursa M. Komplexní výzkum jemnozrnných hutních odpadů. *Final report of project PZ – 01/30/98,* Ostrava: VŠB-TU Ostrava, 1999.

[38] Řepka V., Botula J. Possibilities of recycling of fine-grained metallurgical wastes from old waste depots. *Sborník vědeckých prací VŠB- Technická univerzita Ostrava* 51 (2005) 55-60.

[39] Melecký J., Čtvrtníček A. Technologické ověření hydrometalurgického zpracování cyklovaných ocelárenských úletů. *Hutník* 39 (1989) 166-173.

[40] Gabor R., Seidlerová J. Zhodnocení aplikací postupů vyluhovatelnosti Zn, Cd, Pb, Cr pro jemnozrnné metalurgické kaly. *Chemické listy* 106 (2012) 773-776.

[41] European vehicle market statistics. *The International Council on Clean Transportation*. [online]. 2013 [cit. 2014-06-20]. Available from: *http://www.theicct.org/sites/default/files/publications/EU_vehiclemarket_pocketbook_2013_Web.pdf*

[42] Regulation 715/2007. *Euro V Standards*, 2009.

[43] Regulation 715/2007. *Euro VI Standards*, 2014.

[44] Kittelson D.B. Engines and Nanoparticles: A Review. *Journal of Aerosol Science* 29 (1998) 575-588.

[45] Raber L.R. EPA's Air Standards. *Chemical and Engineering News* 14 (1997) 10-18.

[46] Dockery D.W., Pope C. A., Xu X., Spengler J.D., Ware J.H., Fay M.E., Ferris, Jr. B.G., Speizer F.E. An Association between Air Pollution and Mortality in Six U.S. Cities. *The New England Journal of Medicine* 329 (1993) 1753-1759.

[47] Pope C. A., Thun M.J., Namboodiri M.M., Dockery D.W., Evans J.S., Spezier F.E., Heath C.W. Particulate Air Pollution as a Predictor of Mortality in a Prospective Study of U.S. Adults. *American Journal of Respiratory and Critical Care Medicine* 151 (1995) 669-674.

[48] Ruzer L.S., Halley N.H. *Aerosols Handbook: Measurements Dosimetry, and Health Effects*. Florida: CRC Press, 2005. ISBN 1-56670-611-4.

[49] Thorpe A., Harrison R.M. Sources and Properties of Non-exhaust Particulate Matter from Road Traffic: A Review. *Science and Total Environment* 400 (2008) 270-282.

[50] Vaněk T. *Brzdy osobních silničních vozidel a jejich diagnostika*. Pardubice, 2008. Thesis (Ing.). Univerzita Pardubice. Dopravní fakulta Jana Pernera.

[51] Tomášek V. *Frikční kompozity pro brzdové systémy automobilů a metody jejich charakterizace*, Ostrava: VŠB-Technická univerzita Ostrava, 2009. ISBN 978-80-248-2085-9.

[52] Lee L. *Contribution to development of copper-free automotive brake pads*. Carbondale, 2013. Thesis. Southern Illinois University. Center for Advanced Friction Studies.

[53] Bečka J. *Tribologie*. Praha: Vydavatelství ČVUT, 1997. ISBN 80-01-01621-8.

[54] Eriksson M., Bergman F., Jacobson S. On the Nature of Tribological Contact in Automoitive Brakes. *Wear* 252 (2002) 26-36.

[55] Sanders P.G., Dalka T.M., Xu N., Maricq M.M., Basch R.H. Brake Dynamometer Measurement of Airborne Brake Wear Debris. In: *World Congress Detroit, Michigan 2002*. Society of Automotive Engineers, Inc.

[56] Eriksson M., Jacobson S. Tribological Surfaces of Organic Brake Pads. *Tribology International* 33 (2000) 817-827.

[57] Handa Y., Kato T. Effects of Cu Powder, $BaSO_4$ and Cashew Dust on the Wear and Friction Characteristics of Automotive Brake Pads. *Tribology Transactions* 39 (1996) 346-353.

[58] Zhao Y., Lu Y., Wright M.A. Sensitivity Series and Friction Surface Analysis of Non-Metallic Friction Materials. *Materials and Design* 27 (2006) 833-838.

[59] Lu Y. A combinatorial Approach of Automotive Friction Materials: Effects of Ingredients on Friction Performance. *Composites Science and Technology* 66 (2006) 591-598.

[60] Ostermeyer G.P., Müller M. Dynamic Interaction of Friction and Surface Topography in Brake Systems. *Tribology International* 39 (2006) 370-380.

[61] Sai Balaji M.A., Kalaichelvan Dr.K. Optimization of a Non Asbestos Semi Metallic Disc Brake Pad Formulation with Respect to Friction and Wear. *Procedia Engineering*, 38 (2012) 1650-1657.

[62] Filip P., Kovarik L., Wright M.A. Automotive Brake Lining Characterization. In: *Proceedings of the 15th Annual SAE Brake Colloquium*, Warrendale, 1997.

[63] Querol X., Alastuey A., Ruiz C.R., Artiñano A., Hansson H.C., Harrison R.M., Buringh E., ten Brink H.M., Lutz M., Bruckmann P., Straehl P., Schneider J. Speciation and

Origin of PM_{10} and $PM_{2.5}$ in Selected European Cities. *Atmospheric Environment* 38 (2004) 6547-6455.

[64] Sanders P.G., Xu N., Dalka T.M., Maricq M.M. Airborne Brake Wear Debris: Size, Distribution, Composition and a Comparison of Dynamometer and Vehicle Test. *Environmental Science and Technology* 37 (2003) 4060-4069.

[65] Garg B.D., Cadle S.H., Mulawa P.A., Groblicki P.J. Brake Wear Particulate Emissions. *Environmental Science and Technology* 34 (2000) 4463-4469.

[66] Kukutschová J., Moravec P., Tomášek V., Matějka V., Smolík J., Schwarz J., Seidlerová J., Šafářová K., Filip P. On Airborne Nano/Micro Sized Wear Particles Released from Low-metallic Automotive Brakes. *Environmental Pollution* 159 (2011) 998-1006.

[67] Oberdörster G., Oberdörster E., Oberdörster J. Nanotoxicology: an Emerging Discipline Evolving from Studies of Ultrafine Particles. *Environmental Health Perspectives* 113 (2005) 823-829.

[68] Sternbeck J., Sjödin Å., Andréasson K. Metal Emissions from Road Traffic and the Influence of Resuspension – Results from Two Tunnel Studies. *Atmospheric Environment* 36 (2002) 4735-4744.

[69] Balakrishna S., Lomnicki S., McAvey K.M., Cole R.B., Delinger B., Cormier S.A. Environmentally Persistent Free Radicals Amplify Ultrafine Particle Mediated Cellular Oxidative Stress and Cytotoxicity. *Particle and Fibre Toxicology* 6 (2009) 11.

[70] Peikertová P., Kukutschová J., Vávra I., Matějka V., Životský O., Vaculík M., Lee P.W., Filip P. Water Suspended Nanosized Particles Released from Nonairborne Brake Wear Debris. *Wear* 306 (2013) 89-96.

[71] Kukutschová J., Roubíček V., Malachová K., Pavlíčková Z., Holuša R., Kubačková J., Mička V., MacCrimmon D., Filip P. Wear Mechanism in Automotive Brake Materials, Wear Debris and its Potential Environmental Impact. *Wear* 267 (2009) 807-817.

[72] Uexküll O., Skerfving S., Doyle R., Braungart M. Antimony in Brake Pads – a Carcinogenic Component?. *Journal of Cleaner Production* 13 (2005) 19-31.

[73] Matějka V., Lu Y., Matějková P., Smetana B., Kukutschová J., Vaculík M., Tomášek V., Zlá S., Fan Y. Possible Stibnite Transformation at the Friction Surface of the Semi-metallic Friction Composites Designed for Car Brake Linings. *Applied Surface Science* 258 (2011) 1862-1868.

[74] Jang H., Kim S.J. The Effects of Antimony Trisulfide (Sb_2S_3) and Zirconium Silicate ($ZrSiO_4$) in the Automotive Brake Friction Material on Friction Characteristics. *Wear* 239 (2000) 229-236.

[75] Lee P.W., Filip P. Friction and Wear of Cu-free and Sb-free Environmental Friendly Automotive Brake Materials. *Wear* 302 (2013) 1404-1413.

[76] Characterization of Airborne Brake Wear Debris. *Sustainable Conservation*. [online]. 2006 [cit. 2014-06-20]. Available from: http://www.suscon.org/bpp/pdfs/ADPSDAmendedFinalReport(Jan2006).pdf

[77] Denier van der Gon H.A.C, Hulskotte J.H.J., Visschedijk A.J.H., Schaap M. A Revised Estimate of Copper Emissions from Road Transport in UNECE-Europe and its Impact on Predicted Copper Concentrations. *Atmospheric Environment* 41 (2007) 8697-8710.

[78] Brake Pad Partnership. *Sustainable Conservation*. [online]. 2010 [cit. 2014-06-20]. Available from: http://www.suscon.org/bpp/index.php.

[79] A Metal Whose Use Dates Back Centuries Continues to Fulfill Essential Needs Today – and Standards rom ASTM Committee B05 Address its Applications. ASTM Standardization News, September/October 2010.

[80] Limiting the use of certain substances in brake friction material. *Washington State Legislature*. [online]. 2010 [cit. 2014-06-20]. Available from: http://apps.leg.wa.gov/documents/billdocs/2009-10/Pdf/Bill%20Reports/Senate/6557-S%20SBR%20FBR%2010.pdf

[81] Hazardous materials: motor vehicle brake friction materials. *Official California Legislative Information*. [online]. 2010 [cit. 2014-060-20]. Available from: /http://www.leginfo.ca.gov/pub/09-10/bill/sen/sb_0301-0350/sb_346_bill_20100927_chaptered.pdf

[82] Relating to Roadway Particulate Matter Pollution Control. *Hawaii State Legislature*. [online]. 2012 [cit. 2014-06-20]. Available from: http://www.capitol.hawaii.gov/session2012/bills/SB2342_.HTM

[83] Relating to Motor and Other Vehicles – Brake Friction Material. *State of Rhode Island General Assembly*. [online]. 2010 [cit. 2014-06-20]. Available from: http://webserver.rilin.state.ri.us/BillText/BillText10/HouseText10/H7997.pdf.

[84] Botula J., Řepka V. Možnosti recyklace jemnozrnných hutních odpadů ze starých zátěží. *Conference Proceedings METAL2002,* 2002.

[85] Remon E., Bouichardon J.-L., Cornier B., Guy B., Leclerc J.-C., Faure O. Soil Characteristics, Heavy Metal Availability and Vegetation Recovery at a Former Metallurgical Landfill: Implications in risk Assessment and Site Restoration. *Environmental Pollution* 137 (2005) 316-323.

[86] Karvosenoja N., Tainio M., Kupiainen K., Tuomisto J.T., Kukkonen J., Johansson M. Evaluation of the Emissions and Uncertainties of $PM_{2.5}$ Originated from Vehicular Traffic and Domestic Wood Combustion in Finland. *Boreal Environment research* 13 (2008) 465-474.

[87] Weckwerth G. Origin of Fine Dust in Urban Environmental Zones – Evidence from Element Patterns Received by Dichotomous Collection and INAA. *Applied Radiation and Isotopes* 68 (2010) 1878-1883.

[88] Varrica D., Bardelli F., Dongarrà D., Tamburo E. Speciation of Sb in Airborne Particulate Matter, Vehicle Brake Linings, and Brake Pad Wear Residues. *Atmospheric Environment* 64 (2013) 18-24.

[89] Querol X., Viana M., Alastuey A., Amato F., Moreno T., Castillo S., Pey J., de la Rosa J., Sánchez de la Campa A., Artíñano B., Salvador P., García Dos Santos S., Fernández-Patier R., Moreno-Grau S., Negral L., Minguillón M.C., Monfort E., Gil J.I., Inza A., Ortega L.A., Santamaría J.M., Zabalza J. Source Origin of Trace Elements in PM from Regional Background, Urban and Industrial Sites of Spain. *Atmospheric Environment* 41 (2007) 7219-7231.

[90] Dongarrà G., Manno E., Varrica D. Possible Markers of Traffic-related Emissions. *Environmental Monitoring and Assessment* 154 (2009) 117-125.

[91] Fernández-Espinosa A.J., Ternero-Rodríguez M. Study of Traffic Pollution by Metals in Seville (Spain) by Physical and Chemical Speciation Methods. *Analytical and Bioanalytical Chemistry* 379 (2004) 684-699.

[92] Oral information: Peter Filip, Professor for Materials Engineering, Centre for Advanced Friction Studies, Southern Illinois University Carbondale, Illinois, USA, 2013.

[93] Verma A., Singh S.N. Biochemical and Ultrastructural Changes in Plant Foliage Exposed to Auto-pollution. *Environmental Monitoring and Assessment* 120 (2006) 585-602.

[94] Naszradi T., Badacsonyi A., N´meth N., Tuba Z., Batič F. Zinc, Lead and Cadmium Content in Meadow Plants and Mosses Along the M3 Motorway (Hungary). Journal of Atmospheric Chemistry 49 (2004) 593-603.

[95] Sandahl J.F., Baldwin D.H., Jenkins J.J., Scholtz N.L. A Sensory System at the Interface between Urban Stormwater Runoff and Salmon Survival. *Environmental Science and Technology* 41 (2007) 2998-3004.

[96] Riediker M., Devlin R.B., Griggs T.R., Herbst M.C., Bromberg P.A., Williams R.W., Cascio W.E. Cardiovascular Effects in Patrol Officers are Associated with Fine Particulate Matter from Brake Wear and Engine Emissions. *Particle and Fibre Toxicology* 1 (2004) 1-10.

[97] Mamulová Kutláková K., Tokarský J., Kovář P., Vojtěšková S., Kovářová A., Smetana B., Kukutschová J., Čapková P., Matějka V. Preparation and Characterization of Photoactive Composite Kaolinite/TiO_2. *Journal of Hazardous Materials* 188 (2011) 212-220.

[98] Peikertová P., Rebilasová S., Gröplová K., Kukutschová J., Matějka V. Raman Study of Clay/TiO_2 Nanocomposites. *In:* NANOCON 2011 Conference proceedings, Ostrava: Tanger, Ltd., 2011, 293-297. ISBN 978-80-87294-23-9.

[99] Gröplová K., Rebilasová S., Peikertová P., Kukutschová J., Matějka V. Toxicity Assessment of Vermiculite/TiO_2 and Bentonite/TiO_2 Composites Using Green Algae Desmodesmus Subspicatus. *In:* NANOCON 2011 Conference proceedings, Ostrava: Tanger, Ltd., 2011, 655-658. ISBN 978-80-87294-23-9.

[100] Rebilasová S., Peikertová P., Gröplová K., Neuwirthová L. The Influence of Mechanical Treatment of Vermiculite on Preparation Composites Vermiculite/TiO_2. *In:* NANOCON 2011 Conference proceedings, Ostrava: Tanger, Ltd., 2011, 427-432. ISBN 978-80-87294-23-9.

[101] Dědková K., Matějová K., Lang J., Peikertová P., Mamulová Kutláková K., Neuwirthová L., Frydrýšek K., Kukutschová J. Antibacterial Activity of Kaolinite/NanoTiO_2 Composites in Relation to Irradiation Time, *Journal of Photochemistry and Photobiology B: Biology* 135 (2014) 17-22.

[102] European Standard EN 12457-4:2002: Characterization of waste – Leaching – Compliance test for leaching of granular waste materials and sludges – Part 4: One stage batch test at a liquid to solid ratio of 10 l/kg for materials with particle size below 10 mm (without or with size reduction), 2002.

[103] Welch P.S. *Limnology*. New York: McGraw-Hill Book Co. Inc. 1935.

[104] American Water Works Association, *Water Quality and Treatment: a Handbook of Public Water Supplies*, New York: Mc Graw-Hill Co. Inc. 1971.

[105] Larkin P.J. IR and Raman Spectroscopy; Principles and Spectral Interpretation. New York: Elsevier Inc. 2011. ISBN 978-0-12-386984-5.

[106] Water Absorption Spectrum. *Water Structure and Science*. [online]. 2014 [cit. 2014-06-20]. Available from: http://www1.lsbu.ac.uk/water/vibrat.html

[107] Energy-Dispersive X-Ray Spectroscopy (EDS). *Geochemical Instrumentation and Analysis*. [online]. 2013 [cit. 2014-06-20]. Available from: http://serc.carleton.edu/research_education/geochemsheets/eds.html

[108] The Transmission Electron Microscope. *Nobel Prize*. [online]. 2014 [cit. 2014-06-20]. Available from: http://www.nobelprize.org/educational/physics/microscopes/tem/

[109] Guézennec A.-G., Huber J.-C., Patisson F., Sessiecq P., Birat J.-P., Ablitzer D. Dust Formation in Electric Arc Furnace: Birth of the Particels. *Powder Technology* 157 (2005) 2-11.

[110] Calcium Carbonate (Calcite). *National Institute of Standards and Technology*. [online]. 2011 [cit. 2014-06-20]. Available from: http://webbook.nist.gov/cgi/cbook.cgi?ID=B6004659&Mask=80

[111] van der Marel H.W., Beutelspacher H. *Atlas of Infrared Spectroscopy of Clay Minerals and their Admixtures*. Amsterdam: Elsevier Science Ltd. 1976.

[112] Han S.-M., Park J.-G., Sohn I. Surface Kinetics of Nitrogen Dissolution and its Correlation to the Slag Structure in the $CaO\text{-}SiO_2$, $CaO\text{-}Al_2O_3$, and $CaO\text{-}SiO_2\text{-}Al_2O_3$ Slag System. *Journal of Non-Crystalline Solids* 357 (2011) 2868-2875.

[113] Iwata N., Fujii H., Okamoto T. Magnetic Properties of (Mn,Cr)P and (Mn,Fe)P Compounds. Journal of the Physical Society of Japan 46 (1979) 778-783.

[114] Socrates G. *Infrared and Raman Characteristic Group Frequencies.* New-York: Wiley. 2001. ISBN 978-470-09307-8.

[115] Plachá D., Peikertová P., Kukutshová J., Lee P.W., Čabanová K., Karas J., Kuchařová J., Filip P. Analysis of Organic Compounds Present in Non-airborne Wear Particles Released from Low-metallic Automotive Model Brake Pad. **submitted to** *Atmospheric Research*.

[116] Kukutschová J., Roubíček V., Mašláň M., Jančík D., Slovák D., Malachová K., Pavlíčková Z., Filip P. Wear Perforemance and Wear Debris of Semimetallic Automotive Brake Materials. *Wear* 268 (2010) 86-93.

[117] Ferrari A.C. Raman Spectroscopy of Graphene and Graphite: Disorder, Electron-Phonon Coupling, Doping and Nonadiabatic Effects. *Solid State Communications* 143 (2007) 47–57.

[118] Ferrari A.C., Meyer J.C., Scardaci V., Casiraghi C., Lazzeeri M., Mauri F., Piscanec S., Jiang D., Novoselov K.S., Roth S., Geim A.K. Raman Spectrum of Graphene and Graphene Layers. *Physical Review Letters* 97 (2006) 187401.

[119] Bose S., Kuila T., Mishra A.K., Kim N.H., Lee J.H. Preparation of Non-covalently Functionalized Graphene Using 9-anthracene Carboxylic Acid. *Nanotechnology* 22 (2011) 405603.

[120] Sun J., Zhai Q., Lei Y., Yang X., Du X. Phase Transformations of Graphite and Carbon Black by Laser With Low Power Density. *Transactions of Tianjin University* 13 (2007) 318-321.

[121] Nemanich R.J., Solin S.A. First- and Second-Order Raman Scattering from Finite-size Crystals of Graphite. *Physical Review B* 20 (1979) 392-401.

[122] Wopenka B., Pasteris J.D. Structural Characterization of Kerogens to Granulite-Facies Graphite: Applicability of Raman Microprobe Spectroscopy. *American Mineralogist* 78 (1993) 533-577.

[123] Nistor L.C., Van Landuyt J., Ralchenko V.G., Kononenko T.V., Obraztsova E.D., Strelnitsky V.E. Direct Observation of Laser-induced Crystallization of a-C:H films. *Applied Physics A* 58, 137 (1994).

[124] Robins L.H., Farabaugh E., Feldman A. Line Shape Analysis of the Raman spectrum of Diamond Films Grown by Hot-Filament and Microwave-Plasma Chemical Vapor Deposition. *Journal of Materials Research* 5 (1990) 2456-2468.

[125] Li Y.-S., Church J.S., Woodhead A.L. Infrared and Raman Spectroscopic Studies on Iron Oxide Magnetic Nano-particles and their Surface Modifications. *Journal of Magnetism and Magnetic Materials* 324 (2012) 1543-1550.

[126] McCarty K. F. Inelastic Light Scattering in a α-Fe_2O_3: Phonon vs Magnon Scattering. *Solid State Communications* 68 (1988) 799–802.

[127] Massey M. J., Baier U., Merlin R., Weber W. H. Effects of Pressure and Isotopic Substitution on the Raman Spectrum of alpha- Fe_2O_3: Identification of Two-Magnon Scattering. *Physical Review B* 41 (1990) 7822–7827.

[128] Mosleh M., Blau P.J., Dumitrescu D. Characteristics and Morphology of Wear Particles from Laboratory Testing of Disk Brake Materials. *Wear* 256 (2004) 1128-1134.

[129] 294/2005 Sb. *O podmínkách ukládání odpadů na skládky a jejich využívání na povrchu terénu a změně vyhlášky č. 383/2001 Sb., o podrobnostech nakádání s odpady*: MŽP, 2005.

[130] 376/2001 Sb. *Vyhláška Ministerstva životního prostředí a Ministerstva zdravotnictví o hodnocení nebezpečných vlastností odpadů*: MŽP, 2001.

[131] ČSN EN ISO 6341. *Jakost vod – Zkouška inhibice pohyblivosti Daphnia magna Straus (Cladocera, Crustacea) – Zkouška akutní toxicity*, 1997.

[132] ČSN EN 28692. *Jakost vod – Zkouška inhibice růstu sladkovodních řas Scenedesmus subspicatus*, 1995.

[133] ČSN EN ISO 11348-3: *Jakost vod – Stanovení inhibičního účinku vzorků vod na světelnou emisi Vibrio fischeri (Zkouška na luminiscenčních bakteriích) – Část 3: Metoda s lyofilizovanými bakteriemi*, 2009.

[134] Perrenoud A., Gasser M., Rothen-Rutishauser B., Gehr P., Riediker M. Characterization of Nanoparticles Resulting from Different Braking Behaviors. *International Journal of Biomedical Nanoscience and Nanotechnology* 1 (2010) 17.

[135] Peikertová P., Kuricová M., Lišková A., Tulinská J., Vávra I., Bartušová M., Kukutschová J., Horváthová M., Ilavská S., Jahnová E., Szabová M., Dušinská M., Filip P. Airborne Brake Wear Debris: Characterization and the Effect on Immune Response. *In:* Workshop NANOBASE, Ostrava, 2014. ISBN 978-80248-3436-8.

[136] Peikertová P., Kuricová M., Lišková A., Tulinská J., Vávra I., Bartušová M., Kukutschová J., Horváthová M., Ilavská S., Jahnová E., Szabová M., Dušinská M., Filip P. The Effect of Airborne Brake Wear Debris on Immune Response. Poster presentation In: conference NANOCON2013, Brno, 2013.

[137] Oberdörster G., Oberdörster E., Oberdörster J. Nanotoxicology: an Emerging Discipline Evolving from Studies of Ultrafine Particles. *Environmental Health Perspectives* 113 (2005) 823-829.

[138] Kučová K. Otěrové částice z brzdového obložení automobilů a jejich akutní akvatická toxicita pro sladkovodní zelené řasy. Ostrava, 2014. Bachelor thesis (Bc.). VŠB-Technická univerzita Ostrava. Nanotechnology Center.

[139] Toxicological profile for barium. *U.S. Department of Health and Human Services – Agency for Toxic Substances and Disease Registry*. [online]. 2011 [cit. 2014-06-20]. Available from: http://www.atsdr.cdc.gov/toxprofiles/tp.asp?id=327&tid=57

[140] Magalhães M.O.L., do Amaral Sobrinho N.M.B., Zonta E., de Caravalho M.M., Tolón-Becerra A. Effect of Variations in the Redox Potential of Gleysol on Barium Mobility and Adsorption in Rice Plants. *Chemosphere* 89 (2012) 121-127.

[141] Baldi F., Pepi M., Burrini D., Kniewald G., Scali D., Lanciotti E. Dissolution of Barium from Barite in Sewage Sludges and Cultures of *Desulfovibrio desulfurican*. *Applied and Environmental Microbiology* 62 (1996) 2398-2404.

[142] Ulrich G.A, Breit G.N., Cozzarelli I.M., Suflita J.M. Source of Sulfate Supporting Anaerobic Metabolism in Contaminated Aquifer. *Environmental Science and Technology* 37 (2003) 1093-1099.

[143] Bolze C.E., Malone P.G., Smith M.J. Microbial Mobilization of Barite. *Chemical Geology* 13 (1974) 141-143.

[144] Philips E.J.P., Landa E.R., Kraemer T., Zielinski R. Sulfate-reducting Bacteria Release Barium and Radium from Naturally Occurring Radioactive Material in Oil-field Barite. *Geomicorbiology Journal* 18 (2001) 167-182.

[145] Oskaesson A., Reeves A.L. *Barium*, In: Nordberg G.F., Fowler B.A., Nordberg M., Friberg L.T., *Handbook on the Toxicology of Metals*. London: Academic Press London, 2007.

[146] Senko J.M., Campbell B.S., Henriksen J.R., Elshahed M.S., Dewers T.A., Krumholz L.R. Barite Deposition from Phototropic Sulfide-oxidizing Bacterial Activity. *Geochimica et Cosmochimica Acta* 68 (2004) 773-780.

[147] Gregus Z., Klaassen C.D. *Mechanisms of Toxicity*. In: *Casarett & Doull's Toxicology – The Basic Science of Poisons*. New York: MacGraw – Hill Companies Inc. 2001. ISBN 0-07-134721-6.

[148] Stohs S.J., Bagchi D. Oxidative Mechanisms in the Toxicity of Metal Ions. *Free Radical Biology and Medicine* 2 (1995) 321-336.

[149] Dvořáčková J., Bielniková H., Kukutschová J., Peikertová P., Filip P., Zelenik K., Komínek P., Uvirová M., Přádná J., Čermáková Z., Dvořáček I. Detection of Nano- and Micro-sized Particles in Routine Bioptic Material - Pilot Study. *Biomedical Papers* (2012) DOI: 10.5507/bp.2012.104.

[150] Zeleník K., Kukutschová J., Dvořáčková J., Bielniková H., Peikertová P., Čábalová L. , Komínek P. Possible Role of Nano-sized Particles in Chronic Tonsillitis and Tonsillar Carcinoma: a Pilot Study. *European archives of oto-rhino-laryntology* 270 (2013) 705-709.

[151] Peikertová P. Detection of Metallic Micro- and Nano-sized Particles in Human Soft Tissues and Body Fluids. ISSN-ISBN: 978-80-248-2344-7, VŠB-TUO, 2010, 91-92.

8. PUBLICATIONS AND OTHER OUTPUTS GENERATED DURING PhD. STUDY

Internship abroad

- 3 month internship (25. 3. – 24. 6. 2013) in Center for Advanced Friction Studies, Southern Illinois, Carbondale, USA, (financed by the framework of the Nanotechnology – the basis for international cooperation project, reg. no. CZ.1.07/2.3.00/20.0074 supported by Operational Programme 'Education for competitiveness' funded by Structural Funds of the European Union and state budget of the Czech Republic).
- 1 month internship (26. 11. – 14. 12. 2012) in Department of Immunology and Immunotoxicology in Slovak Medical University in Bratislava, (financed by the European Commission 7th FP for the Quality Nano project (FP7 INFRA-2010-1.1.31, Contract no: 214547-2)).

Invited Lecture

P. Peikertová: Brake Wear Debris and its Potential Impact to the Health and Environment, October 4th 2013, Beijing University of Chemical Technology (BUCT), Beijing, China.

Publications in Impacted International Journals

Publications directly related to dissertation thesis

P. Peikertová, J. Kukutschová, I. Vávra, V. Matějka, O. Životský, M. Vaculík, P.W. Lee, P. Filip, Water suspended nanosized particles released from nonairborne brake wear debris, *Wear* 306 (2013) 89-96.
(IF 1.809)

P. Peikertová, I. Vávra, R. Dvorský, K. Dědková, J. Kukutschová, Water suspended nanosized particles released from fine grained pyrometallurgical sludges, **submitted** to *International Journal of Minerals, Metallurgy, and Materials.*

D. Plachá, P. Peikertová, J. Kukutschová, P.W. Lee, K. Čabanová, J. Karas, J. Kuchařová, P. Filip, Analysis of organic compounds present in non-airborne wear particles released from low-metallic automotive model brake pad, **submitted to** *Atmospheric Research*.

Publications related to the study of metal-based particles, which could be originated from brake wear and industry in human tissues and body fluids

K. Zeleník, J. Kukutschová, J. Dvořáčková, H. Bielniková, P. Peikertová, L. Čábalová, P. Komínek, Possible role of nano-sized particles in chronic tonsillitis and tonsilar carcinoma : a pilot study, *European archives of oto-rhino-laryntology* 270 (2013) 705-709.
(IF 1.458)

J. Dvořáčková, H. Bielniková, J. Kukutschová, P. Peikertová, P. Filip, K. Zelenik, P. Komínek, M. Uvirová, J. Přádná, Z. Čermáková, I. Dvořáček, Detection of nano- and micro-sized particles in routine bioptic material - Pilot study, *Biomedical Papers* (2012) DOI: 10.5507/bp.2012.104.
(IF 0.990)

H. Barošová, J. Dvořáčková, K. Mamulová Kutláková, P. Peikertová, J. Rak, H. Bielniková, J. Kukutschová, Metal-based particles in human amniotic fluids of fetuses with normal karyotype and congenital malformation, **submitted to** *Environmental Science and Pollution Research*.

Publications related to the TiO_2 and its properties – composite kaolinite TiO_2 was used in model brake pad formulation

L. Matějová, M. Cieslarová, S. Daniš, Z. Matěj, P. Peikertová, M. Šihor, J. Lang, V. Matějka, TiO_2 Thin Films Prepared by Chelating Agent Assisted Sol-gel: Their Characterization and Photocatalytic Activity in Oxidation of Azo-dye Acid Orange 7. **Submitted to** *Applied Surface Science.*

L. Matějová, K. Kočí, M. Reli, L. Čapek, A. Hospodková, P. Peikertová, Z. Matěj, L. Obalová, A. Wach, P. Kuśtrowski, A. Kotarba, Preparation, characterization and photocatalytic properties of cerium doped TiO_2 : On the effect of Ce loading on the photocatalytic reduction of carbon dioxide, *Applied Catalysis B: Environmental* 152-153 (2014) 172-183.
(IF 5.825)

K. Dědková, K. Matějová, J. Lang, P. Peikertová, K. Mamulová Kutláková, L. Neuwirthová, K. Frydrýšek, J. Kukutschová, Antibacterial activity of kaolinite/nanoTiO_2 composites in relation to irradiation time, *Journal of Photochemistry and Photobiology B: Biology* 135 (2014) 17-22.
(IF 3.110)

J. Tokarský, L. Neuwirthová, P. Peikertová, L. Kulhánková, K. Mamulová Kutláková, V. Matějka, P. Čapková, Structure and electrical conductivity of pellets pressed from polyaniline/TiO_2/kaolinite composite, *Materials Chemistry and Physics* 146 (2014) 146-152.
(IF 2.072)

Publications related to study of polyaniline

L. Kulhánková, J. Tokarský, P. Peikertová, L. Ivánek, K. Mamulová Kutláková, P. Čapková, Conductivity of polyaniline/montmorillonite nanocomposites prepared under various conditions, *Materials Technology – Advanced Performance Materials* (2014) **in press.**
(IF 0.593)

P. Čapková, V. Matějka, J. Tokarský, P. Peikertová, L. Neuwirthová, L. Kulhánková, J. Beňo, V. Stýskala, Electrically conductive nanocomposite aluminosilicate/graphene, *Journal of the European Ceramic Society* 34 (2014) 3111-3117.
(IF 2.360)

L. Kulhánková, J. Tokarský, V. Matějka, P. Peikertová, S. Vallová, V. Stýskala, P. Čapková, Electrically conductive and transparent PANI/montmorillonite nanocomposite thin films, *Thin Solid Films* 562 (2014) 319-325.
(IF 1.604)

J. Tokarský, M. Maixner, P. Peikertová, L. Kulhánková, J.V. Burda, The IR and Raman spectra of polyaniline adsorbed on glass; comparison of experimental, empirical force field, and quantum chemical results, *European Polymer Journal* 57 (2014) 47-57.
(IF 2.562)

L. Kulhánková, J. Tokarský, L. Ivánek, V. Mach, P. Peikertová, V. Matějka, K. Mamulová Kutláková, P. Čapková, Enhanced electrical conductivity of polyaniline films by postsynthetic DC high-voltage electrical field treatment, *Synthetic Metals* 179 (2013) 116-121.
(IF 2.109)

J. Tokarský, L. Kulhánková, K. Mamulová Kutláková, P. Peikertová, J. Svatuška, V. Stýskala, V. Matějka, V. Vašinek, P. Čapková, Monitoring conductivity and optical homogeneity during the growth of PANI thin films, *Thin Solid Films* 537 (2013) 58-64.
(IF 1.604)

L. Kulhánková, J. Tokarský, P. Peikertová, K. Mamulová Kutláková, L. Ivánek, P. Čapková, Montmorillonite intercalated by conducting polyanilines, *Journal of Physics and Chemistry of Solids* 73 (2012) 1530-1533.
(IF 1.527)

Others publications

D. Plachá, G. Simha Martynková, A. Bachmatiuk, P. Peikertová, J. Seidlerová, M.H. Rümmeli, The influence of pH on organovermiculite structure stability, *Applied Clay Science* 93-94 (2014) 17-22.
(IF 2.342)

K. Mamulová Kutláková, J. Tokarský, P. Peikertová, Functional and eco-friendly nanocomposite kaolinite/ZnO with high photocatalytic activity, *Applied Catalysis B: Environmental* **in press.** DOI: 10.1016/j.apcatb.2014.07.018
(IF 5.825)

S. Jiang, R. Mi, R. Yun, S. Qi, X. Zhang, Y. Lu, V. Matějka, P. Peikertová, J. Tokarský, Properties of intercalated and un-intercalated calcined kaolinite filled nano- and micro-composites with polyamide 1010, *Journal of Reinforced Plastics and Composites* **under review.**

Conferences and proceedings

Outputs directly related to dissertation thesis

P. Peikertová, M. Vaculík, P. Filip, J. Kukutschová, Raman Microspectroscopy as a Tool for Characterization of Brake Wear Debris, *In:* NANOCON 2012 Conference Proceedings. Ostrava: Tanger, Ltd., 2013, 842-846. ISBN 978-80-87294-35-2.

P. Peikertová, M. Kuricová, A. Lišková, J. Tulinská, I. Vávra, M. Bartušová, J. Kukutschová, M. Horváthová, S. Ilavská, E. Jahnová, M. Szabová, M. Dušinská, P. Filip, Airborne brake wear debris : Characterization and the effect on immune response, *In:* Workoshop NANOBASE, 2014 Ostrava. *VŠB – Technická univerzita Ostrava* (2014) 41-44. ISBN 978-80248-3436-8.

Outputs related to the study of metal-based particles, which could be originated from brake wear and industry in human tissues and body fluids

P. Peikertová, Detection of metallic micro- and nano-sized particles in human soft tissues and body fluids. In: Den inetrních doktorandů, 2010 Ostrava. *VŠB – Technická univerzita Ostrava* (2010), 91-92. ISSN-ISBN: 978-80-248-2344-7.

H. Doležalová, J. Dvořáčková, P. Peikertová, H. Bielniková, K. Mamulová Kutláková, J. Kukutschová, Methods for analysis of human amniotic fluids. *In:* NANOCON 2013 Conference Proceedings. Ostrava: Tanger, Ltd., 2014, 151-156. ISBN 978-80-87294-47-5.

Outputs related to the TiO_2 and its properties – composite kaolinite TiO_2 was used in model brake pad formulation

K. Dědková, L. Matějová, K. Matějová, P. Peikertová, K. Mamulová Kutláková, Jana Kukutschová, Study of Antibacterial Activity of Cerium Doped TiO_2 photocatylsts. *In:* NANOCON 2013 Conference Proceedings. Ostrava: Tanger, Ltd., 2014, 479-484. ISBN 978-80-87294-47-5.

K. Dědková, P. Peikertová, J. Lang, J. Kukutschová, Study of the antibacterial activity of composites kaolinite/TiO2. *In:* NANOCON 2012 Conference Proceedings Ostrava: Tanger, Ltd., 2013, 842-846. ISBN 978-80-87294-35-2.

P. Peikertová, S. Rebilasová, K. Gröplová, J. Kukutschová, V. Matějka, Raman study of clay/TiO_2 nanocomposites. *In:* NANOCON 2011 Conference proceedings, Ostrava: Tanger, Ltd., 2011, 293-297. ISBN 978-80-87294-23-9.

S. Rebilasová, P. Peikertová, K. Gröplová, L. Neuwirthová: The Influence of Mechanical Treatment of Vermiculite on Preparation Composites Vermiculite/TiO_2. *In:* NANOCON 2011 Conference proceedings, Ostrava: Tanger, Ltd., 2011, 427-432. ISBN 978-80-87294-23-9.

K. Gröplová, S. Rebilasová, P. Peikertová, J. Kukutschová, V. Matějka, Toxicity Assessment of Vermiculite/TiO_2 and Bentonite/TiO_2 Composites Using Green Algae Desmodesmus Subspicatus. *In:* NANOCON 2011 Conference proceedings, Ostrava: Tanger, Ltd., 2011, 655-658. ISBN 978-80-87294-23-9.

K. Gröplová, S. Rebilasová, P. Peikertová, K. Mamulová Kutláková, V. Matějka, J. Kukutschová: Quartz/TiO_2 composite and its acute aquatic toxicity. Contribution from

Conference Nano Ostrava 2011, *In: Advanced Science, Engineering and Medicine*, 3 (2011) 26-29.

Outputs related to study of polyanilines

J. Tokarský L. Kulhánková, P. Peikertová, K. Mamulová Kutláková, V. Matějka, V. Stýskala, J. Svatuška, P. Čapková, Enhancing the conductivity of PANI thin films by addition of clay. *In:* NANOCON 2013 Conference Proceedings. Ostrava: Tanger, Ltd., 2014, 151-156. ISBN 978-80-87294-47-5.

P. Peikertová, L. Kulhánková, L. Ivánek, V. Mach, J. Tokarský, V. Matějka, K. Mamulová Kutláková, P. Čapková, Study of PANI thin film polymerization in dependence on electrical field. *In:* NANOCON 2013 Conference Proceedings. Ostrava: Tanger, Ltd., 2014, 135-139. ISBN 978-80-87294-47-5.

P. Peikertová, L. Kulhánková, L. Neuwirthová, J. Tokarský, P. Čapková, Study of protonation state of polyaniline thin film in dependence on storage conditions. *In:* NANOCON 2012 Conference Proceedings Ostrava: Tanger, Ltd., 2013, 156-161. ISBN 978-80-87294-35-2.

P. Peikertová, V. Matějka, L. Kulhánková, L. Neuwirthová, J. Tokarský, P. Čapková: Thin polyaniline films: study of the thermal degradation. *In:* NANOCON 2011 Conference proceedings, Ostrava: Tanger, Ltd., 2011, 516-520. ISBN 978-80-87294-23-9.

Conferences without Proceedings

Outputs directly related to dissertation thesis

P. Peikertová, Nano-sized particles emitted from automotive brakes, Oral presentation *In*: Workshop NANOBASE, Ostrava, VŠB-TUO, 2014.

P. Peikertová, M. Kuricová, A. Lišková, J. Tulinská, I. Vávra, M. Bartušová, J. Kukutschová, M. Horváthová, S. Ilavská, E. Jahnová, M. Szabová, M. Dušinská, P. Filip, The effect of airborne brake wear debris on immune response, Poster presentation in conference NANOCON, Brno 2013.

P. Peikertová, Nanometrické částice emitované z dopravy. Oral presentation *In*: Workshop NANOBASE Ostrava, VŠB-TUO, 2012.

P. Peikertová, J. Kukutschová, Fine and ultrafine particles in pyrometallurgical sludges. Poster presentation *In*: Workshop NANOBASE, Ostrava, VŠB-TUO, 2012.

Outputs related to the study of metal-based particles, which could be originated from brake wear and industry in human tissues and body fluids

H. Bielnikova, J. Dvořáčková, J. Kukutschová, K. Čabanová, P. Peikertová, H. Doležalová. P. Delongová, Nanopathology: Metal Particles in Samples of Human Tissues and body Fluids, Poster presentation *In*: NANOCON 2013, Brno, Czech Republic, 2013.

Outputs related to the TiO_2 and its properties – composite kaolinite TiO_2 was used in model brake pad formulation

K. Čabanová, P. Peikertová, V. Matějka, J. Kukutschová, Acute aquatic toxicity of photoactive TiO_2 nanoparticles anchored on kaolinite matrix to freshwater green algae. Poster presentation *In*: NANOSAFE 2012, Grenoble, France, 2012.

P. Peikertová, J. Tokarský, L. Neuwirthová, L. Kulhánková, V. Matějka, K. Mamulová Kutláková, H. Doležalová, P. Čapková, Nanocomposite kaolinite/TiO_2 coated with polyaniline – spectroscopic study. Poster presentation *In*: Workshop on Layered Materials 2013. Liblice, Czech Republic 2013.

K. Mamulová Kutláková, J. Tokarský, P. Peikertová, V. Matějka, Kaolinite/TiO_2: The composite material with high photodegradation activity, *In*: NANOSMAT 2014, Dublin, Ireland (September 2014).

Outputs related to study of polyanilines

P. Peikertová, L. Kulhánková, L. Ivánek, V. Mach, J. Tokarský, V. Matějka, K. Mamulová Kutláková, P. Čapková, After-treatment of polyaniline thin films in high voltage electric field. Poster presentation *In*: NANOSMAT 2013. Granada, Spain, 2013.

P. Peikertová, L. Kulhánková, L. Neuwirthová, J. Tokarský, P. Čapková, Change of protonation state of polyaniline thin films during long time period: Raman study. Poster presentation *In*: NANOSMAT 2013. Granada, Spain, 2013.

P. Čapková, L. Kulhánková, T. Plaček, J. Tokarský, L. Neuwirthová, K. Mamulová Kutláková, V. Matějka, P. Peikertová, V. Stýskala, Nanocomposites conducting

polyaniline/phyllosilicate. Oral presentation *In*: Workshop on Layered Materials 2013. Liblice, Czech Republic, 2013.

P. Čapková, L. Kulhánková, L. Neuwirthová, J. Tokarský, V. Stýskala, P. Peikertová, K. Mamulová Kutláková, V. Matějka, J. Svatuška, V. Vašinek, Structure, conductivity and optical properties of polyaniline thin films. Poster presentations *In*: Nano Ostrava 2013 – 3rd Nanomaterials and Nanotechnology Meeting, Ostrava, Czech republic, 2013.

L. Kulhánková, L. Neuwirthová, J. Tokarský, K. Mamulová Kutláková, P. Peikertová, L. Ivánek, P. Čapková, Effect of preparation method on structure and conductivity of polyaniline/montmorillonite nanocomposites. Poster presentation *In*: 4th International Symposium on Structure-Property Relationships in Solid State Materials – SPSSM4. Bordeaux, France, 2012.

L. Kulhánková, L. Neuwirthová, J. Tokarský, V. Stýskala, P. Peikertová, K. Mamulová Kutláková, V. Matějka, P. Čapková: Polyaniline thin films: technology, structure and properties. Poster presentation *In*: 4th International Symposium on Structure - Property Relationships in Solid State Materials – SPSSM4. Bordeaux, France, 2012.

Other outputs

P. Peikertová, J. Tokarský, V. Matějka, Spectroscopic studies of composites kaolinite/ZnO and montmorillonite/ZnO, *In*: NANOSMAT 2014, Dublin, Ireland (September 2014).

P. Peikertová, K. Mamulová Kutláková, K. Dědková, J. Tokarský, V. Matějka, Characterization of Morphology and Structure of Composite Polyamide1010/kaolinite and influence of UV irradiation, *In*: NANOSMAT 2014, Dublin, Ireland (September 2014).

K. Mamulová Kutláková, M. Trčková, Z. Šrámková Zajacová, P. Alexa, J. Tokarský, P. Peikertová, Antibacterial kaolinite/ZnO nanocomposite: Preparation and characterization, *In*: NANOSMAT 2014, Dublin, Ireland (September 2014).

Functional Samples

K. Dědková, V. Matějka, K. Mamulová Kutláková, P. Peikertová: "Nanostrukturovaný kompozitní materiál kaolinit/TiO_2 s antibakteriálním vlastnostmi" (reg. num. 058/02-06-2014_F), Registered 2014,

Education

„Laboratorní cvičení z fyzikální chemie“ (9360-014/01)

„Chemie“ (9360-0005/01)

„Experimentální metody a nástroje pro nanotechnologie I - chemické“ (9360-0131/02)

Consultation:

Karla Kučová, Otěrové částice z brzdového obložení automobilů a jejich akutní akvatická toxicita pro sladkovodní zelené řasy Bachelor’s thesis, 2014.

Opponent reports:

Veronika Holišová, Biosyntéza nanočástic ušlechtilých kovů, Bachelor’s thesis, 2012

Jiří Karas, Kontaminace životního prostředí organickými látkami z nespalovacích procesů v automobilové dopravě, Thesis, 2013

Participitation in Projects

SGS SP2012/45: „Oxidické systémy – metody jejich charakterizace a environmentální aspekty“ – research leader

SGS SP2011/86: “Environmentální aspekty využití fotokatalyticky aktivních nanokompozitů“ - researcher

CZ.1.07/2.3.00/20.0074: „Nanotechnologie – báze pro mezinárodní spolupráci“ - researcher

GAČR P108/11/1057: „Příprava, struktura a vlastnosti nanokompozitů vodivý polymer/fylosilikát“ – researcher

LH 12184: „Nová nanostrukturovná plniva pro polymerní kompozity“ – researcher

GAČR 14-23274S: „Nekonvenční příprava nanostrukturovaných oxidů kovů pomocí přetlakových a superkritických tekutin“ - researcher

QNANO SMU-TAF-82: „Nano-sized particles from automotive friction composite“ – research leader

9. LIST OF ABBREVIATIONS

AO4D	brake dynamometer wear test procedure
ATR	Attenuated Total Reflectance
a.s.	"akciová společnost" is the Czech Republic legal structure for a public limited liability company
BC	Before Christ
BF	blast furnace sludge sample
BFO	blast furnace sludge overflow sample
BFU	blast furnace sludge underflow sample
CAFS	Center for Advanced Friction Studies
CCD	charge-coupled device
D	diameter
EDS	Energy Dispersive X-Ray detector
e.g.	exempli gratia (for example)
et al.	the collective
etc.	and so on
FTIR	Fourier Transform Infrared Spectroscopy
G6C	model brake pad sample
G6C/KATI	model brake with composite kaolinite/TiO_2 in its formulation
IARC	International Agency for Research on Cancer
i.e.	id est ("that is")
KATI	composite kaolinite /TiO_2
min.	minimum
„N"	marking of category "dangerous" according to the Waste catalog
NAO	non-asbestos organic brakes
„O"	marking of category "others" according to the Waste catalog
OC	notation of oxygene converter sludge sample
"O/N"	marking of waste category which are not mentioned in lists of "N" materials, but the category "N" was assigned to them
PAHs	polycyclic aromatic hydrocarbons
PM	particulate matter
$PM_{2.5}$	particles smaller than 2.5 μm aerodynamic diameter
PM_{10}	particles smaller than 10 μm aerodynamic diameter
ROS	reactive oxygen species
SEM	Scanning Electron Microscopy
SMP1	commercial brake pad sample
SMP2	commercial brake pad sample
SOS	SOS response is the first described DNA repair system
SOSIP	SOS inducing potency
TEM	transmission Electron Microscopy
TF	tandem furnace sludge sample
U.S. EPA	United States Environmental Protection Agency
vol.%	percentage by volume
wt.%	percentage by weight
XRPD	X-Ray Powder Diffraction

10. LIST OF FIGURES

Figure 23: Selected SEM images of the OC (a), TF (b), BF (c), BFO (d), and BFU (e) samples prepared by leaching with corresponding EDS spectra. Crosses in the images show measured points.

Figure 24: TEM images in bright (left side) and dark filed (right side) of the OC (a), TF (b), BF (c), BFO (d), and BFU (e) samples prepared by leaching.

Figure 25: Raman spectra of measured metal compounds in suspension prepared by leaching – TiO_2 (a), $FeCO_3$ (b), $CaSO_4$ (c), and $CaSO_4.2H_2O$ (d) occurrence of these compounds in studied samples is described in text.

Figure 26: Selected SEM images of the OC (a), TF (b), BF (c), BFO (d), and BFU (e) samples prepared by sedimentation with corresponding EDS spectra. Crosses in the images show measured points.

Figure 27: Selected TEM bright field images of water treated samples OC (a), TF (b), BF (c), BFO (d), and BFU (e) prepared by sedimentation

Figure 28: Raman spectra of $BaSO_4$ (a), $PbSO_4$ (b), and organic compound (c).

Figure 29: Selected SEM images with corresponding EDS patterns measured from surface area of the G6C (a), G6C/KATI (b), SMP1 (c), and SMP2 (d) wear debris samples.

Figure 30: Measured FTIR spectra of all collected brake wear debris samples.

Figure 31: Measured XRPD patterns of G6C (a), G6C/KATI (b), SMP1 (c), and SMP2 (d). **1** - Fe, **2** – Fe_2O_3, **3** – Fe_3O_4, **4** – C (graphite), **5** – $(Mg_{0.064}Ca_{0.936})CO_3$, **6** – $ZrSiO_4$, **7** – Sb_2O_5, **8** - Sb_2Fe, **9** – $BaSO_4$, **10** – SiO_2, **11** – FeO, **12** – $BaZrO_3$, **13** – Zn, **14** – CuO, **15**– γ-$Fe_{21.34}O_{32}$.

Figure 32: Measured Raman spectra of amorphous carbon (a), mixture of amorphous carbon and graphite (b), and graphite (c).

Figure 33: Measured Raman spectra of hematite (a) and magnetite (b).

Figure 34: SEM images of detected particles in dried suspensions of brake wear debris with corresponding EDS patterns of G6C (a), G6C/KATI (b), SMP1(c), and SMP2 (d).

Figure 35: Bright field TEM images of G6C (a) and SMP1 (c), with corresponding dark field TEM images of G6C (b) and SMP1 (d).

Figure 36: Bacterially mediated sulfur cycling reactions modulate the solubility of barite. Soluble barium can be released from barite by sulfate reducing bacteria and then reprecipitated as barite by bacterial processes that generate sulfate [146].

Figure 37: Scheme of Fenton reaction modified from [147].

Figure 38: SEM image of particle detected in amniotic fluid (A) with EDS pattern of point analysis (B) [151].

11. LIST OF TABLES